Institute of Immunology
Faculty of Veterinary Medicine
Freie Universität Berlin
and
Division of Biophysics
Department of Molecular Infection Biology
Leibniz-Center for Medicine and Bioscience
Research Center Borstel

Evaluation of Antimicrobial Peptides as Anti-Cancer Agents against Equine Sarcoid and Human Prostate Adenocarcinoma Cells

Thesis submitted
for the fulfilment of a doctoral degree in Veterinary Medicine at
the Freie Universität Berlin

submitted by
Stephanie Groß
Veterinarian from Hamburg, Germany

Berlin 2014
Journal No: 3764

Printed with approval of the Faculty of Veterinary Medicine

of the Freie Universität Berlin

Dean:	Univ.-Prof. Dr. med. vet. Jürgen Zentek
First reviewer:	Univ.-Prof. Dr. rer. nat. Susanne Hartmann
Second reviewer:	Prof. Dr. rer. nat. Jörg Andrä
Third reviewer:	Prof. Dr. med. vet. Robert Klopfleisch

Descriptors (after CAB-Thesaurus):
peptides, anticancer properties, mode of action, target groups, selectivity, membranes

Day of doctorate: 16.06.2015

Bibliografische Information der *Deutschen Nationalbibliothek*
Die Deutsche Nationalbibliothek verzeichnet diese Publikation in der Deutschen Nationalbibliografie; detaillierte bibliografische Daten sind im Internet über <http://dnb.ddb.de> abrufbar.

ISBN: 978-3-86387-615-9
Zugl.: Berlin, Freie Univ., Diss., 2014
Dissertation, Freie Universität Berlin
D 188

Choriner Str. 85 - 10119 Berlin
verlag@menschundbuch.de – www.menschundbuch.de

Twenty years from now you will be more disappointed by the things that you didn't do than by the ones you did do. So throw off the bowlines. Sail away from the safe harbor. Catch the trade winds in your sails. Explore. Dream. Discover.

(Mark Twain)

I. Table of contents

II. List of figures

III. List of tables

IV. List of abbreviations

A633	Alexa Fluor® 633-labelled streptavidin
A647	Alexa Flour® 647, goat-anti-mouse IgG
AMP	antimicrobial peptide
APH-R	adult horse skin cell line
APS	ammonium persulfate
Aqua dem	demineralised water
ATP	adenosine triphosphate
BPV	bovine papillomavirus
BRM	Bionas® Running medium
CS	chondroitin sulfate
DMEM	Dulbecco`s modified eagle`s medium
$DMEM_{add}$	DMEM with additional supplements (see Materials, 3.1.2)
DMSO	dimethylsulfoxide
DSP	dithiobis(succinimidylpropionate)
E 42/02	equine sarcoid cell line
FCS	fetal calf serum
FITC	fluorescein isothiocyanate
FSC	*Forward Scattering*
GAGs	glycosaminoglycans
HaCaT	non-cancerous, spontaneously transformed human keratinocyte cell line
IDES	interdigitated electrode structures
ISFET	ion sensitive field effect transistor
MAL II	*Maackia amurensis* lectin II
MTT	3-[4,5-dimethylthiazol-2-yl]-2,5-diphenyltetrazolium bromide
NANA	N-acetylneuraminic acid
PBS	phosphate buffered saline
PC	phosphatidylcholine
PC-3	human prostate adenocarcinoma cell line
PI	propidium iodide
PNA	peanut agglutinin

PS	phosphatidylserine
SDS	sodium dodecyl sulfate
SNA	*Sambucus nigra* agglutinin
SSC	*Side Scattering*
TFA	trifluoroacetic acid
WGA	wheat germ agglutinin
w/o	without

1 Introduction

The innate immune system of mammals has developed a fast defense against invading pathogens of various types. During evolution, small lytic peptides arose, exhibiting potent activity against a diversity of microorganisms. These so-called antimicrobial peptides (AMPs) are located at the typical entry portals of pathogens such as on skin surface and mucous membranes as guards to prevent the initial entry of any invasion upon onset [1]. However, AMPs are not just protecting the body from foreign invaders; some also exhibit potent activity against cancer cells [2]. This latter ability brought them into the focus of research as possible new anti-cancer agents, which are of urgent need. Cancer is a common disease in humans resulting in over seven million deaths worldwide per year and an increasing morbidity. The application of classical cancer therapeutics is mostly accompanied by severe side effects. Especially the advanced stages of the disease are often incurable. Besides, there is an increasing occurrence of drug-resistant cancer cells, which additionally hamper the therapy of cancerous diseases [3]. Due to these circumstances, intensive research is in effect for finding new and effective anti-cancer agents, which ideally should exhibit a potent and selective activity. If an agent has shown these properties, before drug development takes place, further investigations must include in detail its mode of action, cell responses to compound treatment as well as its serum stability and its transport to the target tissue if it is considered for a parenteral application.

In this study, a selection of naturally occurring peptides and fragments thereof were tested for their anti-cancer cell effectiveness. The cancer types dealt with in this thesis are the equine sarcoid and the human prostate adenocarcinoma. Both are frequently occurring cancers that involve challenging therapies. While the equine sarcoid is a virus-induced localized skin tumor of equidae, the human prostate adenocarcinoma is a malignant tumor of the prostate gland tissue. The equine sarcoid was chosen because a skin tumor is considered much easier to treat as it excludes all the problems that accompany a parenteral application. As the second cancer model, a human prostate cancer cell line was selected because of the high prevalence of prostate cancer in men and in order to include a cancer type involving parenteral treatment. The investigations on peptides' anti-cancer activity were performed using two different cytotoxicity assays,

fluorescence microscopy, as well as measurements with a biosensor indicating changes in cell metabolism and morphology following peptide treatment in real-time. In addition, peptide optimization with regard to effectiveness and serum stability was determined by investigating various sequence variants of one parent peptide. This aimed mainly at a reduction of high synthesis costs since an enhanced effectiveness decreases the required quantity of the drug and shortened effective variants are less expensive to produce.

Secondly, this study aimed to illuminate on the detailed mode of action of AMPs. It is generally accepted that AMPs are mainly effective via direct destruction of the target cell membrane [4]. The targeting itself is assumed to be due to electrostatic interaction between the cationic peptides and an anionic membrane surface [5], which, in contrast to the zwitterionic surface of healthy cells, is found in most cancer cells [6]. However, the exact mode of action of AMPs is still the subject of research. In the present study, the mode of action of AMPs was investigated with regard to i) killing kinetics of peptides including peptide to peptide interaction in the absence and presence of a lipid membrane, ii) putative anionic surface target structures of peptides, and iii) cancer cell selectivity. The kinetics of peptide activity were determined by cytotoxicity assays and metabolic biosensor measurements. Several models for peptide-membrane interaction assume peptide aggregation, especially if membrane destruction might occur via pore formation [7]. Thus, gel electrophoresis was performed to elucidate the peptides' tendency towards aggregation and aggregation changes upon peptide-membrane interaction. For peptide targeting of membranes, three different anionic surface structures that were found to be enhanced on cancer cell membranes were investigated as potential preferred binding structures. Investigations were performed by determining the inhibiting effect of the different structures on the peptides' cytotoxicity as well as the impact of according enzymatic treatment of cancer cell surfaces on peptide activity. This is considered to provide information if some anionic surface structures are more attractive for peptides than others. These results are also important for a better understanding of the cancer cell selectivity of peptides, which not only depends on the individual peptide but may vary for different cancer types.

2 Literature review

2.1 Antimicrobial peptides and their anti-cancer activity

Antimicrobial peptides (AMPs) are widespread in nature being part of the defense system of virtually all life forms, including bacteria, plants, and invertebrate and vertebrate species [1]. They are also named *host defense peptides* due to their diverse functions in the innate immune system. Some peptides show direct killing properties for bacteria, and/or fungi, some parasites and enveloped viruses [1]. In higher life forms, AMPs are suspected to exhibit important immunomodulatory and immunostimulatory properties like the enhancement of phagocytosis, prostaglandine release by mast cell degranulation, anti-endotoxic effect, and promotion of angiogenesis and wound healing. Via chemotactic activities on dendritic cells and T lymphocytes, they seem to work as connecting link between innate and adaptive immunity in vertebrate species [4], [8], [9]. Furthermore, some AMPs were also found to have an activity against cancer cells [2], [10]. It should be mentioned that most AMPs have a broad spectrum of activity but individual peptides do not necessarily possess all of the described properties. Hence, to achieve a defense as broad as possible, most multi-cellular organisms produce several different AMPs [11]. According to their functions, AMPs can be found in vertebrates mainly on sites of increased pathogen exposure, like the skin and mucous membranes as well as within the granules of immune cells. Among other things, they are expressed by epithelial cells and either secreted onto the mucosal surfaces of the respiratory, digestive and urogenital tracts or held in the respective superficial non-viable epithelium [1], [11]. They are also produced in immune cells, being stored in vesicles until release. AMPs are gene encoded and are mainly synthesized in mammals as larger precursors that are proteolytically processed to the active form [11], [12]. How important AMPs are as protective agents is, for example, evidenced by the human disease *Morbus Kostmann*. Patients suffering from this condition are born with a lack of granulocytes, which is treated nowadays with a special cytokine. But despite the successful treatment of granulocyte deficiency, there is still a deficiency of AMP LL-37, which leads to severe periodontal inflammation and infections [13], [14]. The importance of AMPs for the

prevention and the limiting or clearance of infections has also been shown in several animal models [11], [15], [16].

Thus far, nearly 900 naturally occurring AMPs from numerous species have been discovered [17] and several thousands have been synthesized. In spite of having different spectrums of activity and showing diversity in their sequence and structures, most of the AMPs share several common features. They are small with varying sizes of anywhere from nine to up to 100 amino acids, they are hydrophobic and most of them possess a positive net charge provided by arginine, lysine or, in acidic environments, histidine. Their usual membrane activity is achieved by their amphipathic secondary structure. Here, due to the specific shape, hydrophobic, hydrophilic and cationic amino acids are separated by their accumulation on different parts of the molecule [5], [8], [11], which is exemplarily shown for peptide NK-2 in Figure 2-1. Based on their secondary structure, AMPs can be assigned to four classes: (i) α-helical, (ii) β-sheet structures with two to three disulfide bonds, (iii) extended structures, and (iv) loop structures with one disulfide bond [9]. The peptides investigated in this thesis belong to the first class. This class of AMPs generally consist of 12 to 40 amino acid residues and was found to be mostly unstructured in aqueous solutions, adopting the amphipathic α-helical confirmation only in the presence of a membrane or membrane-mimetic environment [12]. Furthermore, there are several peptide families, each of which includes a group of homologues peptides. In mammals, there are two main families named defensins and cathelicidins [15], [18], while magainins are typically found in amphibians [19] and cecropins in insects [20].

In this thesis, peptide effectiveness against tumor cells was investigated. In the following, an overview of the anti-cancer activity of peptides will be provided with special respect to their mode of action, selectivity and therapeutic potential.

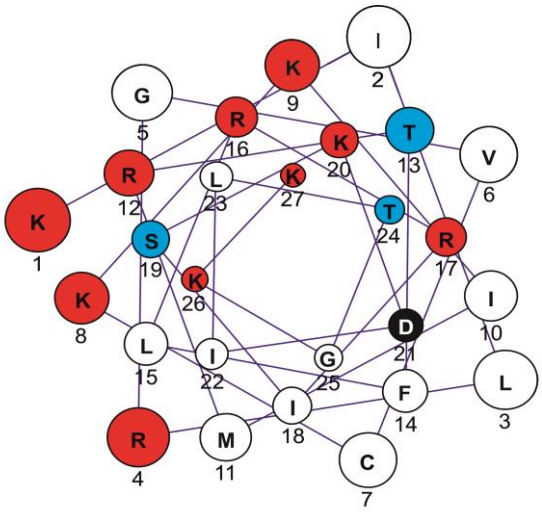

Figure 2-1 Helical wheel diagram of peptide NK-2

Depicted is the helical wheel diagram of peptide NK-2 to exemplarily illustrate the peptides' amphipathic character. Pointed out are the distributions of the cationic (red), anionic (black), hydrophobic (white) and hydrophilic (blue) amino acid residues. Created using the software Lasergene Protean.

2.1.1 Peptides' mode of action

The exact mode of action of AMPs is still not completely understood. However, there is a general consensus that the cationic AMPs target negative cell surfaces via electrostatic interaction [1], [4], [5]. After the attachment of peptides to a cell membrane, several models have been postulated to describe the processes of cell membrane integrity destruction either by disruption or by pore formation. In any case, induction of membrane permeability requires a certain peptide concentration threshold [21]. The loss of membrane integrity induces the collapse of the electrochemical gradient with a resulting increased water and ion flow [22]. The increased permeability causes cellular contents to leak out, thereby leading to rapid cell death. Peptides can also disturb essential membrane functions by reordering lipids through the formation of membrane domains [23]. In addition, for some AMPs, intracellular targets have also been suggested triggering cell death via mitochondrial membrane disruption or inhibition of nucleic acid synthesis, protein synthesis, enzymatic activity, and cell wall synthesis [1], [24], [7], [25]. While cell killing via membranolytic effects occurs within minutes, intracellular modes of action need more time to result in cell death [7], [26]. It has also been postulated that peptide-mediated cell killing might occur as a multihit mechanism

that includes more than one mechanism of action [5], [7]. However, most peptides seem to act via direct and rapid cell membrane lysis.

The first step of peptide-membrane interaction includes the adaptation of an amphipathic secondary structure upon membrane contact for in-solution unstructured peptides. This is common for α-helical AMPs [12], but also occurs in other peptide classes like β-sheet AMPs [27]. Peptides associate on membrane surfaces via electrostatic interaction between their positively charged residues and the negatively charged lipid head groups of the membrane [2], then align parallel to the membrane surface and reorient themselves with their hydrophobic sides toward the membrane. Depending on their hydrophobicity, peptides might already insert to a certain degree into the lipid bilayer causing local membrane thinning and/or increased curvature strain. Below the peptides appear voids in the hydrophobic core that are filled by flexible neighboring lipids or a closer movement of the inner leaflet. Thereby, peptides induce membrane domains of varying thickness, curvature strain, lipid composition and fluidity which result in membrane destabilization [23], [28]. A two-state model was postulated, which demonstrates for some peptides that they adopt two different binding states depending on the peptide-to-lipid ratio. At low peptide-to-lipid ratios, they are in the "S" state and above a threshold peptide-to-lipid ratio in the "I" state. In the "S" state, the AMPs lie inactively in the lipid head group region of the membrane surface. After reaching a certain peptide-to-lipid ratio, peptides adopt a pore-forming state, the "I" state, introducing cell death [28]. This indicates that a critical peptide concentration on the cell surface is needed for cell killing.

For the membrane disruption by AMPs, several models have been postulated in attemps to explain the peptide-membrane interaction describing here only the most common ones. In the "barrel-stave mechanism", peptides aggregate after reaching the critical concentration and insert themselves into the membrane, forming a "barrel-like" ring. Individual peptides or peptide complexes form the transmembrane spokes within this barrel with the hydrophobic side to the lipid layer and the hydrophilic side to the pore lumen. By additional peptide absorption, the pore size increases [7], [29]. Another pore-forming mode of action is described by the "toroidal-pore mechanism". In contrast to the "barrel-stave mechanism", the pores here are lined with peptides and phospholipid head groups, thus minimizing the repulsive forces between the cationic AMPs. These pores have only a finite lifespan and, due to pore collapse, some peptides may enter the cytoplasm to reach intracellular targets [7], [22]. For pore formation, an oligomerization

of the peptide magainin has been postulated [30]. The third model is called “carpet mechanism” and describes the self-association of peptides on the membrane surface in a carpet-like manner [31]. When a threshold concentration is reached, peptides insert into the hydrophobic core and induce membrane disruption in the form of disintegration [29]. In the beginning of membrane destruction too, transient holes may occur in the membrane [5].

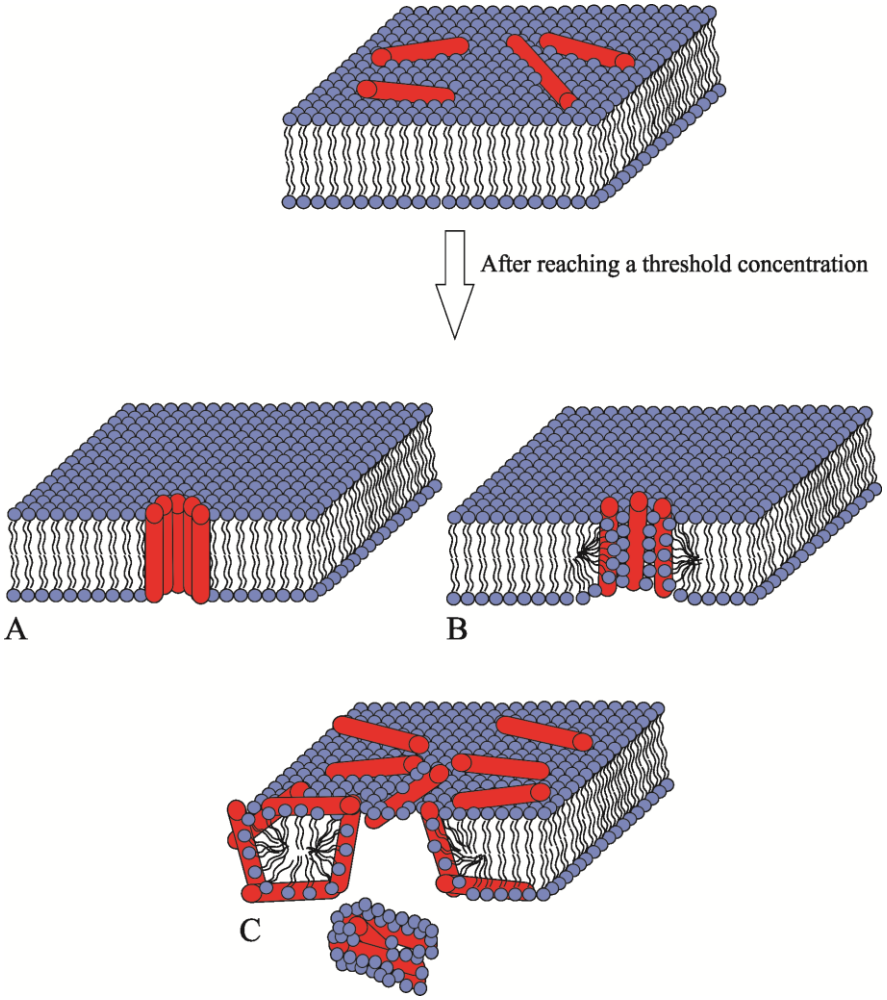

Figure 2-2 Peptides’ models for action

Depicted are the different mechanisms of peptide-membrane interaction. After reaching the respective threshold concentration, pore formation via barrel-stave (**A**) and toroidal-pore mechanism (**B**) might occur as well as membrane disintegration and micelles formation by the carpet mechanism (**C**). Figure modified after [4].

The different modes of action are illustrated in Figure 2-2. It is most likely that different modes of action might occur depending on the peptides’ nature, membrane composition, peptide concentration and environmental conditions.

2.1.2 Selectivity due to different cell membrane composition

As mentioned earlier, some AMPs exhibit selectivity towards one or several cell types like bacteria or cancer cells while affecting healthy mammalian cells to a lesser degree or even not at all. This selectivity seems to be receptor-independent but based on different membrane compositions that influence the electrostatic interactions between peptide and membrane and the membrane stability. In the following, the differences in the membrane composition of healthy and cancer cells, being important in this context, will be pointed out and different membrane surface structures discussed as potential targets for AMPs.

Eukaryotic cell membranes consist of a lipid bilayer with embedded proteins. The outer and inner leaflets of this bilayer show asymmetric lipid distribution [32]. The plasma membranes of healthy cells are mainly non-charged on their outside because predominantly choline phospholipids like zwitterionic sphingomyelin and phosphatidylcholine (PC) can be found here, while aminophospholipids like anionic phosphatidylserine (PS) and zwitterionic phosphatidylethanolamine (PE) are concentrated in the inner leaflet [33]. In contrast, the surface of some cancer cells has a net negative charge due to a higher content of anionic molecules in their outer leaflet, such as PS [34]–[36], O-glycosylated mucins (glycoproteins that are rich in anionic saccharides like sialic acids and sulfates) [37], [38], sialylated gangliosides [39] and heparin sulfates [40]. This is discussed to enable an electrostatic interaction of these anionic molecules with cationic AMPs and might be the important factor determining their selectivity for cancer cells over healthy cells. In addition, the selectivity seemed to be enhanced by a high negative transmembrane potential of some cancer cells [41], which is lower in normal cells. Another difference between healthy and cancerous cells, which might influence the varying sensitivity for peptides, is the higher membrane fluidity of the latter [42]. Eukaryotic cell membranes usually contain cholesterol, which stabilizes the fluid membranes [36], thus making them less susceptible to an insertion of AMPs and subsequent destabilization [29], while in some cancer cell membranes the cholesterol content is decreased [42]. In accordance with this, it had been shown for cecropin and its analogues that an increased cholesterol content reduces the insertion of AMPs into the membrane [43], [44]. Furthermore, membrane stability was found to be enhanced by an interaction of inner leaflet PS with skeletal proteins [45]. Hence, it

should be investigated if the shifting of PS to the outer leaflet in cancer cells further destabilizes the membrane. In addition, cancer cells are reported to have bigger surface areas than normal cells because of an increased number of microvilli. In this case, more peptide molecules could bind on cancer cell surfaces [2], which might enhance the cancer cell-killing effect as well.

The negative surface charge of cancer cells is attributed to the increased quantity of different anionic molecules. In this thesis, the focus was on three of these anionic molecules: PS, sialic acids and sulfated glycosaminoglycans while also considering them as potential peptide targets. As mentioned previously, the asymmetric phospholipid distribution of the normal cell membrane changes in cancerous cells with a shift of PS from the inner to the outer leaflet. Even if it might not happen in all cancerous cells, an enhanced PS content in the outer membrane could be shown for several cancer cell types, thereby suggesting PS to be a possible cancer marker as well [46]. For magainin-2, anionic phospholipids (PS, PG) were found to be essential for peptide action [47] and the effectiveness of synthetic peptides derived from beetle defensins had been shown to depend on PS on the cells' surface [48]. Another anionic group that can be found in extended amounts on cancer cell surfaces are sialic acids as components of glycolipids and glycoproteins [49], [50]. The increase of these terminal sugars might be due to an over expression of certain glycosyltransferases by cancer cells [2]. Some studies determined an influence of sialic acids on peptide action by showing an interaction of peptide and sialic acids [51], [52] or suggesting sialic acids as peptide targets [53]. As a third group of anionic molecules, highly sulfated glycosaminoglycans (GAGs) should be mentioned which are attached to cell surface proteoglycans and have also been shown to be increased in several cancer types [40]. Heparan sulfate (HS) and chondroitin sulfate (CS), two major classes of GAGs, interact with small peptides leading to a partial enhancement of peptide effectiveness [54]. To sum up, all three anionic molecule groups have been shown in various studies to be involved in the cell targeting of peptides, which suggests that different factors might play a role in the recognition of cancer cells by individual AMPs.

2.1.3 Influence of amino acid residues on peptide activity

As shown previously, the cytolytic activity of peptides is assumed to depend mainly on their positive net charge and their amphipathic character. Due to their properties and

position, some amino acids play an important role in the peptides' activity and their deletion induces a reduction or inhibition of peptide effectiveness. This has to be considered for the development of peptide derivates with enhanced selectivity and cancer cell toxicity.

As their positive net charge and their hydrophobicity seem to be key factors in peptide activity, AMPs are characterized by a predominance of positively charged and hydrophobic amino acids. Cationic amino acid residues include only lysine (K), arginine (R) and, in acidic environments, also histidine (H), while there are several hydrophobic amino acid residues like leucine (L), isoleucine (I), tryptophan (W) and methionine (M). Substituting and/or deleting single or several amino acids can investigate their importance for the cytotoxicity of a certain peptide. For example, an enhanced positive net charge of +2 following substitution of aspartatic acid by lysine was shown to increase peptide activity against bacteria [55], as well as the attachment of a cationic amino acid stretch to the C-terminus of a peptide [56]. The deletion of several hydrophobic residues is reported to induce the loss of antitumor activity of lactoferrin- and gaegurin 6-derived peptides [57], [58], while, on the other hand, an increased hydrophobicity has induced a higher haemolytic activity in peptide melittin [30]. It has also been suggested for peptide cateslytin, which adopts a β-sheet secondary structure, that after peptide binding, the lipid-peptide complex is stabilized by aromatic residues like phenylalanine (F) and tyrosine (Y) via van der Waals forces pointing out their importance for the activity of this peptide [27]. Furthermore, some amino acid residues have been found to be essential for the activity of a certain peptide, for example, arginine in melittin peptides while lysine is only minimally important here, although both are cationic [59]. Yang *et al.* [57] determined for short lactoferrin derivates a required net charge of around +7 for high antitumor activity and selectivity. Another study by Andrä *et al.* named, besides a minimal positive net charge of +8, a highly amphipathic anchor point as essential for the antibacterial properties of NK-2 derivates. The anchor point can be formed by only seven amino acids, which are required for two helical turns [55]. As the amphipathic character seems to be extremely important for peptide activity, the order of the amino acid residues that enable the amphipathic conformation of the peptides is suggested to be crucial for the antitumor activity [57], [59]. For melittin, any substitution of an amino acid residue has to maintain the ability for forming the secondary amphipathic structure of the peptide; otherwise, peptide activity might be decreased or lost [59], [60]. Finally, specific details regarding amino

acid influence for the activity of certain peptides are known. But general statements can be barely made so far because of the various results for different peptides.

2.1.4 Prospect of peptides as cancer therapeutics

Conventional cancer therapeutics exhibit severe side effects and more and more multi-drug-resistant cancer cells are arising. Thus, there is an urgent need for new forms of cancer therapy and certain AMPs are promising candidates.

Peptides with anti-cancer activity could be divided into two major classes, both including peptides with high potency against cancer cells, but one class shows no or less activity against normal mammal cells, while the other does not differentiate between healthy and degenerated cells [24]. Of course, for therapeutic purposes, peptides with selective cancer killing properties are of most interest. Several AMPs were documented to be more selective than chemotherapeutics, thereby minimizing side effects [61]. In addition, AMPs are also active against multi-drug-resistant cancer cells [62] and some restistant cell lines have been reported to be even more sentitive for peptides than non-resistant cancer cell lines [63]. Multi-drug resistance can be caused by overexpression of drug transporters, induction of drug-breakdown enzymes, and defects in apoptotic pathways, all of which should be overcome by the direct and fast membranolytic effect of peptides [61]. Nevertheless, several resistance mechanisms of pathogens have been found to inhibit peptide activity [39], and cancer cells have been able to develop a melittin resistance [61]. Besides their membranolytic action, some peptides induce apoptosis in cancer cells via intracellular targeting of mitochondria [4], [25], [26], [64]. It is noteworthy that certain AMPs show anti-angiogenic activity [61], which might be triggered by the anionic surface of tumor blood vessels [35]. Hence, solid tumors are attacked by the peptides from two sides, inducing necrosis and/or apoptosis of the cancer cells and an additional starving out by reducing the blood supply. Furthermore, a recent study demonstrated the use of peptides as anti-cancer vaccine. In this phase I clinical trial, subcutan injections of a multi-peptide vaccine apparently extended the overall survival of pancreatic cancer patients [65].

While there are already more than 100 peptide-based drugs for different diseases on the market, the development of AMPs as new effective cancer drugs still has several obstacles to overcome [66]. Despite the promising *in vitro* activities of AMPs against cancer cells and serious design efforts, there has so far been only limited success with

drug approval [67]. However, antimicrobial peptide-based drugs are indicated, for example, for curing or preventing impetigo and diabetic foot ulcer, oral mucositis, sepsis and catheter-associated infections [68]. To name a few, nisin was demonstrated to prevent mastitis in cows by topical application as a teat dip and cecropin-melittin hybrid peptides were shown to have topical activity against the *Pseudomonas aeruginosa* eye infection of rabbits [16]. The preferred topical application results from the problem of peptide inactivation in serum, either by proteases or anionic serum components [61]. Interestingly, an all-D amino acid analog of magainin exhibits resistance to proteolytic degradation, while having the same anti-cancer activity as its natural counterpart [69], which suggests that this form might enhance serum stability in other anti-cancer peptides as well. Another problem in drug development is the potential toxicity of the peptides, pointing out the need for highly selective peptides. A different approach might be the implementation of additional targeting strategies, like the conjugation of a peptide to a molecule interacting with unique tumor cell structures. An alternative is also targeted liposomal delivery vehicles, which transport the peptide through the blood stream directly to the tumor site, thereby avoiding inactivation and potential immunogenic reactions [61]. One big problem is still the high cost of manufacture. Besides the reduction of the risk of an anaphylactic shock [48], shortening of peptides is carried out to reduce the production costs. A combined application of chemical anti-cancer agents and AMPs might reduce the quantity of both, thus reducing side effects and costs. According to this, promising synergistic effects have been shown for anti-cancer agents and cecropin A [70].

2.2 Characteristics of the appropriated peptides

For this thesis, a selection of representative natural α-helical peptides and fragments was chosen. The peptide in focus is NK-2, for which anti-cancer activity has already been proven [71], and several derivates have been developed [55]. In addition, LL32 was chosen, a fragment of the human LL-37, which itself seems to play a role in the formation of different cancer types [72]. Honey bee melittin served as the reference peptide due to its high and non-selective cytotoxicity [59]. Detailed information on all in this study used peptides is summarized in Table 2-1.

Table 2-1 Peptide properties

Indicated are the used peptides with their amino acid sequence, number of residues (n), net charge (Q) and molecular weight (MW in Da). Amino acid residues in bold exhibit key functions for the design of variants. Red amino acid residues are modifications made compared to the respective parent peptide. Blank gaps mark deletions.

Peptide	Amino acid sequence	n	Q	MW
NK-2	KILRGV**C**KKIMRTFLRRISK**D**ILTGKK-NH_2	27	+10	3202
C7A	KILRGV**A**KKIMRTFLRRISK**D**ILTGKK-NH_2	27	+10	3170
C7A-D21K	KILRGV**A**KKIMRTFLRRISK**K**ILTGKK-NH_2	27	+12	3183.1
C7A-Δ	KILRGV**A**KKIMRTFLRR ILTGKK-NH_2	23	+10	2726.5
NK-11	KI **S**K R ILTGKK-NH_2	11	+ 6	1270.6
LL32	LLGDFFRKSKEKIGKEFKRIVQRIKDFLRNLV-NH_2	32	+ 6	3921.7
Melittin	GIGAVLKVLTTGLPALISWIKRKRQQ-NH_2	26	+ 5	2846.5

2.2.1 NK-lysin and its synthetic derivates

The parent peptide of NK-2 is porcine NK-lysin, a member of the family of saposin-like proteins [73]. NK-lysin was first isolated from the small intestine of pigs and found to be synthesized and released by cytotoxic T lymphocytes and natural killer (NK) cells [74]. It shows relatively narrow antibacterial activity, some antifungal activity against *Candida albicans* and is cytotoxic for the NK-sensitive mouse tumor cell line YAC-1, while not being hemolytic [75]. This natural peptide is 78 amino acid residues in length. Its three-dimensional structure consists of five α-helices, which are folded to a globular domain with a hydrophobic core, a hydrophilic surface and cationic clusters [76]. Peptide NK-2 comprises helices 3 and 4 (residues 39-65) of NK-lysin [77]. It features broad spectrum activity against microbes [77], fungi [77], protozoans [78], lipopolysaccharides [79] and cancer cells [71], [80], but low hemolytic and cytotoxic effects on healthy human cells [77], [80]. NK-2 has a cationic amphipathic α-helical secondary structure. The alternating distribution of hydrophilic and hydrophobic as well as cationic amino acid residues is shown in Figure 2-1. Different variants of NK-2 were synthesized to improve stability, increase positive net charge, and shorten the peptide. The design and the antimicrobial activity of some of these variants were described

previously [55], [81]. NK11, an inactive variant [55], was used as a negative control peptide.

2.2.2 LL32

The only known human cathelicidin is hCAP-18, an 18-kDa cationic antimicrobial protein [82]. The naturally occurring proteolytic C-terminal cleavage product of hCAP-18, LL-37, exhibits an amphipathic α-helical secondary structure and shows a broad-spectrum antimicrobial- and lipopolysaccharide-neutralizing activity [83] as well as several immunofunctional roles [84]. Regarding carcinogenesis, LL-37 shows contradictory roles. In some human malignancies, it is overexpressed and seems to promote the cancer, while in other cancer types it obviously functions as a suppressor [72]. LL-37 is expressed by epithelial cells throughout the body and by different kinds of leukocytes [84]. The deletion of the C-terminal five amino acid residues results in peptide LL32, which was shown to exhibit antibacterial effects [85]. Its secondary structure is also a cationic amphipathic α-helix with the typical characteristic of segregation of the hydrophilic and hydrophobic amino acid residues.

2.2.3 Melittin

Melittin is a well-known component of the venom of the European honey bee and has potent hemolytic activity. Its high interaction with and destruction of various cell membranes is believed to be due to its high content of hydrophobic side chains [59], [71], [77]. A look at the sequence reveals the organization of this peptide into a hydrophobic and a C-terminal hydrophilic part. Besides featuring pronounced hydrophobicity, melittin has a net charge of +6 with four of these charges on the C-terminal end. The amphipathic secondary structure of melittin consists of two α-helices. In aqueous solution, melittin seems to be, depending on the conditions, either monomeric or in a tetrameric aggregate. Melittin has been shown to have different modes of action according to peptide concentration, the membrane composition, and the environmental condition [86]. Here, melittin served as a positive control peptide because of its high and non-specific cytotoxicity.

2.3 Two different cancer types as cell models

Skin cancer is an appropriate model for a topical application of peptides avoiding the complexities that accompany a systemic treatment. Thus, the frequently occurring equine sarcoid was chosen as one of two cancer types to be investigated in this study. As the respective cell model for peptide treatment, a pair of equine cell lines was selected i.e.: equine sarcoid cells (E 42/02) and normal equine skin cells (APH-R). As a second cancer type, human prostate cancer was chosen due to its frequent incidence. This cancer model included a respective cancer cell line (PC-3) and human keratinocytes (HaCaT) as healthy reference cells.

2.3.1 The equine sarcoid

The equine sarcoid is a locally, invasively growing, fibroblastic tumor with a variable epithelial fraction. In principal, the equine sarcoid can occur in the skin of the horse throughout the whole body but most frequently affected are the head, the ventral torso, the genital region and the limbs. The equine sarcoid occurs singularly or in multiples, but does not metastasize into internal organs [87]. It can grow up to fist size and, in advanced stages, bacterial secondary infections often occur. Six different clinical types have been described namely occult, verrucous, nodular, fibroblastic, mixed, and malignant [87], [88]. The equine sarcoid has a high tendency to recurrence [89], but spontaneous regressions have also been reported [90]. The general condition of the affected horses is mainly not impaired.

Looking at the aetiology, it is verified that the bovine papillomavirus (BPV) namely type 1 and 2 play a key role. DNA of both types was found in equine sarcoids in different studies [91]–[94], and expression of the BPV genome in equine sarcoids could also be demonstrated [95]–[97]. Furthermore, BPV DNA was found in mononuclear cells in the peripheral blood of sarcoid-affected horses [98], which might support relapse after treatment. Interestingly, BPV DNA was also found in the unaffected skin of horses with an equine sarcoid as well as of horses without equine sarcoids [99]. Since healthy horses were also found to carry BPV, different co-factors are discussed to be necessary for the clinical development of equine sarcoids, especially a preliminary damage of the skin, but also genetic factors, age, breed, and gender [87], [89], [90],

[100], [101]. Furthermore, it has been observed that the tumor can be transmitted to areas of healthy skin by contact [87].

First described by Jackson in 1936 [102], the equine sarcoid is the most common skin tumor in horses worldwide [89], [101], [103]–[105]. Beside horses, donkeys, mules, and zebras can also be affected [102]. Based on the clinical appearance, only a tentative diagnosis can be made. For a reliable diagnosis of an equine sarcoid, a histological examination should be done. There are several differential diagnoses like equine papilloma, fibroma, and fibrosarcoma, to name only a few [87].

Many therapies are known, like surgical excision, cryosurgery, laser therapy, immunotherapy, brachytherapy, different ointments, topical or injected chemotherapy, and homeopathy [87], [89], [106]–[110]. But despite all these options, a successful treatment of the equine sarcoid is difficult because of the very high relapse rate, especially after surgical intervention [88], [89], [97]. The recurrence itself is often worse than the original tumor, characterized by growing faster and bigger and with a higher invasive potential [108].

The prognosis depends on the localization, size, and inflammation degree. Even if it is often only a matter of aesthetics, equine sarcoids can also cause serious problems and can even culminate in a non-rideable horse. Thus, it is often an enormous economic factor for the owner due to the difficult and mostly repeating treatment.

2.3.2 Human prostate cancer

Prostate cancer is cancer that develops in the prostate, a gland of the male reproductive system that surrounds the upper part of the urethra and produces some of the seminal fluid that protects and nourishes the sperm. The most common prostate cancer is the prostate adenocarcinoma. Prostate cancer mainly grows slowly and is seldom fatal for the patient but malignant types also occur that grow and spread quickly [111]. If the cancer spreads, metastases will develop mainly in local lymph nodes and bones but might also affect other organs. Symptoms of localized prostate cancer may include difficulty in urinating, hematuria, or erectile dysfunction. Of course, metastases may lead to further symptoms depending on the affected tissue.

The causes of the transformation from a normal prostate cell to a prostate cancer cell are not completely known, but several risk factors are suspected to be linked to this disease. Factors that are discussed to promote the development of prostate cancer include high

levels of androgens, an age over fifty, race (prostate cancer is most common in African-American men), and an inherited predisposition. A healthy diet that includes a proportion of vegetables and fruits combined with restrictions on red meat and high-fat dairy products seems to reduce the risk of prostate cancer [111].

Prostate cancer is the most diagnosed cancer in men with the second-highest cancer-related mortality in the US [112]. In Germany, each year, around 58,000 men are diagnosed with prostate cancer and around 12,000 men die of this disease [113]. It is no longer only a common cancer in North America and Europe; increasing rates of incidence and mortality are also reported in Asia, especially in Korea, Japan and Singapore [114], [115]. Mainly elderly men are affected as the incidence is significantly increased in men over 55 years of age [116]. According to the National Cancer Institute, based on data from the US National Institutes of Health, one in six men in the US will be diagnosed with prostate cancer during his lifetime. However, many men with prostate cancer never have symptoms, undergo no therapy and mostly die due to other causes.

Diagnosis is mainly done by screening the amount of prostate-specific antigen (PSA) in a man's blood and/or by digital rectal examination. As there are often no symptoms of the disease before metastasis, these examinations are important for detecting the cancer at an early, more treatable stage. If prostate cancer is suspected by one or both tests, a biopsy of the prostate is taken for a histological examination. If the histology confirms the cancer diagnosis, it is also used to grade the cancer. This grading predicts how fast the cancer will grow and spread. The most common differential diagnosis of a slowly growing prostate cancer is the benign prostatic hyperplasia. An infection or inflammation of the prostate might also show similar symptoms as described for prostate cancer [111].

Therapy depends on the individual case and the grade of the cancer. Slow-growing tumors might not need any treatment, but should be regularly controlled to notice any worsening of their condition (so-called "watchful waiting"). Treatment for more malignant types includes radiotherapy, brachytherapy, hormone therapy, cryosurgery and the radical prostatectomy, all with more or less severe side effects. Radiotherapy, for example, might lead to impotence, urinary and fecal incontinence and chronic diarrhea while radical prostatectomy might cause urinary incontinence and erectile dysfunction [113]. A metastatic prostate tumor is currently non-curable [117], which indicates an urgent need for new therapeutic agents.

Correspondingly, prognosis depends mainly on the stage of the tumor. Watchful waiting might be the best option for most patients with slow-growing tumors, but being diagnosed with cancer without treatment is a challenging task for many men. Furthermore, there is the risk that the cancer develops faster than suspected and reaches into a hard or non-curable stage by not having early treatment. On the other hand, treatment of a harmless tumor might be accompanied by side effects that tremendously restrict the quality of life of the patient. Thus, treatment has to be considered carefully for each individual case.

3 Material and Methods

3.1 Material

3.1.1 Peptides

All peptides used had been synthesized with an amidated C terminus by Reiner Bartels and Volker Grote from the Division of Structural Biochemistry at the Research Center Borstel and were provided in HPLC-purified and lyophilized form. Peptide stock solutions (1 mM and 5 mM) were prepared by diluting the peptides in 0.01% trifluoroacetic acid (TFA) and stored at -20 °C. Detailed information on all peptides is summarized in Table 2-1.

3.1.2 Cell lines and cell culture

For this work adherent healthy and degenerated cell lines of equine and human origin were used. The human cell lines already had been in the laboratory for years. That is why instead of their supplier only their ATCC (American Type Culture Collection) or CLS (Cell Lines Service GmbH) numbers, respectively, are indicated in Table 3-1. The equine cell lines were received as fresh shipments for this study. All cell lines were frozen in nitrogen for long time storage and were only defrosted for experimental use. After a certain passage number the cultured cells were disposed.

Table 3-1 Cell lines

Cell line	Origin
APH-R	Adult horse skin Collection of Cell Lines in Veterinary Medicine, FLI, Insel Riems CCLV-RIE 958 Morphology: fibroblast-like
E 42/02	Equine sarcoid Collection of Cell Lines in Veterinary Medicine, FLI, Insel Riems CCLV-RIE 891 Morphology: fibroblastoid
HaCaT	Adult human skin Boukamp *et al.*, 1988 [118] Cell Line Service No. 300493 Morphology: keratinocyte
PC-3	Human prostate adenocarcinoma, derived from metastatic site (bone) ATCC No. CRL-1435™ Morphology: epithelial

All cells were cultured in DMEM, supplemented with 10 % heat-inactivated FCS and 2 % L-glutamine/penicillin/streptomycin. Heat inactivation of FCS was reached by incubation for 30 min at 56 °C. These complete cell culture media are named in the following as $DMEM_{add}$.

Cells were cultured in $DMEM_{add}$ in a humidified atmosphere with 5 % CO_2 at 37 °C, and split after reaching 90-100 % confluency, and harvested either by accutase or trypsin/EDTA treatment. Adherent cells are detached more gently by accutase, resulting in higher cell viability and the conservation of epitopes. The latter is highly advantageous for flow cytometry measurements. Depending on the size of the tissue culture flask, 1 ml (75 cm^2 flask) or 0.5 ml (25 cm^2 flask) of the respective substance was added to the cells. After incubation for a few minutes at 37 °C, followed by gentle shaking, detached cells were resuspended, counted using a Neubauer counting chamber, and adjusted to the required cell density.

Table 3-2 Substances for cell culturing

Substances	Supplier
Bionas running medium (BRM)	Bionas GmbH, Rostock, Germany
Dulbecco's modified eagle's medium (DMEM)	Biochrom AG, Berlin, Germany
Gibco® Cell Dissociation Buffer	Life Technologies, Carlsbad, CA, USA
HEPES	Merck KGaA, Darmstadt, Germany
L-glutamin	Biochrom AG, Berlin, Germany
phosphate buffered saline (PBS) 1 x, pH 7.4	Biochrom AG, Berlin, Germany
Penicillin G/Streptomycin (Pen/Strep)	Biochrom AG, Berlin, Germany
fetal calf serum (FCS),	LINARIS Biologische Produkte GmbH, Dossenheim, Germany
trypsin-EDTA	Biochrom AG, Berlin, Germany
accutase	PAA Laboratories GmbH, Pasching, Austria

3.1.3 Chemicals/reagents and kits

Table 3-3 Chemicals/reagents and kits

Substances	Supplier
acetic acid	Merck KGaA, Darmstadt, Germany
acryl/bisacrylamid (37.5:1) 40 %	Merck KGaA, Darmstadt, Germany
ammonium persulfate (APS)	SERVA, Heidelberg, Germany
Annexin V-FITC	Biolegend, San Diego, CA, USA
Aqua B. Braun	B. Braun, Melsung, Germany
Bionas kit for cell suspension Bionas *metabolic chip* SC1000 Agarose ready-to-use solution Membrane disc	Bionas GmbH, Rostock, Germany
borat	Sigma Life Sciences, St. Louis, MO, USA

Substances	**Supplier**
calcium chloride ($CaCl_2$)	Merck KGaA, Darmstadt, Germany
chloroform	Merck KGaA, Darmstadt, Germany
dimethylsulfoxide (DMSO)	Merck KGaA, Darmstadt, Germany
DSP-crosslinker Pierce DSP (Lomant's Reagent) dithiobis(succinimidylpropionate)	Thermo Scientific, Waltham, MA, USA
ethanol	Merck KGaA, Darmstadt, Germany
gaze TG100	Schleicher und Schuell, Dassel, Germany
glutardialdehyde (25 %)	Sigma-Aldrich, St. Louis, MO, USA
glycerol (87 %)	neoLab Migge Laborbedarf-Vertriebs GmbH, Heidelberg, Germany
hydrochloric acid (HCl)	VWR International SAS, Fontenay-sous-Bois, France
isopropanol	Sigma Life Sciences, St. Louis, MO, USA
magnesium chloride ($MgCl_2$)	Riedel-de Haën, Seelze, Germany
methanol	Merck KGaA, Darmstadt, Germany
molecular weight marker for peptides	Sigma-Aldrich, St. Louis, MO, USA
orange G	Sigma-Aldrich, St. Louis, MO, USA
potassium chloride (KCl)	AppliChem GmbH, Gatersleben, Germany
propidium iodide (PI)	Invitrogen, Eugene, OR, US
Roti-blue (5 x)	Carl Roth GmbH + Co, Karlsruhe, Germany
sodium azide (NaN_3)	Merck Schuchardt OHG, Hohenbrunn, Germany
sodium chloride (NaCl)	Merck KGaA, Darmstadt, Germany
sodium dodecyl sulfate (SDS)	neoLab Migge Laborbedarf-Vertriebs GmbH, Heidelberg, Germany
sodium hydroxide (NaOH)	VWR International SAS, Fontenay-sous-Bois, France
Sytox® green	Invitrogen, Eugene, OR,US

Substances	Supplier
tetramethylenediamine (TEMED)	AppliChem GmbH, Gatersleben, Germany
tetrazolium salt 3-[4.5-dimethylthiazol-2-yl]-2.5-diphenyltetrazolium bromide (MTT)	Sigma-Aldrich, St. Louis, MO, USA
tricine	neoLab Migge Laborbedarf-Vertriebs GmbH, Heidelberg, Germany
trifluoroacetic acid (TFA)	Merck KGaA, Darmstadt, Germany
tris-base	neoLab Migge Laborbedarf-Vertriebs GmbH, Heidelberg, Germany
triton X-100	Sigma-Aldrich, St. Louis, MO, USA
trypan blue	Merck KGaA, Darmstadt, Germany

3.1.4 Carbohydrates

Table 3-4 Carbohydrates

Substances	Supplier
chondroitin sulfate B sodium salt (CS)	Sigma, Steinheim, Germany
N-acetylneuraminic acid (sialic acid, NANA)	Sigma, Steinheim, Germany

3.1.5 Lipids

Table 3-5 Lipids

Lipid	Supplier
PC: L-α-phosphatidylcholine (egg, chicken)	Avanti Polar Lipids, Alabaster, AL, USA
PS: L-α-phosphatidylserine (brain, porcine)	Avanti Polar Lipids, Alabaster, AL, USA

3.1.6 Proteins

Table 3-6 Proteins

Protein	Supplier
asialofetuin (AF)	Sigma-Aldrich, St. Louis, MO, USA
fetuin (FE)	Sigma-Aldrich, St. Louis, MO, USA
lectines: *Maackia amurensis* lectin II (MALII) peanut agglutinin (PNA) *Sambucus nigra* agglutinin (SNA) wheat germ agglutinin (WGA)	Vector Laboratories, Burlingame, CA, US
N-glykosidase F of *Flavobacterium meningosepticum,* recombinant from *E. coli*	Roche Diagnostics GmbH, Mannheim, Germany
neuraminidase from *Athrobacter ureafaciensis*	Roche Diagnostics GmbH, Mannheim, Germany

3.1.7 Immunoreagents

Table 3-7 Immunoreagents

Immunoreagent	Supplier
anti-PS antibody, mouse monoclonal [4B6] to phosphatidylserine (PS)	Abcam, Cambridge, UK
Alexa Fluor® 647, goat-anti-mouse IgG (A647)	Invitrogen, Molecular Probes, Eugene, OR, US
Alexa Fluor® 633-labelled streptavidin (A633)	Invitrogen, Molecular Probes, Eugene, OR, US

3.1.8 Stock solutions and buffers

Throughout this thesis, the abbreviation “aqua dem” refers to sterile filtered demineralized water, obtained from pre-demineralized water further strained by a Millipore filter system. Unless otherwise specified, aqua dem was used as solvent or diluting agent.

3.1.8.1 Buffers and solutions for SDS-PAGE

ammoniumpersulphate solution

40 % APS (w/v)

Anode buffer (10 x)

2 M tris base

titrated with HCl to pH 8.9

Buffer S (stock buffer for sample buffer)

6.06 g tris base

0.4 g SDS

0.01g NaN_3

ad 80 ml

titrated with HCl to pH 6.8

ad 100 ml

Cathode buffer (10 x)

1 M tris base

1 M tricine

1 % SDS (w/v)

titrated with HCl to pH 8.25

Coomassie destaining solution

10 % acetic acid (v/v)

50 % ethanol (v/v)

Gel buffer (3 x)

36.3 g tris base

0.3 g SDS

0.01 g NaN_3

ad 80 ml

titrated with HCl to pH 8.45

ad 100 ml

Gel fixation solution

0,4 M borat

titrated with NaOH to pH 8.5

5 % glutardialdehyde (v/v)

Roti-blue solution (1 x)

20 % methanol (v/v)

20 % Roti-blue (5 x) (v/v)

Sample buffer (2 x)

2.5 ml buffer S

2 g SDS

40 mg orange G

20 ml glycerol (87 %)

ad 100 ml

Separating gel composition	13 %	15 %	17 %
acryl/bisacrylamid (37.5:1) (40 %)	3.25 ml	3.75 ml	4.25 ml
gel buffer (3 x)	2.25 ml	2.25 ml	2.25 ml
glycerol (87 %)	2.0 ml	2.0 ml	2.0 ml
aqua dem	2.5 ml	2.0 ml	1.5 ml
TEMED (100 %)	9 µl	9 µl	9 µl
APS (40 %)	12 µl	12 µl	12 µl

Spacer gel composition	9 %
acryl/bisacrylamid (37.5:1) (40 %)	2.25 ml
gel buffer (3 x)	3.3 ml
glycerol (87 %)	1.0 ml
aqua dem	3.45 ml
TEMED (100 %)	5 µl
APS (40 %)	9 µl

Stacking gel composition	4 %
acryl/bisacrylamid (37.5:1) (40 %)	1.0 ml
gel buffer (3 x)	3.3 ml
glycerol (87 %)	---
aqua dem	5.7 ml
TEMED (100 %)	5 µl
APS (40 %)	9 µl

3.1.8.2 Solution for MTT assay

Stop solution

90 % isopropanol (v/v)

10 % triton X-100 (v/v)

0.8 % HCl 32 % (v/v) 480 µl

3.1.8.3 Solution and buffer for flow cytometry

Annexin V binding buffer (10 x)

100 mM HEPES
1.5 M NaCl
50 mM KCl
10 mM $MgCl_2$
18 mM $CaCl_2$
titrated with NaOH to pH 7.4
ad to 100 ml

Annexin V incubation reagent

1 % Annexin V binding buffer (v/v)
1 % Annexin V-FITC (v/v)

3.1.9 Equipment and tools

Table 3-8 Equipment and tools

Equipment and tools	**Supplier**
automatic weighing scales:	
Satorius Research	Satorius AG, Göttingen, Germany
Satorius Extend	Satorius AG, Göttingen, Germany
Bionas® 1500[2] analyzing system	Bionas® GmbH, Rostock, Germany
breathable Sealing Films AeraSeal	EXCEL Scientific, Victorville, CA, USA
cell counting chamber from Neubauer 0.1 mm depth, 0.0025 mm^2 size	Assistent, Sondheim/Röhn, Germany
gel electrophoresis system with a Power Pac 200 generator and a MiniProtean 3 Cell apparatus	Bio-Rad Laboratories, Inc., Hercules, CA, USA

Equipment and tools	**Supplier**
camping gas Bunsen burner Labogaz	Camping gaz, France
carbon dioxide incubator "Thermo scientific Heraeus"	Thermo Scientific®, Braunschweig, Germany
centrifuges: Biofuge 17RS, Heraeus Sepatech Centrifuge 5415R Varifuge K, Heraeus Christ	 Heraeus Instruments, Berlin, Germany Eppendorf, Hamburg, Germany Heraeus Instruments, Berlin, Germany
clean bench: Gelaire BSB4	Bioflow Technik, Meckenheim, Germany
Eppendorf reaction tubes (0.5 ml, 1.5 ml, 2 ml)	Eppendorf, Hamburg, Germany
FACSCalibur™ flow cytometer	Becton Dickinson Biosciences, Heidelberg, Germany
folded capillary cell (cuvettes)	Malvern Instruments GmbH, Malvern, UK
glass bottle with screwtop (100 ml, 1000 ml)	Schott, Jena, Germany
heating block BT 100	Kleinfeld Labortechnik GmbH&Co, Gehrden, Germany
laminar flow hood: LaminAir® HB2472	Heraeus Instruments, Berlin, Germany
magnetic stirrer, M5 CAT	Neo Lab, Heidelberg, Germany
metabolic biosensor chip (SC1000)	Bionas® GmbH, Rostock, Germany
microscopes (transmission light) Zeiss 46 70 85 Zeiss ID02	 Carl Zeiss AG, Oberkochen, Germany Carl Zeiss AG, Oberkochen, Germany
microscopes (fluorescence) Olympus IX 70-S8F2 with a black and white digital camera C848-05G Leica TCS SP5 confocal laser scanning microscope	 Olympus Corporation, Tokyo, Japan Hamamatsu Photonics Deutschland GmbH, Herrsching, Germany Leica Microsystems GmbH, Wetzlar, Germany
microscope (incident light) Di-Li 2009 – 3 with a digital camera MP3	Di-Li® Distelkamp Electronic, Kaiserslautern, Germany

Equipment and tools	**Supplier**
microtiter plate reader, Rainbow	Tecan, Crailsheim, Germany
Milli-Q Advantage A10 with sterile filter Millipak 20 (0.22 µM)	Merck Millipore, Billerica, MA, USA
multi-channel pipettes Eppendorf research 100 and 300	Eppendorf, Hamburg, Germany
multi-well culture plates, flat bottom (6- and 96-well)	Costar tissue culture treated, Corning Incorporated, NY, US
µ-Slides VI 0.4	Ibidi, Martinsried, Germany
orbital shaker SSM1	Stuart Scientific Co. Ltd., Redhill, Surrey, UK
petri dishes w/o cams (92 x 16 mm)	Sarstedt, Nümbrecht, Germany
pH meter, Microprocessor pH537	Wissenschaftlich-Technische Werkstätten (WTW), Weilheim, Germany
pipetboy acu Integra	Integra Biosciences, Fernwald, Germany
pipettes eppendorf Research 10, 20, 100, 200, 1000	Eppendorf, Hamburg, Germany
pipette tips (2 µl – neutral, 200 µl – yellow, 250 µl – neutral, 1000 µl – blue)	Sarstedt, Nümbrecht, Germany
polystyrene Round Bottom Tube 12 x 77 mm style (5 ml)	BD Falcon, Heidelberg, Germany
scanner hp scanjet 2400	Hewlett-Packard Company, Palo Alto, CA, USA
stripettes (5 ml, 10 ml, 25 ml)	Costar, Corning, NY, USA
tissue Culture Flasks (25 cm^2, 75 cm^2)	Sarstedt, Newton, NC, USA
tubes (100 x 16 mm PP (13 ml), 120 x 17 mm PS (15 ml), 114 x 28 mm PP (50 ml))	Sarstedt, Nümbrecht, Germany
ultrasonic device Cell Disruptor B15	Branson Sonifer, Heusenstamm, Germany
vortexer IKA® MS3 digital	IKA, Staufen, Germany
water bath Haake W19	Haake, Karlsruhe, Germany
ZetaSizer Nano	Malvern Instruments, Malvern, UK

3.1.10 Computer software

Table 3-9 Computer software

Software	Manufacturer
CELLQuest Pro V 6.0	Becton Dickinson Biosciences, Heidelberg, Germany
Coral DRAW Graphics Suite X5	Corel Corporation, Ottawa, Canada
Easy Win fitting 6.1	Tecan, Crailsheim, Germany
ImageJ software	Wayne Rasband, National Institutes of Health, Bethesda, MD, USA
Lasergene Protean	DNASTAR Inc., Madison, WI, USA
Leica LAS AF software	Leica Microsystems GmbH, Wetzlar, Germany
Office 2003	Microsoft, Redmond, USA
Origin 6.0	OriginLab Corporation, Northampton, MA, USA
WinMDI, Version 2.8	Joe Trotter, Scripps Research Institute, La Jolla, CA, USA
Wasabi	Hamamatsu Photonics Deutschland GmbH, Herrsching, Germany
B 1500^2 adv CS V1.04	Bionas® GmbH, Rostock, Germany

3.2 Methods

3.2.1 Liposome preparation

Liposomes are vesicles, prepared of natural or synthetic membrane lipids, used as mimics of different cell membranes depending on their lipid composition. To mimic those cancer cells with a negatively charged surface due to a higher content of PS in their outer membrane [34], [35], [46], liposomes were prepared with zwitterionic phosphatidylcholine (PC) and anionic phosphatidylserine (PS).

The preparation started with the production of 10 mM stock solution of each PC and PS in chloroform, both were incubated for 1 min at 60 °C. After cooling down 90 µl PC solution was mixed with 10 µl PS solution. Subsequently, this mixture was evaporated completely to dryness with gaseous nitrogen. For complete solvent removal the sample was further dried for 30 sec at 60 °C before the residuals were rehydrated in 1 ml PBS to a 1 mM PC/PS (90/10) solution. The solution was sonified using an ultrasonic nozzle for 1 min to break the evolved multilamellar vesicles (MLVs) to small unilamellar vesicles (SUVs). Finally the prepared solution underwent a thermal cycle with 3 times change between 30 min at 8 °C and 30 min at 60 °C to establish phase equilibrium of the lipids. Afterwards, the liposomes were stored in a refrigerator for up to 14 days.

3.2.2 SDS-polyacrylamide gel electrophoresis

Gel electrophoresis was used to investigate the oligomerization of single peptides in solution and in presence of cell membrane mimicking liposomes. By denaturing polyacrylamide gel electrophoresis (PAGE) the different oligomers of the peptide separate in an electric field. The electrophoretic mobility of the molecules generally depends on their charge, size, and shape. The addition of sodium dodecyl sulfate (SDS) to the peptide solution induces the denaturing of the peptides and an equal negative charge of all molecules as SDS itself is negatively charged and forms complexes with the peptides. After the addition of SDS and heating of the samples up to 100 °C for 5 min, the secondary and tertiary structures are destroyed with the exception of the covalent bindings such as disulfide bonds. Here, due to the sequences of the peptides no covalent bindings were suspected to exist, neither within a single peptide nor between

two peptide molecules. Thus, no reductive agent was added. As the peptides were denatured and equally charged, the resulting separation was based on the size (number of amino acid residues) rather than different migration patterns due to various shapes or charges. The smaller the oligomers are the faster they move through the gel. DSP, an amine-reactive crosslinker, fixes covalently and non-covalently linked molecules together. Thus, the addition of DSP before denaturing of the peptides allows the separation of heat- and SDS-instable oligomers. Here, instead of using the standard gel for protein separation with two layers as described by Ulrich Laemmli [119], a spacer gel was added as a third layer with the intent to improve the separation of the quite small peptides. In addition, glycine was replaced by tricine as trailing ion shifting the stacking limit to the low-molecular-mass range. These improvements in the separation of small proteins were first described by Schägger and von Jagow [120].

Before pouring the gel, the glass plates were cleaned carefully with alcohol. Initially, different compositions of the separating gel (13 %, 15 % and 17 %) were tested. The lower the percentage of the polyacrylamide gel is the smaller are the pores through which the molecules have to migrate. As the 15 % separating gel proved best, this composition was chosen for all following tests. For pouring the gel one after the other 2.4 ml separating gel (15 %) and 0.8 ml spacer gel were filled into the gel chamber, before the remaining space was completed with stacking gel. TEMED and APS were added to the gel solutions immediately ahead of pouring as polymerization is initiated by these substances. The three different gel solutions were filled directly one after another allowing them to polymerize together. Combs were rubbed with APS (40 %) and inserted carefully into the fluid gel to avoid any air bubbles. After polymerization, the gels were used either immediately or packed in wet towels and foil and stored for up to 8 days at 8 °C.

This approach was meant to determine differences in peptide oligomerization in solution and after attachment to lipid membranes respectively. Peptide stock solutions of 1 mM were used, PC/PS liposomes were prepared as described under 3.2.1, and the DSP crosslinker was diluted in DMSO to a 2 mM stock solution directly before use. Then three preparations were made for each peptide: peptide alone, peptide with liposomes and peptide with liposomes and DSP crosslinker. Stock solutions of these components were mixed and diluted with PBS to the required concentrations. The sample preparations were incubated for 30 min at room temperature. Following, each preparation was mixed 1:1 with sample buffer (2 x) and incubated for 5 min to 100 °C.

Directly before and after heating the preparations were briefly spun down. After the preparation of the system as described above, lanes were loaded with 1 µg peptide, 500 µM liposomes, 100 µM DSP. The molecular weight marker was solved in aqua dem and diluted 1:1 in sample buffer (2 x) to 1 µg/µl. As reference 10 µg were loaded per lane.

The gels were run with 10 to 20 mA for approximately 3.5 hrs. After careful detachment from the glass plates the gel was fixed by shaking in fixation solution for 30 min. Afterwards, the gel was washed three times for 5 min with aqua dem and then stained with Roti®-blue solution over night on an orbital shaker at 70 revolutions per minute. Roti®-blue is a colloidal Coomassie G250 staining agent with a high bound specificity for proteins combined with minimal gel matrix staining. Destaining was done over 30 min with Coomassie destaining solution. After removal of the destaining solution, the gel was washed with aqua dem, and scanned immediately with a flat bed scanner without image editing. For better printing results brightness and contrast of the gels were adapted.

3.2.3 MTT assay

As a cytotoxic endpoint test the MTT (3-[4.5-dimethylthiazol-2-yl]-2.5-diphenyltetrazolium bromide) assay was chosen. This test provides information about the viability of cells after the treatment with peptides in different concentrations by measuring their metabolic activity. Living cells reduce the yellow tetrazolium base of the MTT to purple formazan crystals by mitochondrial activity. The viability of the cells could be calculated via the degree of color change from yellow to purple.

Cells were harvested with trypsin/EDTA, counted and suspended in $DMEM_{add}$. Cell density was adjusted and 2.5 x 10^4 cells per well were placed in a sterile 96-well flat bottom plate. Cells were cultivated for 24 h (PC-3 and E 42/02) and 48 h (APH-R), respectively, at 37 °C in a humidified atmosphere with 5 % CO_2. Because of differences in cell growth rates, varying cultivation times were necessary to achieve a comparable confluency for all cell lines at the beginning of the test.

From stock solutions peptides were diluted in PBS + 10 % $DMEM_{add}$ or in full $DMEM_{add}$ for the time kinetic test series (dilution stages: 0.1, 0.3, 1, 3, 10, 30, 100 µM). Culture plates with adherent E 42/02, APH-R or PC-3 cells, respectively, were washed three times with 37 °C warm PBS + 10 % $DMEM_{add}$ (full $DMEM_{add}$ for killing kinetic

assays). Afterwards 100 µl peptide solution of each dilution stage were added immediately to the wells. The plates were then incubated in general for 4 h or for 30 min, 2 h, 4 h and 24 h in the killing kinetic test series, respectively, at 37 °C in a humidified atmosphere with 5 % CO_2. Subsequently, 10 µl freshly prepared MTT solution (5 mg/ml in PBS) were added to each well (50 µg/well) and the wells were incubated another 2 h under the same conditions as before. To stop the metabolic activity of the cells and dissolve the formed formazan crystals, 100 µl stop solution were added to each well. The color change was measured photometrically in a microtiter-plate reader with absorbance and reference wavelengths of 570 and 690 nm respectively. Cells incubated with PBS + 10 % $DMEM_{add}$ or with full $DMEM_{add}$, respectively, (M_{PBS} = 100 % viability) served as negative control and cells incubated with 5 % triton X-100 in PBS (M_T = 0 % viability) as positive control. All experiments were done in duplicates and performed at least twice. For all duplicates the arithmetic mean was calculated to determine the metabolic activity (% M) of the cells incubated with peptides (M_{Exp}), the negative (M_{PBS}) and the positive (M_T) control using the following equation: $\% M = 100 \times ((M_{Exp}-M_T)/(M_{PBS}-M_T))$. The metabolic cell activities of the equal, but independently performed, experiments were then again arithmetically averaged and depicted graphically using Origin 6.0. By sigmoidal fitting of the curves IC_{50} values were calculated. These indicate the respective peptide concentration at which the viability of cells was reduced by 50 % compared to control. Due to a steep curve shape not all curves could be fitted. In this case the IC_{50} values of the affected curves were estimated.

As a variant of the standard experiment described so far, four different incubation times were tested to obtain information about the killing kinetic in peptide activity. A second variant of the standard experiment was performed to investigate peptides potential targets on cell surfaces. Chondroitin sulphate, N-Acetylneuraminic acid, fetuin and asialofetuin were used as imitators of different carbohydrate membrane components to investigate whether the presence of any of them has an inhibitory effect of the activity of the tested AMPs. Thus, 1 mg of each carbohydrate was solved in 1 ml PBS + 10 % $DMEM_{add}$ and 10 µl (10 µg/well) of the different solutions were poured on the cells directly before adding 100 µl peptide. Wells without the substances served as reference values and were loaded with 10 µl PBS + 10 % $DMEM_{add}$ alone.

3.2.4 Fluorescence microscopy

Fluorescence microscopy was used to show directly the effect of NK-2 on PC-3 cells and delineate the significance of sialic acids and oligo-/polysaccharids on the cell surface for the activity of NK-2. Peptide induced membrane permeability was measured with Sytox® green. This dye penetrates only compromised membranes and shows a > 500-fold fluorescence enhancement upon binding to nucleic acids. Therefore, dead and damaged cells could be easily detected by their bright green fluorescence, while the living cells and the medium remained unstained.

PC-3 cells were harvested by trypsin/EDTA treatment, counted and suspended in $DMEM_{add}$. Cells were seeded with a density of 4 x 10^5 into 6-well plates and incubated for 24 h at 37 °C in a humidified atmosphere with 5 % CO_2. After washing the wells twice with PBS, either 0.1 U neuraminidase or 0.1 U glycosidase F in 1 ml PBS were added each to one well. As a control cells were treated with PBS alone. Then the plate was incubated in the dark for 2 h in a humidified atmosphere at 37 °C and 5 % CO_2. After incubation, Sytox® green was added to each of the wells from a 5 mM stock solution in DMSO to reach a final concentration in the wells of 5 µM. The dye was mixed with the buffer in the wells by gentle shaking. Then NK-2 was added from a 1 mM stock solution in 0.01 % TFA to reach a final concentration in the wells of 3 µM, again, mixed by gentle shaking. Fluorescent microscopy images with 40-fold magnification, 100 ms exposure time and high gain were taken at defined time intervals using Wasabi software. The invert fluorescent microscope Olympus IX 70-S8F2 with the lens located below the sample was used. Sytox® green was excited by a light source (100 W mercury-vapour lamp) of 460 to 490 nm and fluorescence emission was measured at wavelengths over 510 nm. Unless taking pictures, the sample was sheltered from light. Serial pictures of the different wells were taken immediately by moving the plate. This allows for monitoring not the same sections of the wells over the time. The black and white camera used provides grey-scaled pictures where bright dots represent cells with high fluorescent intensity. Quantification of fluorescence positive cells per image was performed using the ImageJ software. The image sequence of a whole experiment was adjusted regarding brightness/contrast and threshold to define which particles should be counted by the particle analyzer. An example thereof is given in Figure 3-1.

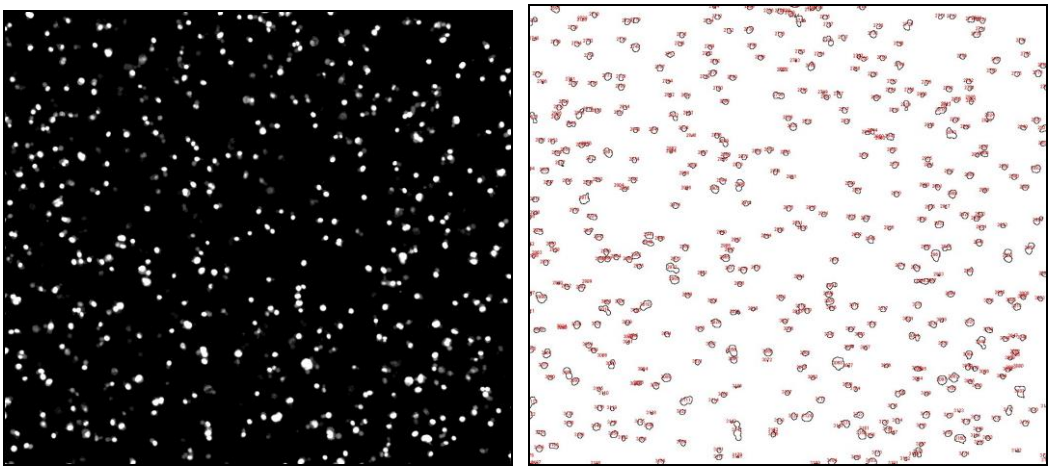

Figure 3-1 Particle counting

One exemplary fluorescence image with the associated drawing indicating the counted cells (red) by ring marks (blue) is depicted.

In addition, confocal laser scanning microscopy was chosen for a more detailed observation of cell reactions to peptide treatment. This microscopy has several advantages over conventional widefield optical microscopy, including the ability to control depth of field, blocking of out-of-focus light, and the capability to collect serial optical sections from thick specimens. In this thesis, the interest was mainly on the higher resolution of the produced images and the chance of indicating individual fluorophores. Peptides NK-2 and NK11 were labelled to the fluorophore rhodamine (Rh) to visualize membrane binding, while membrane permeabilization was again shown by Sytox® green influx. In the fluorescent images peptides are indicated in red and Sytox® green in green color.

For confocal fluorescence microscopy of living cells, cells were seeded in $DMEM_{add}$ in µ-Slides at a density of 3×10^4 cells/well or 4.8×10^4 cells/well as indicated and incubated for 24 h at 37 °C in a humidified atmosphere with 5 % CO_2. Rh-NK-2 and Rh-NK11 (1 mM) were each diluted in PBS to 1 µM, 3 µM, and 5 µM. To each of these solutions 5 µM Sytox® green was added. Cells were then washed twice and incubated unfixed with 100 µl of each solution at room temperature. Control cells were incubated with pure PBS and 5 µM Sytox® green respectively. Subsequently, samples were analysed with the confacal laser scanning microscope TCS SP5 from Leica Microsystems. This is an inverted microscop that is equipped with different lasers which are individually adjustable via acusto-optical tunable filters. Five separate

photomultiplier tubes (PMTs) allow the simultaneous recording of five different wavelengths. The here used fluorophores have their excitation/emission maxima at 510/524 nm (rhodamine) and 504/523 nm (Sytox® green). For rhodamine the DPSS 561 laser was chosen and for Sytox® green the Argon 488 laser. The PMTs were set in accordance to the emission. The power level of the lasers was set to 20 % and brightness and contrast were optimized by adjusting the smart gain. Cells were observed at least for 30 min. All images were acquired using identical settings with Leica LAS AF software. Images were saved as lif-files and exported as jpg-files.

3.2.5 Flow cytometry

Flow cytometry allows the distinction of individual cells in a fluid flow based on their optical characteristics. The used FACSCalibur™ flow cytometer uses excitation wavelengths of 488 nm and 635 nm. Individual cells of a cell suspension are separated one after the other so that every single cell could be analyzed with regard to its size and its granularity. Cell size is measured by light absorption, referred to as *Forward Scattering* (FSC), and cell granularity by light scattering, termed *Side Scattering* (SSC). Additionally, fluorescence emissions for up to four different wavelengths (FL1 to FL4) can be measured simultaneously.

Before each experiment, a fit of the standard settings for the test series was confirmed. Using a dot plot display of sideward to forward scatter, confirmation was achieved that the targeted cell population was within a previously defined gate and necessary adjustments were performed. During the experiment 10,000 cells (events) were measured for each sample within a given gate. The detection channel was chosen depending on the emission of the used fluorophore. Annexin V, excited at 488 nm, was measured with channel FL1 between 500 and 560 nm. Emission of propidium iodide (PI), which was also excited at 488 nm, was measured with FL2 at a range of 543 to 627 nm. A633 and A647 were both excited with wavelength of 635 nm and measured by channel FL4 at a range of 645 to 677 nm. In the following, the fluorescence intensity values of the unstained cells, the negative controls, were confirmed as being below the pre-defined background level. If necessary, appropriate changes in the setting were performed. Settings were defined for every single cell line and kept constant during each experiment. The FACSCalibur™ is operated with the CellQuest software for data acquisition.

For the evaluation of the raw data the WinMDI 2.8 freeware was used. For all experiments done with propidium iodide (PI), cell lysis (%L) was calculated from the percentage of PI positive cells in buffer alone (PI_b) and in the presence of peptides (PI_{exp}): $\%L=100 \times ((PI_{exp}-PI_b)/(100-PI_b))$. For this purpose a dot plot display of FL2 to forward scatter was horizontally divided into two identical parts with PI positive cells lying in the upper part. The values of cell lysis (%L) for the experiment were calculated by the arithmetic mean of the cell lysis (%L) of the duplicates. Shown values in the results are arithmetic means of all equal experiments. For all other test series the targeted cell population was first re-gated to exclude dead cells from the evaluation. The mean fluorescence intensity for each cell population was displayed in the measurement results by the Y-mean value. For all duplicate values the arithmetic average was calculated. The fluorescence intensities in the result chapter are arithmetic means of all equal experiments.

Seven different measurement series were performed using flow cytometry. All cells were freshly harvested with accutase, and re-suspended with PBS to achieve the desired cell density. Following one (PS staining assay and the peptide inhibition tests) or two (all other tests) wash cycles with PBS, cell preparation was completed by sedimenting cells. Every cell washing mentioned in this chapter includes the addition of PBS to the cell suspensions followed by a centrifugation step with 400 x g for 5 min at room temperature and discarding the supernatant.

Peptide induced cell membrane permeabilization of E 42/02 and APH-R cells was determined by measuring cellular uptake of the membrane-impermeable DNA-intercalating dye propidium iodide (PI). Dilution series in PBS were prepared from peptides 1 mM stock solutions (dilution stages: 0.1, 0.3, 1, 3, 10, 30, 100 µM). Then 100 µl of the different dilution stages were added to the cell pellets (2×10^5 cells). As controls pure PBS and TFA diluted in PBS (same dilution stage as in peptide dilutions) were used. The suspensions were gently vortexed and incubated for 30 min at 37 °C in the dark. Subsequently, all tubes were put on ice before 0.5 µg PI per tube was added. After 5 min incubation at 4 °C in the dark 900 µl ice-cold PBS was added and cells were analyzed with the FACSCalibur™ flow cytometer. All experiments were done in duplicates and at least twice.

Comparing the effectiveness of peptides on the two equine cell lines with and without neuraminidase pre-treatment was expected to support whether desialylation of the cell surface influences the activity of the tested peptides. Either PBS alone (1 ml per 1×10^6

cells) or neuraminidase (1 ml 0.1 U neuraminidase diluted in PBS per 1 x 10^6 cells) was added to the cells (3.4 x 10^6 cells of each cell line per tube) followed by 2 h incubation in the dark at room temperature. After washing cells were split up into FACS tubes (2 x 10^5 cells per tube) and washed once more. Then experiments were performed and evaluated as described above. All experiments were done in duplicates and repeated once.

To confirm the successful desialylation of the cell surface by neuraminidase, the binding of four biotinylated lectins (SNA, PNA, MALII, WGA) with different carbohydrate binding specificities was compared with and without enzyme pre-treatment on both equine cell lines. Detection of cell-bound biotinylated lectins is possible via streptavidin, a biotin-binding protein, which is covalently attached to the fluorescent label A633. Cell pellets (two tubes per cell line with 1.2 x 10^6 cells) were incubated with neuraminidase (1 ml 0.1 U diluted in PBS per 1 x 10^6 cells) or without neuraminidase (1 ml PBS per 1 x 10^6 cells), respectively, for 2 h in the dark at room temperature. Between two washings the enzyme treated and untreated cells were each split up into FACS tubes (2 x 10^5 cells per tube). Biotinylated lectins diluted in PBS (100 µl, 10 µg/ml) were added and the mixture was incubated in the dark for 30 min at 4 °C. Then cells were washed again, re-suspended with streptavidin-A633 in PBS (100 µl, 2 µg/ml) and incubated again for 30 min at 4 °C. After another wash cycle cells were diluted in 1000 µl ice-cold PBS, put on ice and analyzed by flow cytometry. Experiments were done twice in duplicates.

The content of phosphatidylserine (PS) in the outer membrane of E 42/02, APH-R, PC-3, and HaCaT cells was determined by measuring the amount of anti-PS antibody binding on the cells surfaces via a fluorophore-coupled secondary antibody. For this, 0.05 µg mouse monoclonal anti-PS antibody in PBS (0.5 µg/ml) was added to each cell pellet (2 x 10^5 cells). For each cell line a cell pellet was incubated with pure PBS as control. The suspensions were gently vortexed and incubated for 60 min in the dark at room temperature. Then cells were washed once again with PBS, re-suspended with 0.2 µg goat anti-mouse IgG-A647 in PBS (2 µg/ml), and incubated in the dark for 30 min. After another wash cycle, cells were diluted in 1 ml PBS and kept on ice until they were analyzed by flow cytometry. Experiments were done four (PC-3 cells) and three (all other cell lines) times respectively.

Another way to determine the content of PS in the outer membrane of cells is to measure the amount of Annexin V binding on these cells. Fluorochrom-conjugated

Annexin V is a phospholipid-binding protein with a high PS affinity. Herewith again E 42/02, APH-R, PC-3, and HaCaT cells were tested. To each cell pellet (2 x 10^5 cells) 0.05 µg FITC Annexin V (1 % in aqua dem with 10 % Annexin V binding buffer (10 x)) were added. For each cell line a cell pellet was incubated with binding puffer (1 x) alone to serve as a control. The suspensions were gently vortexed, and after 15 min incubation in the dark 400 µl ice-cold binding buffer (1 x) was added to each FACS tube. Cells were kept on ice until undergoing FACSCalibur™ flow cytometry. All experiments were conducted twice.

In the search of possible binding structures for the peptides on the cell surfaces two different approaches were used for FACS analysis. First it was tried to inhibit the activity of NK-2 with anti-PS antibody assuming that phosphatidylserine (PS) might be a possible binding structure for AMPs. To inhibit NK-2 0.05 µg anti-PS antibodies in PBS or PBS alone, respectively, were added to the PC-3 cell pellets (2 x 10^5 cells). Suspensions were vortexed and incubated in the dark at room temperature for 60 min, followed by a washing step. In the meantime a dilution series of NK-2 from 1 mM stock solution was prepared (dilution stages: 0.1, 0.3, 1, 3, 10, 30, 100 µM in PBS). Then 100 µl of the different dilution stages were added to the cell pellets. Controls were performed by adding pure PBS or TFA dilution in PBS respectively. After vortexing, the solutions were incubated in the dark at 37 °C for 30 min. Subsequently, all tubes were put on ice before 0.5 µg PI per tube was added. After 5 min incubation at 4 °C in the dark, 900 µl ice-cold PBS was added, and cells were analyzed with the FACSCalibur™ flow cytometer. Experiments were done twice in duplicates.

As second inhibition test peptides were incubated together with cells and different dilution stages of liposomes prepared of phosphatidylcholine (PC) and phosphatidylserine (PS) (90/10), to determine if there is a concentration dependent peptide inhibition by the liposomes. It was assumed that if PS is the target of the peptides these might bind in high content to the PS of the liposomes and therefore were lost for cell interaction. For this assay the liposomes were prepared as described in 3.2.1. Dilution series in PBS were produced from 1 mM stock solution of liposomes (12 µM, 25 µM, 50 µM, 100 µM, 200 µM, 400 µM). Then 90 µl of the different dilution stages were added to the PC-3 cell pellets (2 x 10^5 cells). The peptides NK-2, C7A-D21K, and LL32 were diluted in PBS to 100 µM and peptide melittin to 50 µM, respectively. Of these peptide dilutions 10 µl were added to the cell pellets/liposomes to reach a final concentration of 10 µM NK-2, C7A-D21K, and LL32 and 5 µM melittin,

respectively. These different peptide concentrations showed similar cytotoxicity in the MTT test and were thus chosen for this test series. Untreated controls were performed with unstained and PI stained cells. The latter were also combined with TFA, diluted in PBS with and without 200 µM liposomes. After vortexing, the cell-liposome-peptide mixtures were incubated in the dark at 37 °C for 30 min. Thereafter, all tubes were put on ice before 0.5 µg PI per tube was added. After 5 min incubation at 4 °C in the dark 900 µl ice-cold PBS was added and cells were analyzed using flow cytometry. Experiments were done three times in duplicates.

3.2.6 Online monitoring of cell metabolism and morphology

Kinetic real-time measurements of cell metabolism and morphology were performed with the Bionas analyzing system 1500[2], which consists of two bio modules, each of them equipped with a metabolic biosensor chip. These silicon-chips serve as the bottom of small culture plates with a size comparable to a 48-well microtiterplate. To monitor dynamic parameters of cell physiology they have three different types of electrodes which measure medium oxygen consumption (Clark-type sensors), acidification of the medium (ISFET sensors), as well as the cell impedance (IDES sensor) [121]. This device provides the possibility not only to distinguish between live and dead cells, but to monitor the metabolic and morphologic responses of cells to solvent substances over extended periods of time.

The measured changes in oxygen content and pH-value of the medium are induced by the metabolic activity of the cells. Acidic breakdown products are resulting especially from glycolysis in form of carbon dioxide (aerobe metabolism), which is hydrated to carbonic acid in solution, and lactate (anaerobe metabolism). Both exit the cell through the membrane, either actively or passively, thus decreasing the pH of the cell surrounding. Other glycolysis breakdown products are passed to the mitochondria where they are needed to generate ATP. In the mitochondria, ATP is synthesized in the respiratory chain by oxidative phosphorylation, which is the dominant process of cellular oxygen consumption. ATP is the energy reserve of the cell, which is needed for all energy-dependent processes. Any activation of energy-consuming reactions increases the ATP production, concomitantly, oxygen consumption, and the secretion of metabolic acids. Active substances can also affect just one of the two values, for example by inhibiting glycolysis or the respiratory chain itself. If cells are critically

damaged they cannot sustain their metabolism, which leads to decreased acidification and oxygen consumption. The third value, impedance, is a measure of adhesion strength or confluency of the cell layer. Changes in impedance are usually the result of modified cell morphology. The cell layer works as insulation so that for an increase of the impedance the cells might move closer together, “duck” in the bottom and/or increase their gap junctions. This may be interpreted as a stress reaction. A decrease in impedance might occur by cells that round up, loose their contact to each other and to the chip surface. In the case of dying cells are completely detached from the surface of the chip [122].

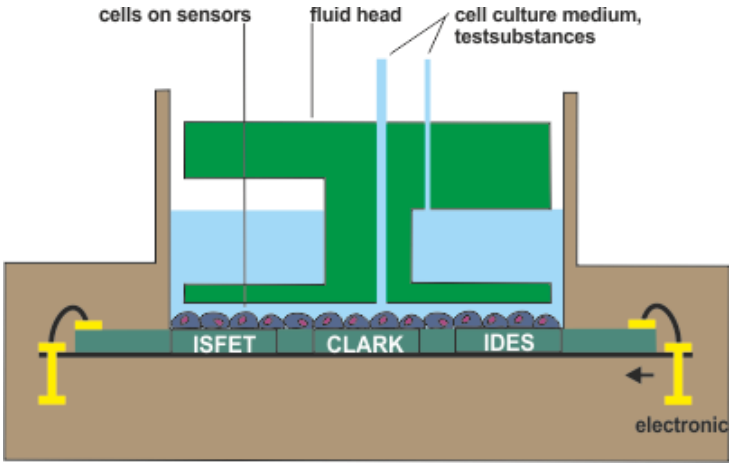

Figure 3-2 Biosensor chip with cell layer and sensor head

Depicted is a scheme of the biosensor chip with adherent cells directly on the chip surface. The housing forms a cylinder, which is open on the top. Here, the fluid head is placed supplying the cells with fresh medium or compound solution.

Before each usage, chips were disinfected for 10 min with 70 % ethanol, rinsed twice and were then covered with $DMEM_{add}$ and conditioned over night at 37 °C in a humidified atmosphere with 5 % CO_2. For each measurement, 2×10^5 with trypsin/EDTA freshly harvested PC-3 or HaCaT cells, respectively, were seeded on the chips, placed 2 h at room temperature to achieve an optimal distribution of the cells on the chip surface and then cultivated for 24 h at 37 °C and 5 % CO_2 in a humidified atmosphere. Before the chips were inserted into the device the cell layer was controlled via an incident light microscope. As the equine cells did not grow with a sufficient

adherence on the chips they had to be immobilized. For this purpose, cells were embedded in agarose and fixed on a membrane disc using the Bionas kit for cell suspensions as described by the manufacturer. In brief, after melting in a 100 °C water bath, one volume of agarose ready-to-use solution was mixed with two volumes of a cell suspension with a cell density of 6 x 10^7 cells/ml. Then 10 µl of this agarose-cell mixture were dropped on a sterile membrane disc (4 x 10^5 cells/membrane) to harden. The sensor chips had been prepared as described above with additional fresh $DMEM_{add}$ inside. The membrane disc was then placed into the sensor chip in that way that the agarose-cell drop was at the bottom with the membrane on top. With embedding in agarose the option for measuring cell morphology changes (IDES sensor) of the two equine cell lines was no longer available.

The tube system of the device was cleaned with 70 % ethanol, rinsed with PBS, and conditioned with Bionas running medium (BRM) before each experiment. The system was operated during experiments with BRM, which is a cell culture medium without bicarbonate buffer, but with 1 mM HEPES, pH 7.4, 4.5 g/l glucose, 0.1 % FCS, 100 U/ml penicillin and 100 µg/ml streptomycin. This low buffered medium allows the assessment of changes in pH. The system works with 4 min "go" and 4 min "stop" phases at a flow rate of 56 µl per min. During the "go" phase, fresh medium/compound inflow combined with removal of used medium occur, while in the "stop" phase the cells change the medium composition due to their metabolism. Oxygen consumption and acidification in the cell supernatant of each chip are measured continuously during the "stop" phase. For each "stop" phase the change of the parameter is calculated and represents the metabolic activity of the cells. Therefore, every 8 min a single data point for the acidification and the oxygen content of the supernatant of each chip is provided. The cell impedance is measured continuously during the whole experiment but only the data during the "stop" phase are taking into account. This avoids any influence of flow rate and substances added to the medium. The given data point for impedance every 8 min is the mean value of the impedance data points over the "stop" phase. After the peptide treatment the cells received another pure BRM flow to determine if there is any cell recovering. Rinsing the sensor chips with 2 % triton X-100 in BRM in the end leads to complete cell lysis and detachment from the surface. This cell-free sensor surface provides the baseline for the measured values.

The calculated values for the acidification and respiration rates between the beginning and the end of the "stop" phase and the mean value for the cell adhesion are the raw

data. For further evaluation the data were normalized to the controls. The raw data measured at the beginning of the experiment, just before the addition of the compound, were averaged and standardized to 100 % and the cell-free values from the triton X-100 treatment were set to 0 %. The other values are set in relation to this, representing the relative values [121]. This was done using the data analyzer of the manufacturer's software (B 1500^2 adv CS V1.04).

In the experiments either one chip served as a control with only BRM flow or both chips were treated with compounds. During the entire experiment, the device remained heated to 37 °C. After each experiment the tube system of the device was flushed with Aqua B. Braun and cleared with air. In a typical experiment, after placing one sensor chip in each of the two biomodules, the chips were flushed with BRM for 4 h to adapt the cells to the new conditions followed by a 12 h feed with pure BRM (as control) or peptides in BRM respectively. Peptides were diluted in BRM from stock solutions to varying concentrations as depicted in the results. After another 4 h pure BRM flow cells were completely lysed by 2 h triton X-100 treatment.

To investigate the impact of sialic acids on the cell surface on the effectiveness of the tested peptides, sensor chips with adherently grown PC-3 cells were first treated with neuraminidase. Cell layer was washed carefully with PBS once, trying to avoid any cell detaching. Subsequently, one chip was filled with 400 µl neuraminidase in PBS (0.1 U/ml) and the other one with pure PBS (as reference). Both chips were incubated in the dark for 2 h in a humidified atmosphere at 37 °C and 5 % CO_2. Then chips were placed in the biomodules and experiments were performed as described above.

For cells with a relative low metabolism rate the device can be equipped with a different sensor head. Both applicable sensor heads differ in the height of the measuring chamber. To investigate the impact of the different sensor heads on the metabolic values, some experiments were also done with the lower sensor head (50 µm) that causes a reduced volume of the measuring chamber compared to the generally used sensor head (200 µm). The smaller measuring chamber, with a reduced amount of medium for the same amount of cells, should make the system more sensitive as little changes in the acidification or oxygen content could be recognized more precisely. This enhances the possibility to monitor cells with low metabolism rates in order to detect also minor changes in medium composition.

3.2.7 Zeta potential

The surface charge of particles is compensated in electrolytic media by ions with an opposite charge (counter ions), resulting in a neutralization of charges. These counter ions form an electrochemical double-layer around the particles. The first layer, called Stern-layer, is attached rather firmly to the particle surface, while the second layer, the diffuse layer, is much more loosly associated with the particle. A gradual decrease of counter ions from the surface of the particle toward the medium can be observed. The Zeta potential can be determined by applying an electric field to the suspension and measuring the velocity of the particles. In the electric field charged particles will move towards an electrode and doing so, counter ions of the diffuse layer are partly removed. The interface between the counter ions that stay with the particle and the surrounding medium is called slipping plane. The electrostatic potential at the slipping plane is the Zeta potential. The electrophoretic mobility of the particles increases proportional to field strength and their Zeta potential [123], [124], [125].

For Zeta potential measurements E 42/02 and APH-R cells were harvested by treatment with enzyme-free cell dissociation buffer (Gibco), filtered through gaze to achieve cell separation and adjusted to 10^6 cells/ml in 40 mM HEPES, pH 7.4. Then, 200 µl of cell suspension was diluted in 800 µl HEPES to a final concentration of 2 x 10^5 cells/ml. This cell solution was placed in a folded capillary cell after this cuvette was washed with ethanol and water. Measurements were performed using a ZetaSizer NanoSeries. The velocity (v) of cells in a driving electric field (E) was measured by Dynamic Light Scattering and the corresponding electrophoretic mobilities (v/E) were calculated. The associated Zeta potentials were automatically calculated from electrophoretic mobility based on the Smoluchowski equation. For each cell preparation, six measurements, each with 20 runs, were performed and averaged for E 42/02 and APH-R cells respectively. Data presented are the mean of two independent cell preparations. All measurements were performed at the lab of Prof. Dr. Mathias Winterhalter at the Jacobs University in Bremen.

4 Results

4.1 Design of NK-2 variants

This thesis aims to determine the various anti-cancer efficacies of three new variants of NK-2. They were synthesized to achieve improved stability, increased positive net charge, as well as a shortened length. The most basic modification of the NK-2 sequence was the replacement of the non-functional sole cysteine (C) residue on position seven with an alanine (A) residue (C7A). This replacement was expected to improve stability by reducing peptide sensitivity to oxidation. Moreover, an enhanced positive net charge of +2 was achieved by substituting the C7A sequence on position twenty-one, the aspartic acid (D) residue, by a lysine (K) residue (C7A-D21K). A shortened variant of C7A was achieved by the deletion of amino acid residues 18 to 21 (C7A-Δ). It may be said that all three variants of NK-2 should have an improved refractiveness against oxidation. In addition, C7A-D21K has an enhanced positive net charge, which might make it more effective in fighting cancer cells, and C7A-Δ, a shortened variant, can reduce production cost if it is at least as effective as its parent peptide, NK-2. NK11, another shortened but inactive variant of NK-2 [55], was used as a negative control peptide. The amino acid sequence, net charge, and the molecular weight for each peptide are shown in Table 2-1.

4.2 Activity of peptides against cancerous equine and human cells

In this thesis, a selection of representative natural α-helical peptides and their fragments were investigated for their effectiveness into fighting malignancies. As example cell lines, two common cancers, the equine sarcoid cell line E 42/02 and the human prostate cancer cell line PC-3, were chosen. To determine selectivity, AMPs were also tested against two healthy cell lines, the equine skin cell line, APH-R, and the human keratinocyte cell line, HaCaT. For the anti-cancer cell efficacy of antimicrobial peptides, the focus was on the α-helical peptide NK-2 [77] and its three synthetic derivates. The study also included peptide LL32, derived from human LL-37, which has

contradictory roles in carcinogenesis [72], and peptide melittin for its high cytotoxicity for all cells [86]. In addition, the different cancer-cell-killing potantials of the NK-2 variants and their parent peptide gave insights into the significance of the amino acid sequence for peptide activity. In the following sections, several assays will point out the anti-cancer cell effectiveness and cancer cell selectivity of these peptides.

4.2.1 Peptide-induced reduction of cell metabolism

To find out whether the selected AMPs were effective against the equine sarcoid cell line, the MTT assay was chosen as a simple cytotoxic endpoint test. In this assay, the viability of cells were found to correspond to the degree of color change caused by living cells metabolizing the yellow tetrazolium base of the MTT into purple formazan crystals; the less the metabolic cells, the less color change. Thus, this assay provided information about the residual metabolic activity of peptide-treated cells. AMPs were also tested on healthy equine skin cells to determine their selectivity for cancerous cells.

As depicted in Figure 4-1, the AMPs possess various degrees of effectiveness against the equine sarcoid cells E 42/02. At a peptide concentration of 1 µM, C7A-D21K and melittin reduce metabolic cell activity, which further declines at a concentration of 3 µM to 25 % and 5 % respectively. At 3 µM NK-2 there is almost a 30 % reduction in the metabolic cell activity, while LL32 has no visible effect at this concentration. Cells treated either with 10 µM C7A-D21K or melittin no longer show any viability. Likewise, the metabolic activity of cells treated with NK-2 decreases to 10 % at this concentration. In contrast, 10 µM of LL32 reduces the metabolic cell activity to approximately 50 %. NK-2 and LL32 kill all cells at a concentration of 30 µM, with metabolic cell activity down at 0 %. The table shows the peptide concentrations at which cell viability is reduced to 50 % of control (IC_{50}). This reveals an improvement in the derivate C7A-D21K compared to its parent peptide NK-2 with regard to cytotoxicity indicated by the IC_{50} value of C7A-D21K, which is similar to that of melittin. The peptide least effective against the equine sarcoid cells is LL32. No selectivity for the cancerous E 42/02 cells above the APH-R cells could be noticed. The equine skin cells are affected a bit more by the AMPs than the equine sarcoid cells.

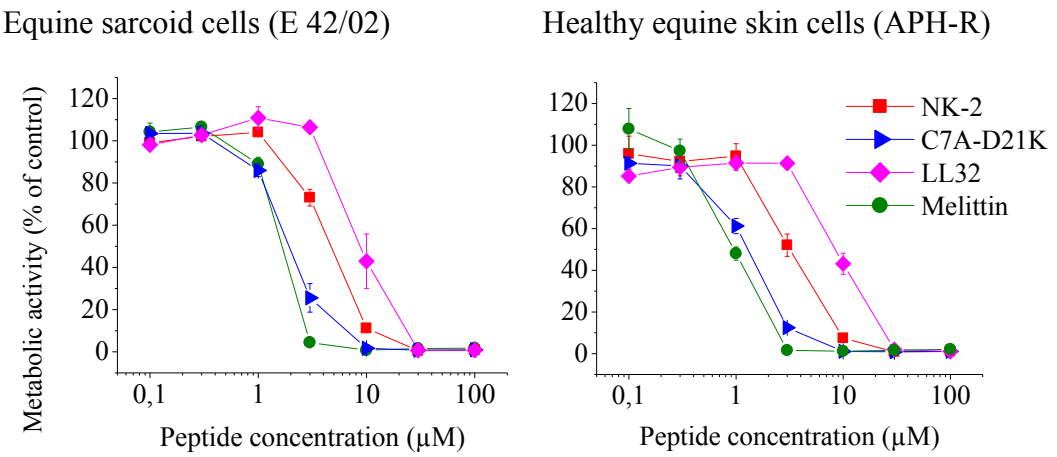

Peptide IC_{50} (µM)	NK-2	C7A-D21K	LL32	Melittin
E 42/02	4.3 ± 0.3	1.9 ± 0.02	≈ 9	1.4 ± 0.1
APH-R	3.2 ± 0.2	1.3 ± 0.02	≈ 10	0.9 ± 0.1

Figure 4-1 Peptide cytotoxicity against equine cell lines

Cytotoxicity of peptides against E 42/02 and APH-R cells was determined by MTT test. Cells (2,5 x 10^4 per well) were incubated with different peptide concentrations (0.1, 0.3, 1, 3, 10, 30 and 100 µM in PBS, pH 7.4, + 10 % $DMEM_{add}$) over 4 h at 37 °C. Viability of cells was measured photometrically. All experiments were done in duplicates (calculating arithmetic means) and were performed at least twice. Depicted are graphical representations of the cytotoxic effects of NK-2 (red filled quartes), C7A-D21K (blue filled triangles), LL32 (magenta filled quarters), and reference peptide melittin (olive filled cicles) against the equine sarcoid and the healthy equine skin cell lines. The table shows IC_{50} values as mean ± SD (µM). The values were derived from titration curves by sigmoidal fitting. IC_{50} values were estimated from curves (≈ values) in cases where fitting was unsuccessful.

The results of the MTT assay do not so far give any indication of the time needed for the peptides to exert cytotoxicity. Thus, a series of tests with incubation times of 30 min, 2, 4 and 24 h was performed with various amounts of peptides diluted in $DMEM_{add}$ instead of PBS + 10 % $DMEM_{add}$. This was done to avoid impairment of cell viability or dying due to lack of nutrients during the 24 h incubation. Results are summarized in Table 4-1.

Table 4-1 Time kinetics of peptide activity

Time-dependent peptide activity against equine sarcoid (E 42/02) and equine skin cells (APH-R) was assessed using the metabolic MTT test. Cells (2,5 x 10^4 per well) were incubated with different peptide concentrations (0.1, 0.3, 1, 3, 10, 30 and 100 µM in $DMEM_{add}$) over 30 min, 2, 4 and 24 h at 37 °C. Viability of cells was measured photometrically. All experiments were done in duplicates (calculating arithmetic means) and were performed at least twice. Shown are IC_{50} values as mean ± SD (µM). The values were derived from titration curves using sigmoidal fitting. IC_{50} values were estimated from curves (≈ values) in cases where fitting was unsuccessful.

Peptide					**Cell line**
IC_{50} (µM)	**30 min**	**2 h**	**4 h**	**24 h**	
NK-2	≈ 70	≈ 53	≈ 50	≈ 39	**E 42/02**
	≈ 67	≈ 58	≈ 53	≈ 45	**APH-R**
C7A	10.6 ± 0.4	13.0 ± 1.0	12.1 ± 1.6	37 ± 4.3	**E 42/02**
	8.9 ± 0.3	11.1 ± 0.3	11.8 ± 1.2	15.0 ± 2.4	**APH-R**
C7A-D21K	8.4 ± 0.2	12.3 ± 2.0	8.3 ± 0.5	12.3 ± 1.0	**E 42/02**
	6.9 ± 0.5	10.9 ± 0.6	10.7 ± 1.0	13.1 ± 1.2	**APH-R**
C7A-Δ	7.5 ± 0.4	13.7 ± 2.0	9.3 ± 1.5	13.1 ± 0.9	**E 42/02**
	6.2 ± 0.2	9.8 ± 0.7	9.4 ± 1.2	12.4 ± 0.9	**APH-R**
NK11	≥ 100	≥ 100	≥ 100	≥ 100	**E 42/02**
	≥ 100	≥ 100	≥ 100	≥ 100	**APH-R**
LL32	≈ 62	≈ 45	≈ 30	≈ 18	**E 42/02**
	≈ 49	≈ 36	≈ 29	≈ 17	**APH-R**
Melittin	3.2 ± 0.06	2.1 ± 0.05	1.8 ± 0.03	1.4 ± 0.04	**E 42/02**
	3.2 ± 0.05	2.6 ± 0.08	2.2 ± 0.07	1.3 ± 0.04	**APH-R**

Regarding the time-dependence of peptide-induced cell-killing, the NK-2 derivates, except the inactive NK11, act on the cells within the first 30 min, while NK-2, LL32, and melittin step up their action over time. C7A shows an unexpected decrease in activity with increasing incubation time, which might be explained by adsorption or slow proteolytic digestion of the AMP. All derivates of NK-2 investigated in these tests, except of inactive NK11, exhibited higher cytotoxic activity than the parent peptide. The substitution of the reactive cysteine residue on position seven by an alanine (C7A) residue improved the IC_{50} value of NK-2 at 4 h incubation time by a factor of four.

When all cysteine/alanine exchange derivates are considered, substitution (C7A-D21K) or deletion (C7A-Δ) of the negatively charged aspartate residue induces a slight increase in activity. Here, LL32 has a slightly higher potency than NK-2. As expected, the reference peptide NK11 is inactive, while melittin shows the highest activity level. Again, there is no selectivity for the equine sarcoid cells beyond those of the equine skin cells.

AMPs, noteably, show a rather low effectiveness in $DMEM_{add}$ (Table 4-1) compared to their values in PBS + 10 % $DMEM_{add}$ (Figure 4-1). NK-2 has a 12-fold lower activity rate against E 42/02 cells in $DMEM_{add}$ than in PBS + 10 % $DMEM_{add}$. Moreover, C7A-D21K and LL32 are less effective with four-fold and three-fold lower activities. Only melittin remains almost unaffected by the different buffers.

To summarize, the results of the MTT assays show that all tested peptides, except inactive NK11, are cytotoxic against equine sarcoid cells but lack selectivity for E 42/02 cells over healthy APH-R. With respect to time taken for killing cells, the main action of the peptides appears to be completed within 30 min. Considerable improvement in effectiveness compared to their parent peptide is seen for all the NK-2 derivates, except NK11. The cytotoxicity of LL32 in pure $DMEM_{add}$ is comparable to that of NK-2, while it is less in PBS + 10 % DMEM. Further, it is noted that peptides show a clearly decreased activity in pure $DMEM_{add}$ compared to PBS + 10 % $DMEM_{add}$.

4.2.2 Peptide-induced membrane permeabilization

Peptide-induced permeabilization of cell membrane was assessed by measuring cellular uptake of a membrane-impermeable DNA-intercalating fluorescent dye, propidium iodide (PI), after the treatment of cells with AMPs. PI-positive cells were distinguished from intact cells using flow cytometry, the higher amounts of PI-positive cells representating greater peptide effectiveness. Membrane permeability is increased in necrotic/apoptotic cells and a change in permeability is also observed with cell exposure to many of the peptides.

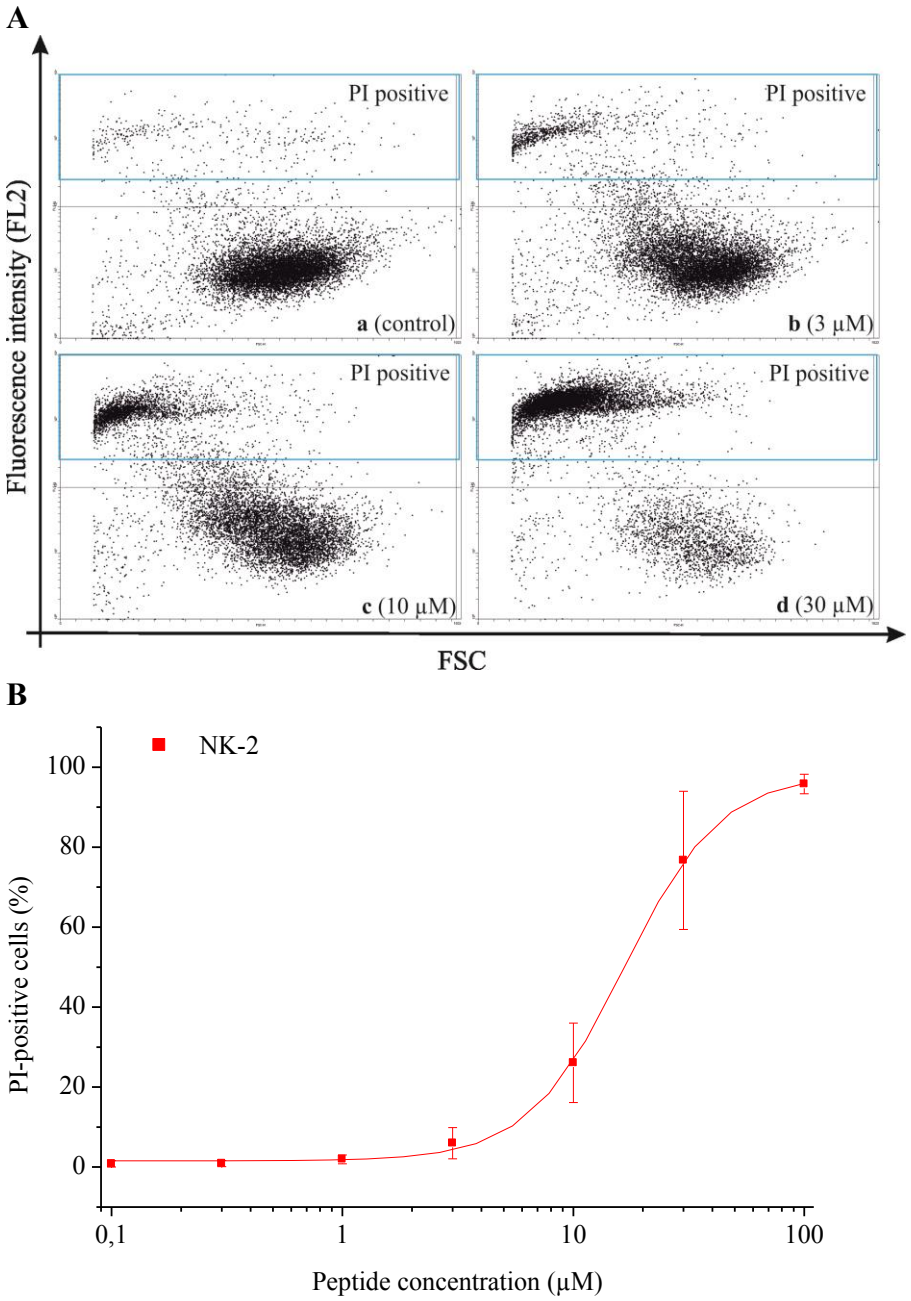

Figure 4-2 NK-2 induced membrane permeabilization of E 42/02 cells

E 42/02 cells, with a density of 2 x 10^5, were incubated in the dark at 37 °C for 30 min with peptide NK-2 (0.1, 0.3, 1, 3, 10, 30 and 100 µM) before adding 0.5 µg propidium iodide (PI). Peptide-induced cell membrane permeabilization was determined by measuring PI-positive cells using flow cytometry. **A** exemplifies the dot plots (FL2 is drawn against FSC) for untreated control cells (a) and cells treated with 3 (b), 10 (c), 30 (d) µM NK-2. Blue rectangles enclose PI-positive cells. **B** depicts sigmoidal fitted curve of NK-2. The percentage of PI-positive cells (%PI) was calculated from the percentage of PI positive cells in buffer alone (PI_b) and in the presence of peptides (PI_{exp}): $\%PI = 100 \times ((PI_{exp}-PI_b)/(100-PI_b))$. Data are shown as mean ± SD of four independent experiments.

Figure 4-2 shows dot plots from experiments with NK-2 against E 42/02 cells where the PI fluorescence intensity of the cells is plotted against the cell size (FSC). Dot plots represent untreated control cells and cells treated with various NK-2 concentrations (3, 10 and 30 µM). Most PI-positive cells are in the cell population treated with 30 µM NK-2, shown by the cell accumulation in the left upper corner. Only few intact cells can be found here in the control cell range. With decreasing NK-2 concentration, the PI-positive cell group becomes smaller, while the amount of fluorescent-negative intact cells increases. Only a few PI-positive cells remain at 3 µM NK-2 concentration. The left shift of PI-positive cells indicates a decreasing cell size caused by the leaking of the cells owing to loss of membrane integrity. Graph B plots the percentage of PI-positive cells against peptide concentrations and shows the sigmoidal-fitted curve of NK-2, indicating the effectiveness of this peptide.

For an easier comparison of the effectiveness of the various peptides, Table 4-2 shows EC_{50} values. They indicate the peptide concentrations at which 50 % of the cells are PI-positive, i.e. the concentrations that give the peptide 50 % of its maximal effectiveness.

As shown in Table 4-2, all seven AMPs were tested against E 42/02 and APH-R cells at various concentrations. All peptides, barring the inactive NK11, changed the membrane permeability of both cell lines. Again, the newly designed variants were found to have greater potency than their parent peptide, NK-2. Here, C7A is with an EC_{50} of 6.8 µM, the most effective one against E 42/02 cells, and even more effective than melittin. The lowest efficacies are observed for NK-2 and LL32 with no selectivity for the E 42/02 sarcoid cells. Here, the peptides affected the APH-R cells more than their cancerous counterparts.

Table 4-2 Peptide-induced membrane permeabilization of equine cells

E 42/02 and APH-R cells, with a density of 2 x 10^5, were incubated in the dark at 37 °C for 30 min with peptides (0.1, 0.3, 1, 3, 10, 30 and 100 µM) before adding 0.5 µg PI. Peptide-induced cell membrane permeabilization was determined by measuring PI-positive cells with a FACSCalibur. The percentage of PI-positive cells (%PI) was calculated from the percentage of PI-positive cells in buffer alone (PI_b) and in the presence of peptides (PI_{exp}): $\%PI = 100 \times ((PI_{exp}-PI_b)/(100-PI_b))$. Experiments were done two (APH-R) to four (E 42/02) times and in duplicates (mean values were calculated) and data is presented as mean ± SD. The data was derived from sigmoidally fitted titration curves.

Peptide	E42/02 EC_{50} (µM)	APH-R EC_{50} (µM)
NK-2	16.6 ± 0.6	6.6 ± 0.4
C7A	6.8 ± 0.4	5.7 ± 0.7
C7A-D21K	13.7 ± 0.9	4.1 ± 0.3
C7A-delta	12.6 ± 0.7	8.1 ± 0.3
NK11	>> 100	>> 100
LL32	17.8 ± 2.1	16.5 ± 0.6
Melittin	12.7 ± 0.2	5.0 ± 0.4

NK-2 induced killing of E 42/02 cells was also monitored by confocal laser scanning fluorescence microscopy. Cells were seeded on microscopic slides and monitored in an unfixed, viable state, while incubated with the membrane impermeable DNA-intercalating fluorescent dye Sytox® green and various concentrations of NK-2 and NK11. Here, both peptides were labelled with the fluorophor rhodamine (Rh-NK-2, Rh-NK11). As shown in Figure 4-3 the addition of 1 µM Rh-NK-2 (D-F) caused a pale red seam at the cells that was visible already after a few minutes. Individual cells were killed by membrane permeabilization, indicated by Sytox® green influx. The number of dead cells did not increase significantly over the incubation time of up to 60 min. Addition of 3 µM of Rh-NK-2 (G-I) caused immediately a red seam at the cells. After a few minutes, first cells were permeabilized and after 30 min approximately two thirds of cells were Sytox® green positive. Here, also the staining of intracellular membranes by the peptide could be observed as well as the influx of the peptide into the nucleus. The latter was indicated by bright yellow fluorescence as a result of the mixture of red and green fluorescence. The addition of 5 µM Rh-NK-2 (J-L), caused cell

permeabilization within 1 min and almost all cells were killed within minutes. Bleb formation could be observed for several cells. In contrast to NK-2, the non-cytotoxic peptide NK11, showed only a marginal binding to the cell surface. This was expressed in a scarcely apparent red stain (not shown) and not followed by membrane passage of Sytox® green. Here, cellular morphology was indistinguishable to control cells.

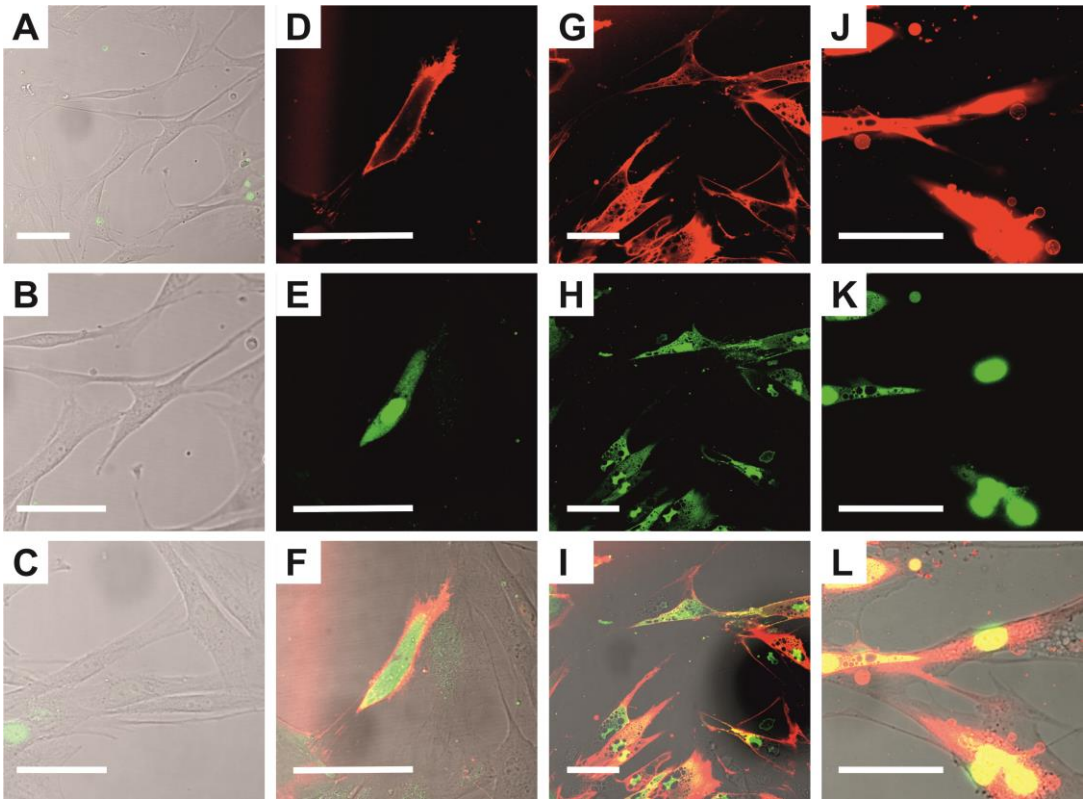

Figure 4-3 NK-2 binding to E 42/02 cells and subsequent cell lysis

NK-2-induced binding and cell-membrane permeabilization of E 42/02 cells were visualised by confocal fluorescence microscopy. The figure shows representative images. Cells were incubated in buffer with membrane-impermeable dye Sytox® green (green fluorescence) and three concentrations of rodamin-labelled (Rh) NK-2 (red fluorescence). (D-F) 1 µM for 13 min; (G-I) 3 µM for 6 min; (J-L) 5 µM for 6 min. Red channel and green channel are presented in the upper (B, F, J) and middle row (D, G, J) respectively. Bottom row (F, I, L) represents an overlay of brightfield, green and red channel. Untreated (control) cells (A, B, C) are shown as brightfield channel. Experiments were performed once (1 µM and 3 µM) or twice (5 µM). Scale bar = 50 µm.

To summarize, the investigation into peptide-induced membrane permeabilization confirmed that NK-2 derivates had improved potency compared to their parent peptide, with C7A being the most effective against E 42/02 cells. But selectivity for cancerous cells over healthy cells was found to be lacking. The anti-cancer cell activity of LL32 was similar to that of NK-2. Confocal fluorescence microscopy was used to visualize membrane permeabilization by NK-2 which occured very fast and was accompanied by morphological changes in the form of cell membrane blebbing.

4.2.3 Peptide-induced modulation of cell metabolism and morphology

To get a deeper insight into peptide-induced changes in cell metabolism and morphology, a chip-based sensor was used to monitor acidification and oxygen consumption rates as well as cell adhesion (impedance) in real time over extended time periods. Cells were routinely flushed for 4 h with pure Bionas running medium (BRM with 1 mM HEPES, pH 7.4, 4.5 g/l glucose, 0.1 % FCS, 100 U/ml penicillin and 100 µg/ml streptomycin) to adapt them to the system, establish constant metabolic rates and morphology prior to initiating a 12 h peptide treatment. This was followed by flushing the cells again for 4 h with pure BRM to monitor any cell recovery. To obtain a zero baseline for the metabolic and morphology values, cells were killed ultimately with triton X-100.

Additionally, absolute metabolic values of untreated cells were calculated from the raw acidification and respiration data of metabolic biosensor experiments. Each biosensor is equipped with five sensors measuring the acidification rate and five measuring the oxygen consumption. Thus, five data for acidification and for respiration were displayed by each chip. During “stop” phases, acidification and oxygen consumption rates increased because of cell metabolism and decreased during “go” phases due to fresh medium inflow. As the slopes of the curves vary, two representative curves out of five were chosen for each value. Then, the difference of the maximum to the lowest points of one representative peak of each curve was taken and the two values were averaged, each for acidification and oxygen consumption. For this, stop phases shortly before the addition of the compound were chosen, because the cells by then had already adapted to the new conditions, and probably showed their normal metabolism. It must be noted that the adhesive PC-3 and HaCaT cells might be more or less concentrated (seeded with

2 x 10^5 cells per chip and incubated for 24 h) than the immobilized E 42/02 and APH-R cells (4 x 10^5). Since the embedment of the equine cells could influence the metabolic value, the metabolic activity of the tested human and equine cells should be considered separately.

Table 4-3 Cells' absolute values of acidification and oxygen consumption rates/4 min

Absolute metabolic values of the cells were gathered from experiments with the Bionas® 1500[2] analyzing system at the end of the first 4 h BRM flow using the raw data curves for acidification and oxygen consumption. For both metabolic values, the difference of the maximum to the lowest point of two peaks, which arise during the 4 min stop-phase, was calculated. Then, out of several experiments, arithmetic means for absolute values of acidification rate (ISFET) and oxygen consumption (Clark) were calculated for the different cell lines. Impedance (IDES) values represent the arithmetic mean of the measured impedance at the beginning of the experiments. Besides values from experiments with the generally used sensor head (200 µm), values from experiments with a smaller sensor head (50 µm) are shown. The number (n) of evaluated experiments represents the number of bio modules (two biomodules per each independent experiment). Measuring the impedance of E 42/02 and APH-R cells was non applicable (n.a.).

Cell line	IDES (nF)	ISFET (V)	Clark (nA)	n
Sensor head 200 µm				
PC-3	23.1 ± 3.7	0.021 ± 0.003	0.162 ± 0.1	74
HaCaT	10.6 ± 2.4	0.015 ± 0.002	0.154 ± 0	10
E 42/02	n.a.	0.018 ± 0.01	0.411 ± 0.3	10
APH-R	n.a.	0.018 ± 0.003	0.593 ± 0.2	10
Sensor head 50 µm				
PC-3	20.9 ± 3.3	0.042 ± 0.01	0.363 ± 0.1	4
E 42/02	n.a.	0.019 ± 0.001	1.025 ± 0.2	2
APH-R	n.a.	0.02	1.238 ± 0.2	4

The absolute metabolic values of the different cells are shown in Table 4-3. Experiments with a smaller sensor head were only performed with PC-3, E 42/02, and APH-R cells. A comparison of PC-3 and HaCaT cell values, measured with the 200 µm sensor head, revealed a remarkable difference in impedance. The impedance of HaCaT cells is more than 50 % lower than that of PC-3 cells. The metabolic rates of HaCaT

cells are also slightly lower than that of PC-3 cells. The equine cell values show no difference in the acidification rates, but E 42/02 cells have a lower respiration rate than their healthy counterparts. All values double when cell lines are compared among each other by using the lower sensor head with the exception of the acidification rates for both equine cell lines which remains the same. Nevertheless, the 50 µm sensor head improves the measurement of metabolic rates and should, therefore, be considered for all cells with a low metabolism.

NK-2 and the three derivates C7A, C7A-D21K, and C7A-Δ were tested against PC-3 cells using the chip-based sensor to investigate the effects of the peptides on metabolism and morphology of this cancer cell line. It was also intended to determine if the NK-2 derivates possessed greater effectiveness against PC-3 cells compared to their parent peptide as it had been shown for the equine sarcoid cells using MTT assays and flow cytometry. Again, peptide melittin was used as positive control.
The effectiveness of 10 µM of NK-2 and three of its derivates on PC-3 cells is depicted in Figure 4-4. The effects of peptide treatment become evident almost immediately after the addition of peptides resulting in an immediate increase of impedance and oxygen consumption (left arrow in the graphics), and an immediate decrease followed by an increase in acidification. These reactions could be considered as the attempt by the cells to counteract the deleterious effects of the peptides, resulting in morphological changes to tighter cell-to-cell contacts, cell flattening, and enhanced metabolic rates. Against PC-3 cells, the derivate with a substitution of the cysteine residue on position seven to alanine (C7A) exhibit no visible potency improvement compared to the parent peptide NK-2. The medium acidification and the oxygen consumption are similar. NK-2, in fact, causes more morphologic reaction by increasing the impedance by more than what is achieved by C7A. Only the additional substitution (C7A-D21K) or deletion (C7A-delta) of the aspartate residue on position 21 of C7A improved peptide effectiveness against PC-3 cells. The one showing the maximum improvement is C7A-D21K, which, with 10 µM, nearly matches the activity of 3 µM melittin. No cell recovery, which would have been indicated by the metabolic rates and impedance returning to the initial values during the BRM flow after peptide treatment, was observed.

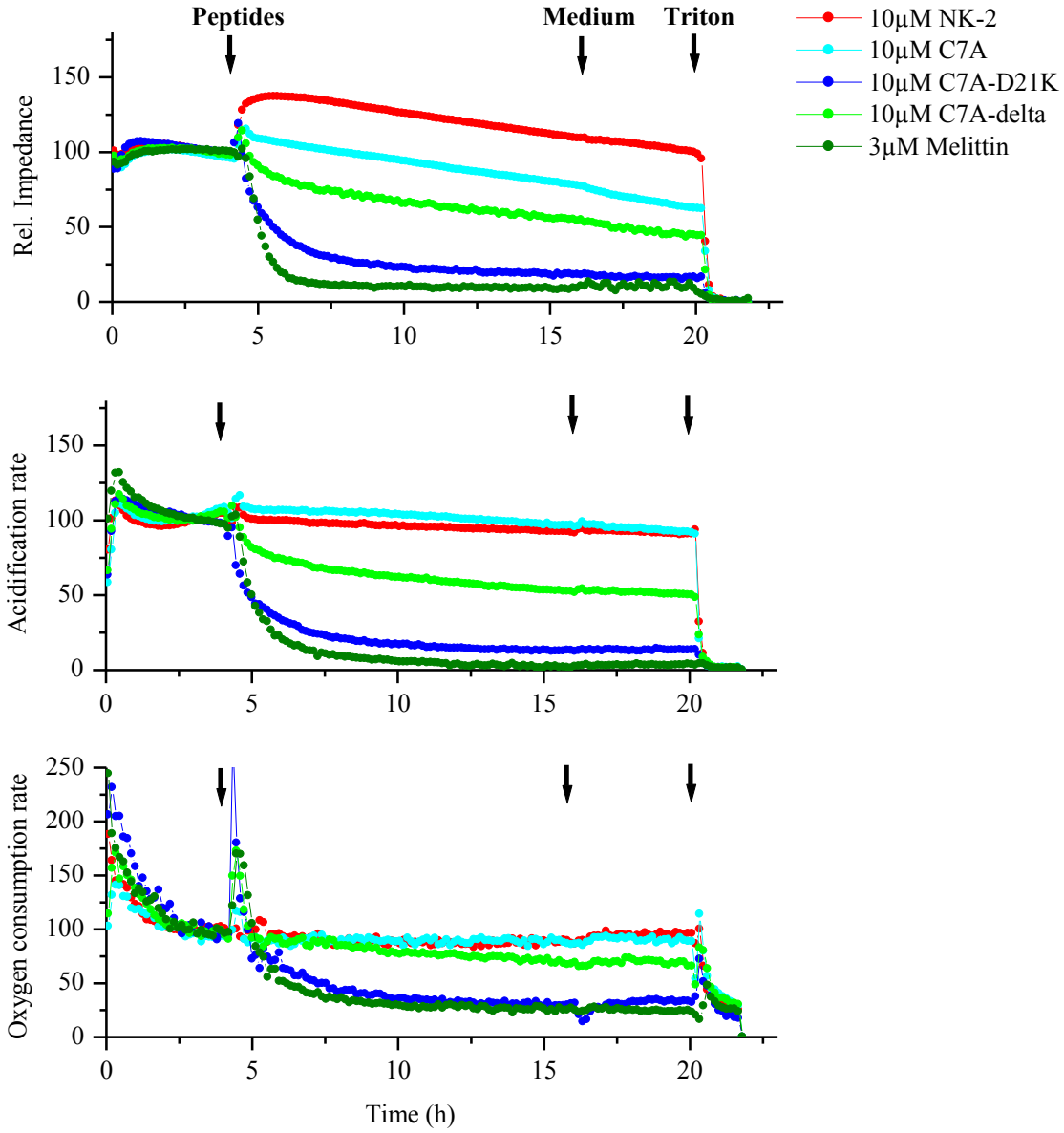

Figure 4-4 Impact of sequence modification on peptide effectiveness

The Bionas® 1500[2] analyzing system was used for metabolic biosensor monitoring of peptide treatment on PC-3 cells to compare the effectiveness of NK-2 and some of its derivates. Cells (2 x 10^5) were grown adherently on biosensor-chips and after an initial 4 h BRM flow were treated for 12 h with peptides (time between left and middle arrow), followed by another 4 h BRM flow and final cell lysis by triton X-100 (right arrow). Depicted are 10 µM of NK-2 (red), C7A (cyan), C7A-D21K (blue), and C7A-delta (green). For each peptide, two to three independent experiments were done. Morphologic (impedance) and metabolic values (acidification and oxygen consumption rate) are represented by their arithmetic means. As reference 3 µM melittin (olive) was used.

To point out the improvement of the effective derivate C7A-D21K compared to its parent peptide NK-2, Figure 4-5 shows the impedance, acidification, and respiration of PC-3 cells exposed to different concentrations of NK-2 and C7A-D21K.

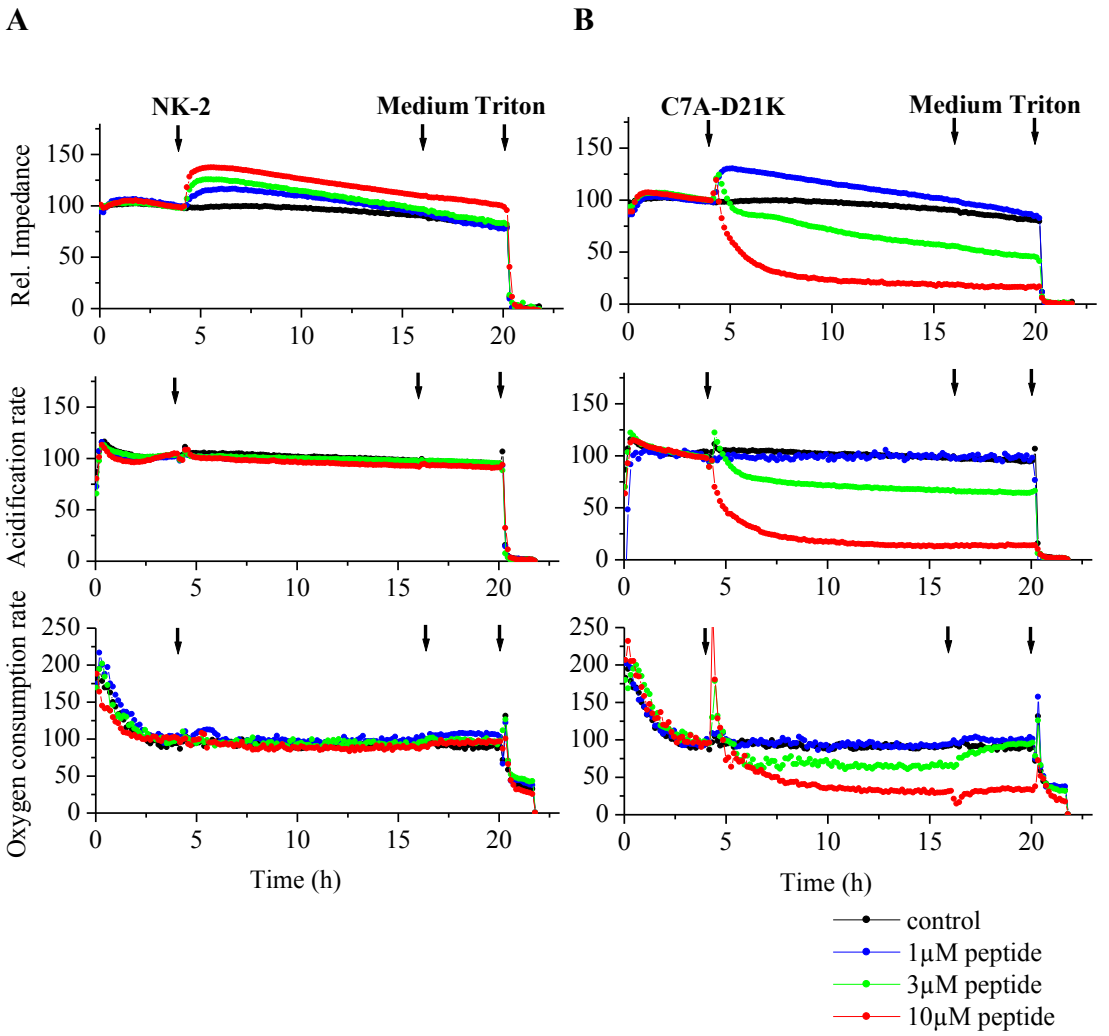

Figure 4-5 PC-3 cell response to NK-2 and C7A-D21K treatment

Depicted is the response of PC-3 cells to treatment with peptides NK-2 (**A**) and C7A-D21K (**B**), measured in real-time with the Bionas® 1500[2] analyzing system. Cells (2 x 10^5) were grown adherently on biosensor-chips and after an initial 4 h BRM flow were treated for 12 h with peptides (time between left and middle arrow), followed by another 4 h BRM flow and final cell lysis by triton X-100 (right arrow). Peptides were used in different concentrations: 1 (blue), 3 (green) and 10 (red) µM. For each concentration, two to three independent experiments were done which are presented by their arithmetic means. Black curves represent untreated control cells.

Cells react immediately to the addition of peptides except in case of the oxygen consumption rate, which is not influenced by the shown NK-2 concentrations. All NK-2 concentrations induce increased impedance across the entire peptide treatment, indicating changes in cell morphology towards a denser cell layer in response to cell stress. Conversely, as little as 3 µM of C7A-D21K decreases the impedance by 50 %, which might be considered compatible with the beginning of cell detachment. Detached dead cells are observed at 10 µM. Perfusion with parent peptide NK-2 has only minor effects on the metabolic acidification and respiration rates. On the contrary, C7A-D21K shows a significant potency improvement indicated by a decrease in both metabolic values at a concentration of 3 µM and cell killing at 10 µM. After the first cell activation through the peptides, impedance and oxygen consumption rates either decrease to control cells level or reach even lower levels compatible with the first signs of cell death. Only a minimal recovery could be observed in the oxygen consumption rate of cells treated with 3 µM C7A-D21K. For PC-3 cells, cell impedance was the most sensitive value, already showing morphologic changes while metabolic parameters remained stable.

Since C7A-D21K showed the strongest activity against PC-3 cells among all the NK-2 derivates, this peptide was further tested for its selectivity of cancerous cells. Therefore, the effectiveness of 3 and 10 µM of C7A-D21K was monitored by the metabolic biosensor not only against PC-3 cells but also against HaCaT cells, a spontaneously transfered human keratinocyte cell line (Figure 4-6).

At the two tested concentration levels, 3 and 10 µM, C7A-D21K shows different influences on the impedance of both cell lines. The morphology of HaCaT cells is comparatively less influenced at both concentrations than that of PC-3 cells. While HaCaT cells show an increase in impedance at 3 µM, a slight decrease is observed at 10 µM. PC-3 cell impedance decreases at 3 µM and cells detach almost completely from the chip surface at 10 µM of C7A-D21K. Acidification rates of HaCaT cells at 3 µM show a greater decline than that of PC-3 cells, but in accordance to the control cells, while the rates of both cell lines go down equally to almost zero at 10 µM peptide concentration. Oxygen consumption rates also decrease for both cell lines but with a greater decline for PC-3 cells. Thus, it can be said that C7A-D21K affects HaCaT cells also but is comparatively more active against cancerous PC-3 cells than against healthy HaCaT cells.

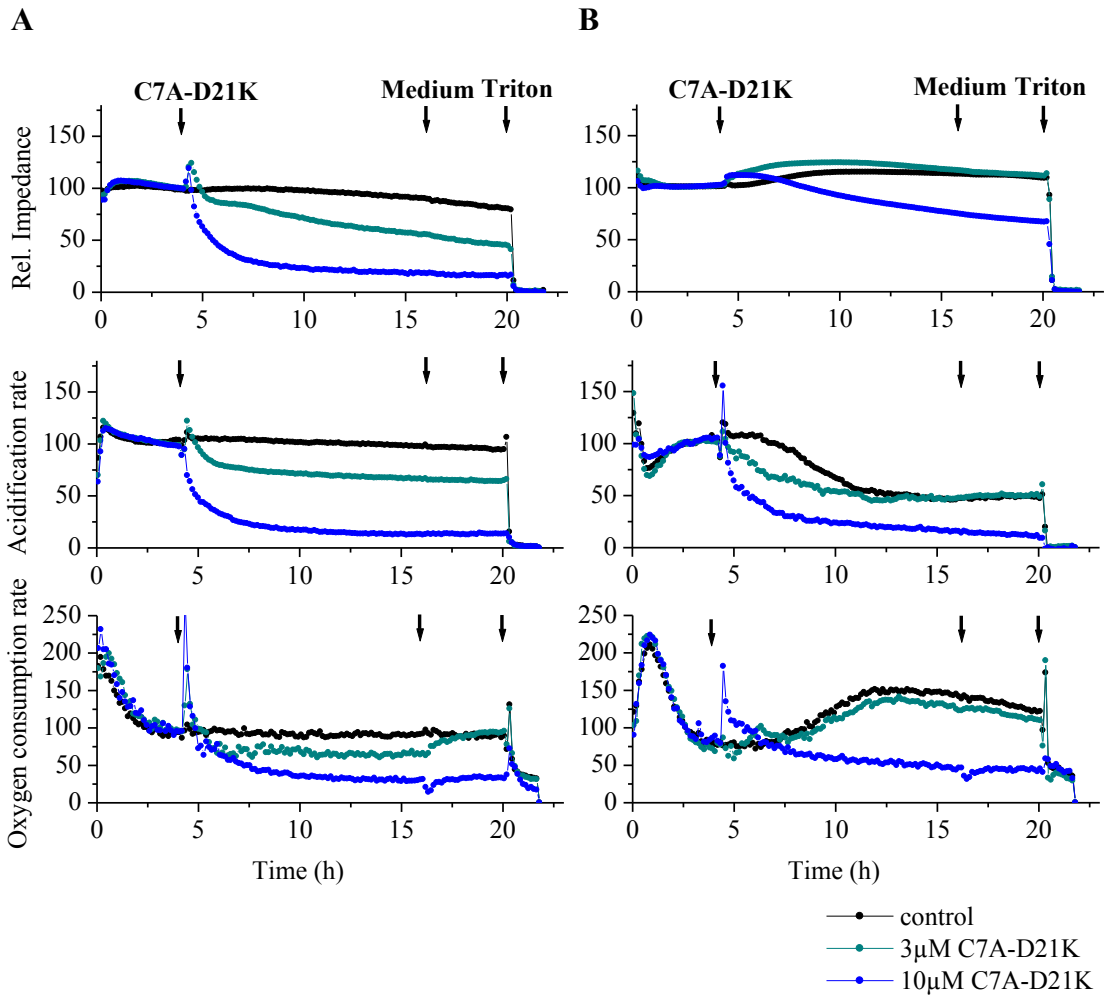

Figure 4-6 Peptide activity on cancerous PC-3 and healthy HaCaT cells

PC-3 (**A**) and HaCaT (**B**) cells were treated with 3 (dark cyan) and 10 (blue) µM C7A-D21K using the Bionas® 1500[2] analyzing system to determine peptide selectivity against cancerous cells. Cells (2 x 10^5) were grown adherently on biosensor-chips and after an initial 4 h BRM flow were treated for 12 h with peptide (time between left and middle arrow), followed by another 4 h BRM flow and final cell lysis by triton X-100 (right arrow). For both cell lines two independent experiments were done. The graph

The effectiveness of NK-2, C7A-D21K and melittin against both equine cell lines was determined also by metabolic biosensor measurements. As the equine cells did not grow adherently on the sensor chips, they had to be embedded in agarose. Hence, the measurement of impedance was not possible; only the metabolic rates could be observed for both equine cell lines (Figure 4-7).

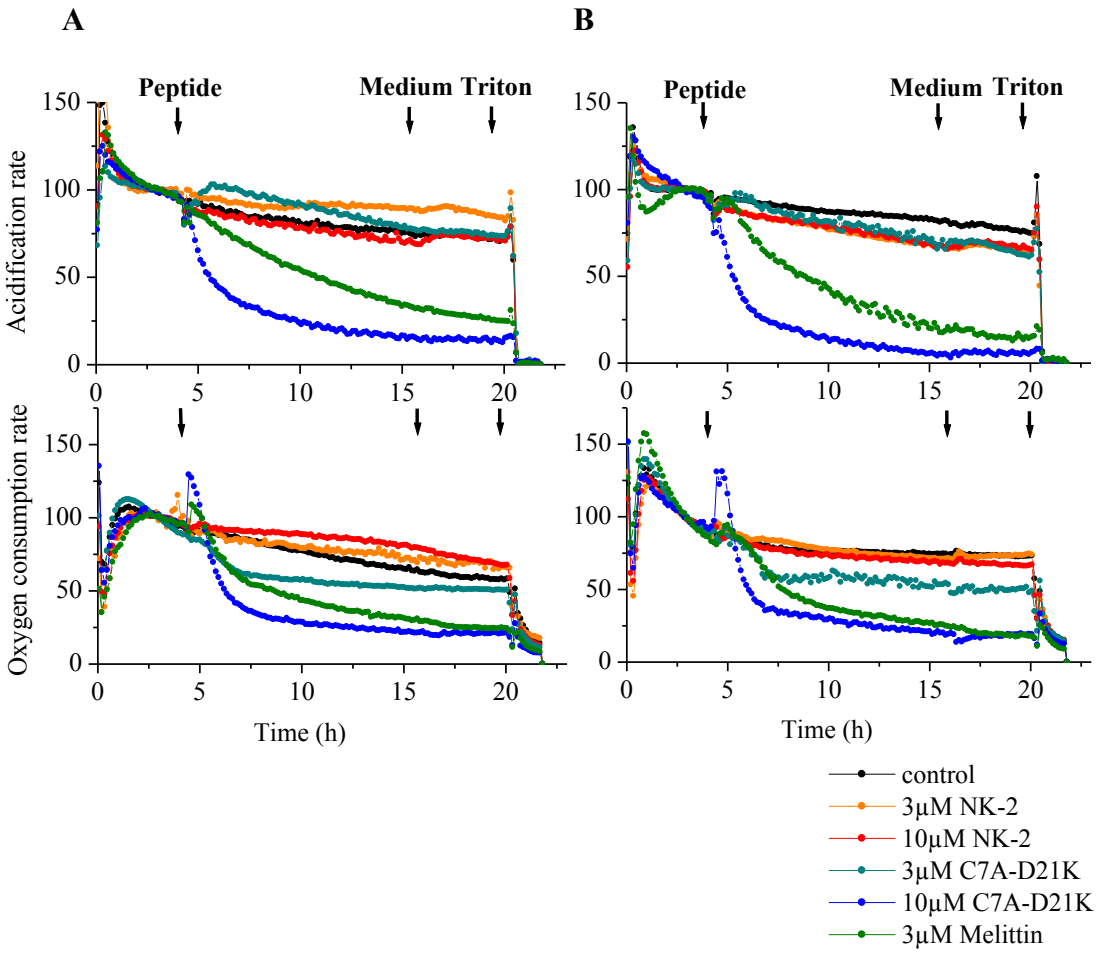

Figure 4-7 E 42/02 and APH-R cell response to peptide treatment

E 42/02 (**A**) and APH-R (**B**) cells were treated with peptides NK-2 and C7A-D21K and metabolic cell responses were measured in real-time with the Bionas® 1500[2] analyzing system. Agarose embedded cells were brought on biosensor-chips and after an initial 4 h BRM flow were treated for 12 h (left to middle arrow) with peptides, followed by another 4 h BRM flow and final cell lysis by triton X-100 (right arrow). Because of the cell embedment impedance measurement was not possible. Peptides were used in different concentrations: 3 µM (orange) and 10 µM (red) NK-2, 3 µM (dark cyan) and 10 µM (blue) C7A-D21K. Olive curves represent 3 µM of reference peptide melittin, black curves untreated control cells. For the different concentrations of each peptide, two to three independent experiments were done which are presented by their arithmetic means.

Here, C7A-D21K again shows improved potency compared to NK-2. The acidification rate of E 42/02 cells is affected only minimally by 3 and 10 µM NK-2 and 3 µM C7A-D21K, while 10 µM C7A-D21K leads to a steep decline to near zero. Reference peptide melittin induces, at 3 µM, a decrease in both metabolic values. The acidification continued to fall after a change to pure BRM flow, indicating non-reversible cell

damage. The oxygen consumption rate is marginally increased by both NK-2 concentrations. C7A-D21K decreases the respiration rate of E 42/02 cells to nearly 50 % (3 µM) and to 25 % (10 µM) respectively. Melittin has a flatter curve than 10 µM C7A-D21K but, in the end, goes down to the same level. Again, no selectivity for the sarcoid cells above the skin cells is visible. Like the PC-3 cells, both equine cell lines react immediately to peptide treatment.

In view of a possible drug development, online experiments were performed with repeated short-duration peptide treatment on PC-3 cells. It was aimed at determining if short treatments with peptides had any cumulative effect. For this, peptide C7A-D21K, the most effective NK-2 derivate against PC-3 cells, was selected. Cells were treated five times for 32 min with either 3 or 10 µM C7A-D21K. Between the treatments, 2 (3 µM) to 6 (10 µM) h pure BRM flow were conducted. This intermediate BRM flow was extended to the 10 µM treatment to monitor cell responses over a longer period of time.

Figure 4-8 shows that, unexpectedly, 3 µM as well as 10 µM of C7A-D21K had almost no influence on both metabolic values during repeated treatments of 32 min. Only impedance clearly increased at 3 µM and slowly decreased at 10 µM, indicating a cell reaction due to peptide treatment. However, for the latter, no recovery of cell impedance was visible during the final 4 h pure BRM flow. Obviously, the 32 min treatment was not sufficient here for inducing fatal cell damage, although this incubation time was enough for peptide-induced cell killing in MTT assays. A possible reason could be the loss of peptide activity under full medium condition, as documented earlier. In order to review this, the medium for online monitoring was adjusted from BRM to PBS with 10 % BRM.

Indeed, now the results from the MTT assays could be confirmed (Figure 4-9). NK-2 (10 µM) in pure BRM induces an impedance increase but has almost no effect on both metabolic values, indicating only a minimal attack on cell integrity. The same concentration of NK-2 in PBS + 10 % BRM results in a slow, two-step decrease of impedance, a complete halt to acidification after 5 h of treatment, and a first steep increase of the oxygen consumption with subsequent decrease. All in all, same NK-2 concentrations induce, in pure medium, only minor reactions among treated cells, while in PBS + 10 % medium cells lose contact with each other, ceasing their aerobe and

anaerobe metabolism. At first, there is a clear increase in oxygen consumption, indicating a high energy demand. It subsequently decreases, probably due to the lack of metabolites for ATP synthesis and progressive cell damage. At this point, the impedance shows its second drop with acidification stopping completely.

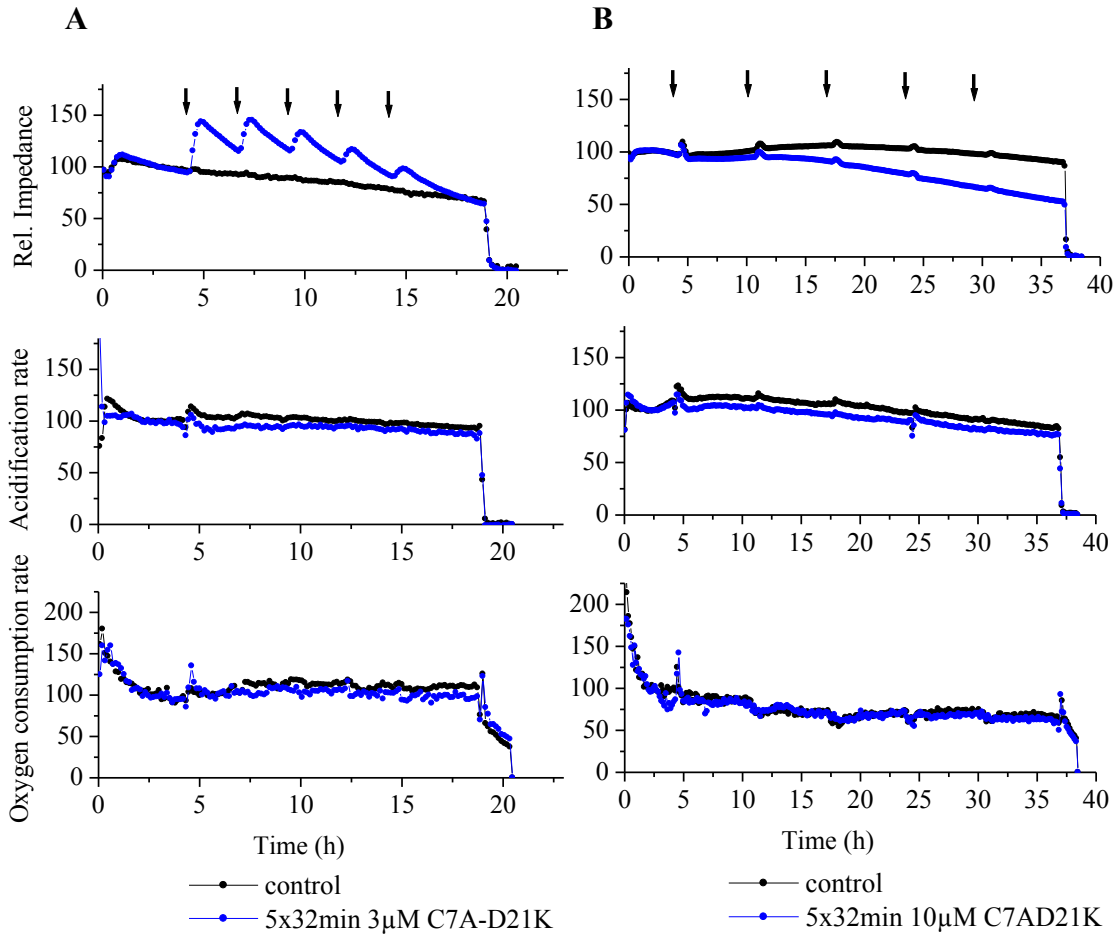

Figure 4-8 Repeated short-duration peptide treatment on PC-3 cells

The effect of repeated short-duration peptide treatment on PC-3 cells was tested using the Bionas® 1500[2] analyzing system. Cells were grown adherently on biosensor-chips and after an initial 4 h BRM flow were treated five times for 32 min with C7A-D21K (blue curves). **A**: 3 µM with 2 h BRM flow in between; **B**: 10 µM with 6 h BRM flow in between. Peptide treatment is indicated by arrows. After the last treatment another 4 h BRM flow followed before final cell lysis by triton X-100. Untreated control cells are represented by the black curves. For each approach, two independent experiments were done; their arithmetic means are depicted.

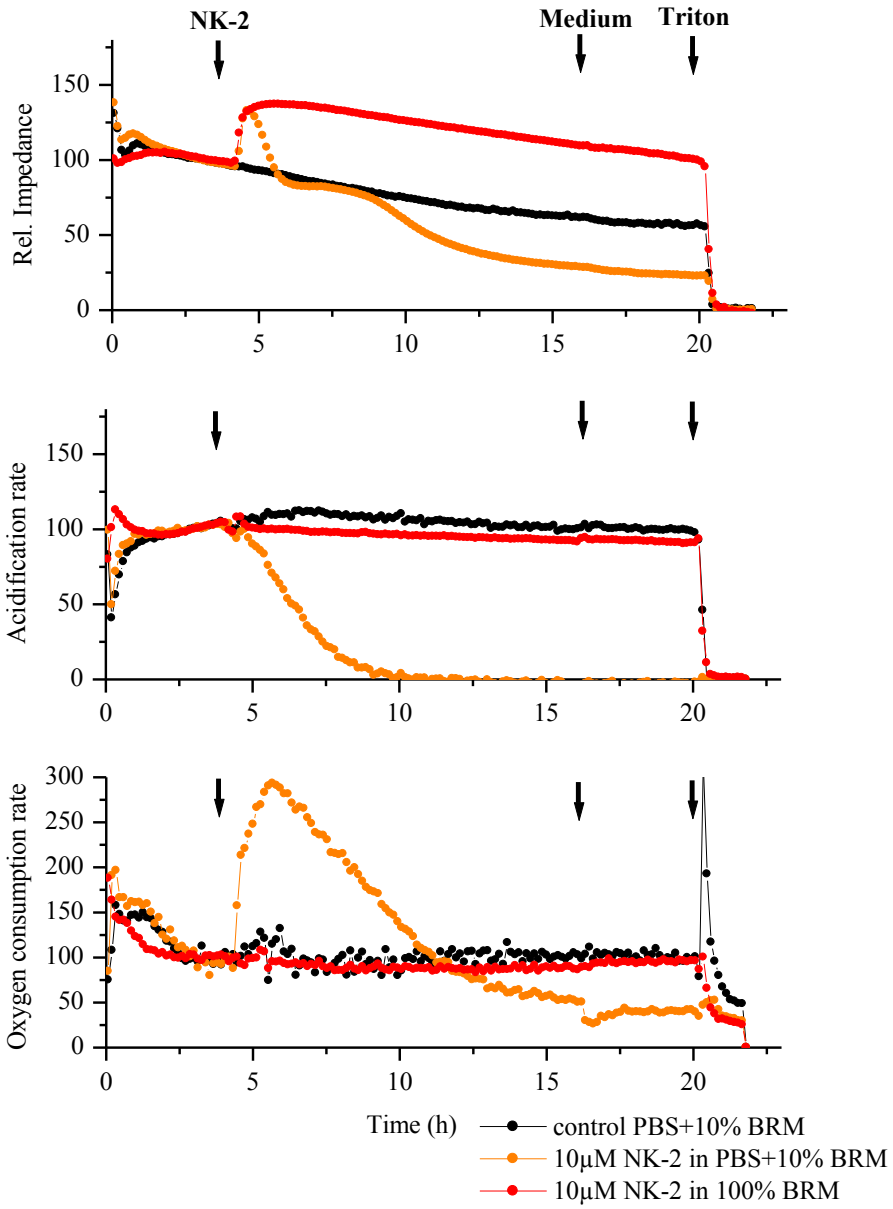

Figure 4-9 Peptide activity in PBS + 10 % BRM compared with 100 % BRM

Online measurements of PC-3 cell response to peptide treatment in PBS + 10 % BRM and 100 % BRM, respectively, were done with the Bionas® 1500[2] analyzing system. After an initial 4 h BRM flow, cells were treated with 10 µM NK-2 for 12 h (time between left and middle arrow), followed by another 4 h BRM flow and final cell lysis by triton X-100 (right arrow). Depicted are the values for cell impedance, acidification and oxygen consumption for cells in PBS + 10 % BRM (orange curves) and 100 % BRM (red curves). Four independent experiments were done; the graphic represents their arithmetic means.

To summarize, metabolic biosensor experiments confirmed a potency improvement in C7A-D21K compared to NK-2 on E 42/02 cells. All three derivates were tested on PC-3 cells but only derivates C7A-D21K and C7A-Δ were found to induce a higher cell

response than NK-2, while C7A showed an activity very similar to its parent peptide. Again, no peptide selectivity for the equine sarcoid cells over the equine skin cells was visible, but PC-3 cells were more affected by C7A-D21K than healthy HaCaT cells. The activity loss of peptides in complete medium detected in the MTT assays has also been confirmed by experiments with the metabolic biosensor. This might be the reason for the ineffective 32 min treatment (which was done in pure BRM), although MTT tests indicated that peptide activity was almost complete after 30 min of incubation.

These real-time experiments document, in particular, metabolic and morphologic cell responses to cell-affecting compounds even without fatal cell damage. Immediate stress reactions of the cells to added peptide, indicated by an increase of impedance and oxygen values but without permanent cell damage, could be seen. Besides, it was possible to compare the metabolic activity of different cell lines by monitoring the metabolic rates of untreated cells. For cells with a low metabolism, the device could be fitted with a lower sensor head, increasing its sensitivity to changes in medium ingredients.

4.3 Impact of different cell surface structures on peptide activity

As there are different negatively charged structures on cell surfaces, investigations were done to determine if any one of them is essential for the activity of the cationic AMPs. In this study, three different anionic membrane surface components were investigated for their impact on peptide activity. Phospatidylserine (PS) was one prominent candidate because of its evidently increased content on several cancer cell surfaces [34], [46]. Moreover, inhibitory effects of two anionic carbohydrate structures were tested to determine the impact of sulphated glycostructures like chondroitin sulphate (CS) and neuraminic acids like N-acetylneuraminic acid (NANA) on peptide activity. Further investigations were done with focus mainly on neuraminic acids to compare peptide effectiveness on desialylated and untreated cells using different approaches. One approach included an extensive deglycosylation of the cell surface by enzymatic cell treatment.

4.3.1 Impact of PS on peptide activity

As anionic PS is suspected to be one of the possible targets for AMPs on cancer cells, initial testing involved the determination of relative amounts of PS on the surface of different cells using flow cytometry. The binding of a PS-specific antibody and Annexin V was used for PS detection. Both the cancerous and healthy cell lines were tested for postulated higher PS content on the surface of cancer cells [34], [46].

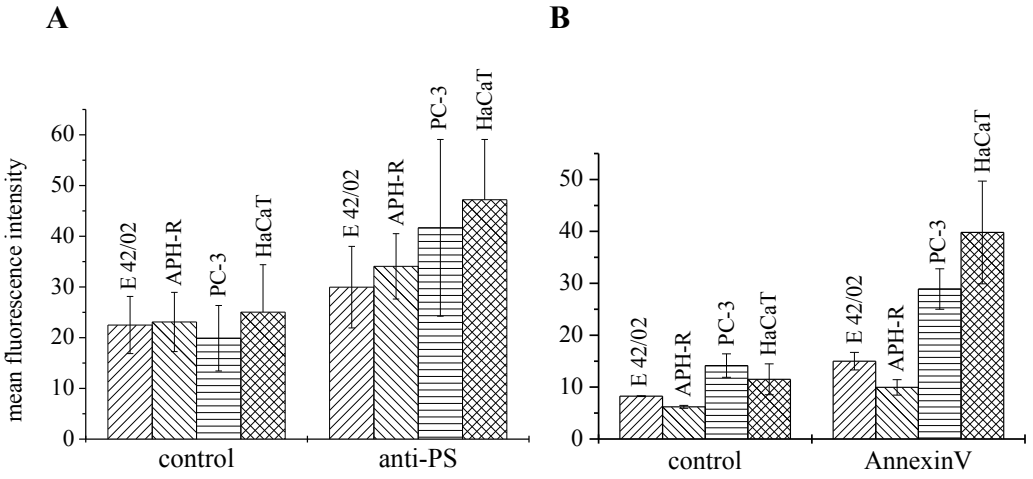

C

Fluorescence intensity increase	E 42/02	APH-R	PC-3	HaCaT
Anti-PS	7.47	10.97	21.77	22.17
AnnexinV	6.75	3.75	14.75	28.3

Figure 4-10 Determination of the PS content on cell surfaces

The PS content on cell surfaces of the different cell lines was investigated by flow cytometry. Cells (2×10^5) were incubated either with (**A**) 0.05 µg of mouse monoclonal anti-PS antibody for 60 min, followed by 30 min incubation with 0.2 µg goat anti-mouse IgG-A647, or with (**B**) 0.05 µg FITC Annexin V for 15 min, respectively. All experiments with anti-PS antibody were done at least three (for PC-3 cells four) times; experiments with Annexin V were done twice. Diagrams depict respective mean fluorescence intensities for stained and unstained E 42/02, APH-R, PC-3, and HaCaT cells. **C** shows the specific increase of fluorescence intensity calculated by subtracting the mean fluorescence intensites of respective control cells from the fluorescence intensities of cells incubated with anti-PS antibody or Annexin V.

As depicted in Figure 4-10, the accessible membrane PS content varies, depending on the binding substance, while the ratio of the PS content of the different cell lines stays mainly the same. Using the anti-PS antibody, the highest PS content was detected on the surface of HaCaT cells, followed by PC-3 cells. A lesser presence of PS was seen on the surfaces of both equine cells. It should be mentioned that for PC-3 cells, the value of one anti-PS experiment was removed because a test by Graf-Henning showed this value to be an outliner. In this outliner test, a value is identified to be so when it is beyond the range of the mean value ± 3 times standard deviation. Annexin V, which is highly specific for PS, also bound mainly on HaCaT cell surfaces, followed by PC-3 cell surfaces. Again, the equine cells had only a very low PS content on their outer cell membranes. The table shows the individual increases in fluorescence intensities of the different cell lines after adding anti-PS antibody or Annexin V respectively. This shows that the anti-PS antibody detected a larger amount of PS on the surface of the APH-R cells than on the cancerous E 42/02, while PC-3 and HaCaT cells show a similar PS content on their surfaces. Using Annexin V for PS detection E 42/02 cells show a higher PS content than APH-R cells, and the PS content on HaCaT cells is nearly doubled compared to PC-3 cells. These results do not show the expected PS content, as there was no significant higher surface PS amount detected on cancerous cells than on healthy cells.

The PI-uptake of peptide-treated cells was also measured to determine the involvement of cell surface PS as peptide-target structure. Therefore, PC-3 cells were first incubated with an anti-PS antibody to occupy PS on the cell surface and, thereby, inhibit a possible NK-2 binding on PS. Control cells without anti-PS antibody incubation served as reference. Then, both cell groups were treated with various NK-2 concentrations.
Figure 4-11 clearly shows that the PI-uptake for the anti-PS antibody treated and untreated cells is the same, negating any PS role in membrane targeting of PC-3 cells by NK-2. Otherwise, covering of PS by its antibody should have lead to decreased NK-2 activity. Successful antibody binding to PC-3 cells was shown in Figure 4-10.

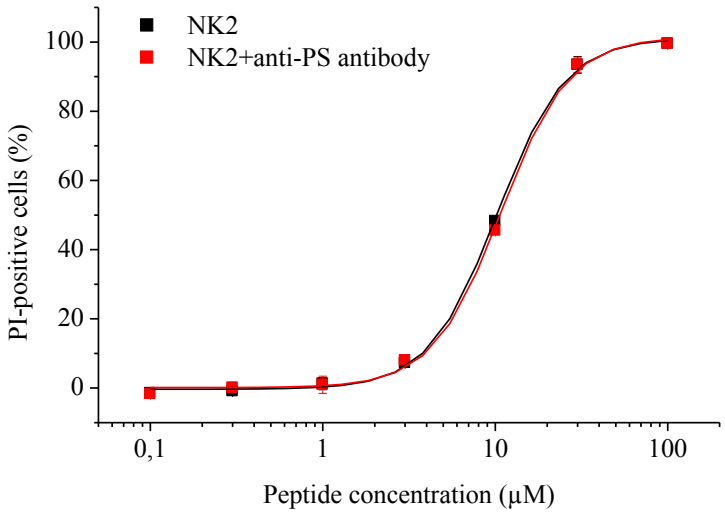

Figure 4-11 Anti-PS antibody impact on NK-2 activity

Flow cytometry was used to clarify whether previous cell incubation with an anti-PS antibody has an influence on the effectiveness of NK-2. PC-3 cells (2 x 10^5) were either incubated with (red trace) or without (black trace) 0.05 µg of mouse monoclonal anti-PS antibody for 1 h in the dark at room temperature. Following peptide addition (0.1, 0.3, 1, 3, 10, 30 and 100 µM in PBS, pH 7.4) cell suspensions were incubated for another 30 min at 37 °C. NK-2 activity was assessed by adding 0.5 µg PI and measuring PI-positive cells with a FACSCalibur. Data is shown as mean ± SD of two independently conducted experiments.

Another PI-uptake assay was performed by adding PC/PS (90/10) liposomes to cell suspensions to determine a possible role of PS in membrane targeting by AMPs. PC-3 cells were incubated with different concentrations of liposomes, and 10 µM of NK-2, C7A-D21K, LL32 or 5 µM of melittin. A lower melittin concentration was chosen due to its higher potency. If PS were a peptide target, a decreased cell membrane permeabilization could be expected with increasing liposome concentration.

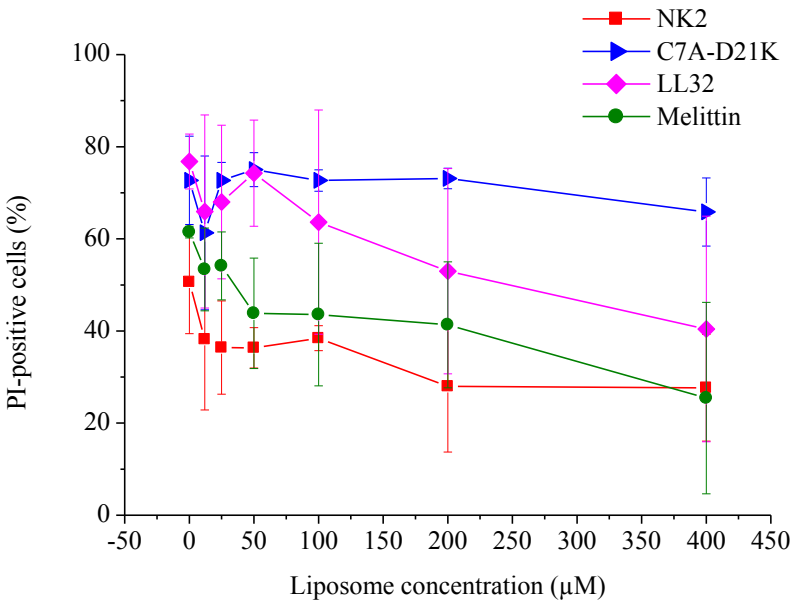

Figure 4-12 Peptide activity on cells in the presence of PC/PS (90/10) liposomes

The impact of the presence of PS containing lipid layers on the activity of peptides was determined using flow cytometry. To PC-3 cells (2 x 10^5) different concentrations of liposomes (12, 25, 50, 100, 200 and 400 µM in PBS, pH 7.4) were added, subsequently followed by addition of either NK-2 (10 µM; red trace), C7A-D21K (10 µM, blue trace), LL32 (10 µM, magenta trace) or melittin (5 µM, olive trace). These suspensions were incubated for 30 min in the dark at 37 °C. Proof of peptide activity was made by adding 0.5 µg PI and measuring PI-positive cells with a FACSCalibur. All experiments were done in duplicates (arithmetic mean values were calculated) and performed three times. The graph depicts the % of PI-positive cells on different liposome concentrations for NK-2, C7A-D21K, LL32 and melittin.

Figure 4-12 shows that the activity of melittin and LL32 clearly decreased with increasing liposome concentration. Yet, the effects of liposomes on NK-2 and, especially, C7A-D21K activities were minimal. This points to distinct cell membrane-targeting by melittin and LL32 compared to NK-2 and its variant. Interestingly, LL32 had a much higher activity than in the previous experiments, being as effective here as C7A-D21K at low liposome concentrations. Figure 4-13 shows representative dot plots of cells treated with C7A-D21K and melittin.

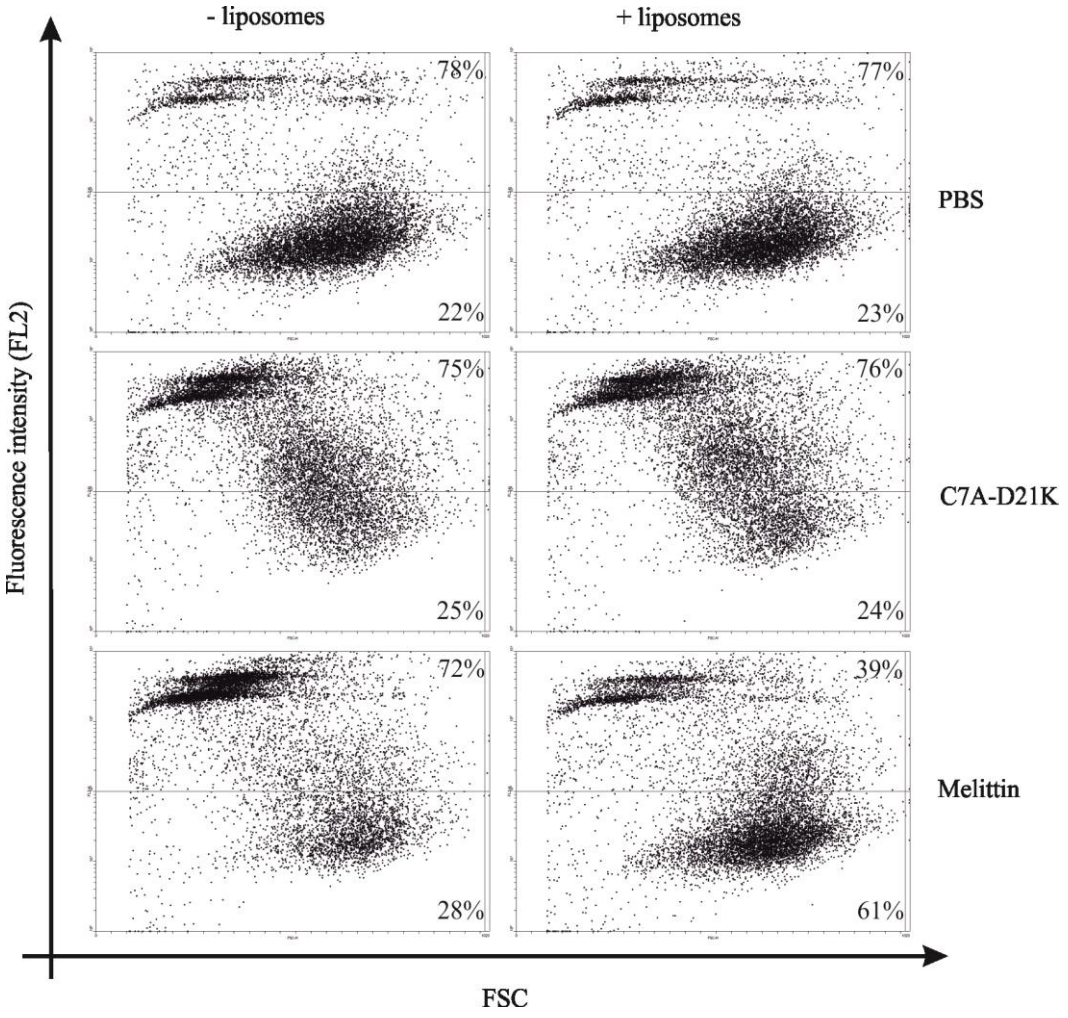

Figure 4-13 Membrane permeabilization by peptides in the presence of liposomes

The figure shows exemplary dot plots belonging to Figure 4-12 which depict the impact of the presence of PS containing lipid layers on the activity of peptides. Shown are the dot plots out of one experiment of untreated PC-3 cells and PC-3 cells treated with 10 µM C7A-D21K with and without 400 µM liposomes as well as 5 µM melittin with and without 400 µM liposomes. A line was drawn above the intact cells to distinguish them from dead cells. The percentage values specify the amount of cells in the two areas.

To summarize, the results for NK-2 and PS as its target structure are somewhat contradictory. The occupation of the anionic membrane lipid PS by an anti-PS antibody had no influence on the effectiveness of NK-2, while the approach with PS-containing liposomes confirmed NK-2 interaction with this phospholipid. The liposomes had a concentration-dependent inhibitory effect also on peptides LL32 and melittin against PC-3 cells, but peptide C7A-D21K was almost unaffected, pointing to different target preferences of individual peptides.

4.3.2 Impact of anionic carbohydrates on peptide activity

The relevance of cellular surface anionic carbohydrates on *in vitro* cytotoxicity of peptides against PC-3, E 42/02, and APH-R cells was first determined using the metabolic MTT assay. As representative glycostructures chondroitin sulfate (CS), N-acetylneuraminic acid (NANA), the more complex fetuin (FE), a sialic acid containing glycoprotein, and its desialylated counterpart asialofetuin (AFE) were chosen. To analyze their inhibitory effects on peptide activity, 10 µg of each of these compounds was added to the cells just before the peptide was added.

Table 4-4 Impact of different cell surface glycostructures on peptide cytotoxicity

Cytotoxicity of peptides against E 42/02, APH-R and PC-3 cells in the absence and presence of chondroitin sulphate (CS) and N-acetylneuraminic acid (NANA) was assessed by the metabolic MTT test after an incubation of 4 h at 37°C with peptide dilution series of 0.1, 0.3, 1, 3, 10, 30 and 100 µM in PBS, pH 7.4, + 10 % $DMEM_{add}$. Against PC-3 cells also inhibitory effects of fetuin (FE) and asialofetuin (AFE) were tested in accordance with the above. Viability of cells was measured photometrically. All experiments were done in duplicates (calculating arithmetic means) and were performed at least twice. Depicted are IC_{50} values as mean ± SD (µM). These values were derived from sigmoidal fits of titration curves. IC_{50} values were estimated from curves (≈ values) in cases where fitting was unsuccessful. None of the used inhibitors alone had any influence on the viability of the cells. Inhibition of C7A-D21K by FE and AFE was not done (n.d.).

Peptid					**Cell line**
IC_{50} (µM)	**NK-2**	**C7A-D21K**	**LL32**	**Melittin**	
PBS	2.9 ± 0.1	1.1 ± 0.01	6.6 ± 0.5	1.1 ± 0.01	E 42/02
with CS	≈ 28	4.5 ± 0.9	≈ 70	2.1 ± 0.2	E 42/02
with NANA	≈ 3	1.2 ± 0	6.4 ± 0.4	1.4 ± 0.02	E 42/02
PBS	3.9 ± 0.3	1.2 ± 0.02	9.6 ± 0.3	1.4 ± 0.01	APH-R
with CS	≈ 38	5.8 ± 0.5	≈ 90	2.4 ± 0.1	APH-R
with NANA	4.4 ± 0.5	1.4 ± 0.1	9.8 ± 0.3	1.8 ± 0.1	APH-R
PBS	3.0 ± 0.1	1.8 ± 0.05	15.8 ± 0.6	1.2 ± 0.04	PC-3
with CS	≈ 55	13.5 ± 2.3	≈ 100	2.6 ± 0.1	PC-3
with NANA	3.6 ± 0.5	1.9 ± 0.1	14.8 ±1.1	1.6 ± 0.2	PC-3
with FE	3.4 ± 0.7	n.d.	≈ 19	0.9 ± 0.05	PC-3
with AFE	6.6 ± 1.3	n.d.	≈ 20	1.4 ± 0.05	PC-3

Here, again, an improved activity of C7A-D21K compared to its parent peptide NK-2 is shown (Table 4-4). LL32 has the lowest effectiveness of the tested peptides, while melittin and C7A-D21K both cause a similar high weakening of metabolic cell activity. The different compounds added show various influences on the peptides. The activity of NK-2 and LL32 is clearly impaired against all three cell lines in the presence of CS, showing the highest effect on PC-3 cells. The activity of C7A-D21K is also inhibited by CS, but on a lesser degree. Cytotoxicity of melittin is only minimally influenced. The addition of NANA and fetuin has no measurable inhibitory effect on the activity of all the peptides while the desialylated asialofetuin slightly reduces the activity of NK-2.

Sialic acids, a common part on cell surfaces, have been shown to influence peptide activity [51], [53]. To further determine the influence of sialic acids on the activity of the in this study tested AMPs different experiments were performed with untreated and desialylated cells. Desialylation of cells was achieved by neuraminidase treatment, thereby cutting off all terminal sialic acids on the cell surface. As pre-testing for these experiments, the enzymatic activity of neuraminidase was proven on both equine cell lines by flow cytometry. For this, cells were incubated with four biotinylated lectins with different carbohydrate binding specificities and fluorescently labelled streptavidin, with high fluorescence intensity indicating high lectin binding.

Figure 4-14 shows a pronounced binding of SNA and a lower, but clear, binding of WGA and MAL II to both untreated equine cell lines. MALII and SNA exhibit high specificity for terminal sialic acids, while WGA binds to NeuNAc (a residue of N-acetylneuraminic acid) and GlcNAc. Owing to its affinity for non-sialylated O-glycans, almost no binding could be seen for PNA. After neuraminidase treatment of cells, the binding of SNA, MALII and WGA was reduced 5, 13 and 1.3 fold on E 42/02 cells, and 3, 9 and 1.2 fold on APH-R cells. The lesser decrease for WGA binding to the desialylated cells may have been caused by its residual binding capacity to GlcNAc, which is not removed by the neuraminidase. The binding of PNA was enhanced 18 (E42/02) and 10 fold (APH-R) respectively. These results confirmed a successful desialylation of the cells.

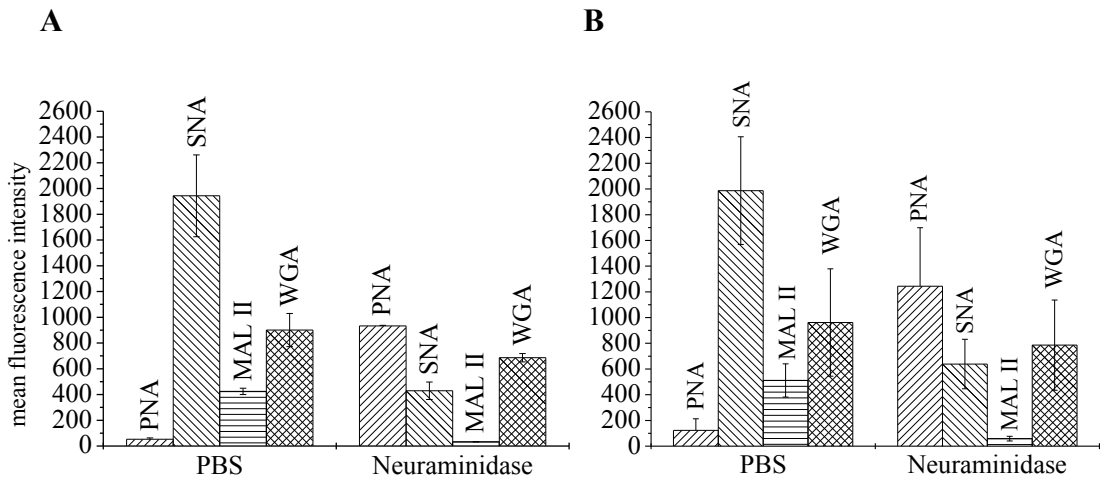

C

Binding of lectins after neuraminidase treatment	PNA	SNA	MAL II	WGA
E 42/02	+ 1664 %	- 78 %	- 92 %	- 24 %
APH-R	+ 913 %	- 68 %	- 88 %	- 18 %

Figure 4-14 Effect of cell desialylation on lectin binding

E 42/02 (**A**) and APH-R (**B**) cells were treated with 0.1 U neuraminidase or PBS for 2 h at room temperature. Then 2 x 10^5 cells were incubated with 10 µg of biotinylated lectins (PNA, SNA, MAL II or WGA, respectively) for 30 min at 4 °C. Proof of desialylation was done by adding 0.2 µg biotin-binding streptavidin-A633 for another 30 min at 4 °C. Experiments were done twice in duplicates. The mean fluorescence intensity for all cells is shown. **C** shows the percentage change of lectin binding after neuramindase treatment of cells.

To determine the impact of terminal sialic acids on cell surfaces for peptide activity, three different experimental setups were performed. Cell surface sialic acids were removed by neuraminidase treatment to subsequently compare peptide effectiveness on untreated and desialylated cells. Then peptide effectiveness was tested on untreated and desialylated cells using fluorescence microscopy, flow cytometry, and a chip-based biosensor. Additionally, the significance of various terminal carbohydrates on cell surfaces was also tested by fluorescence microscopy. Using N-glycosidase, carbohydrate residues from glycopeptides and glycoproteins of the outer cell membrane were removed.

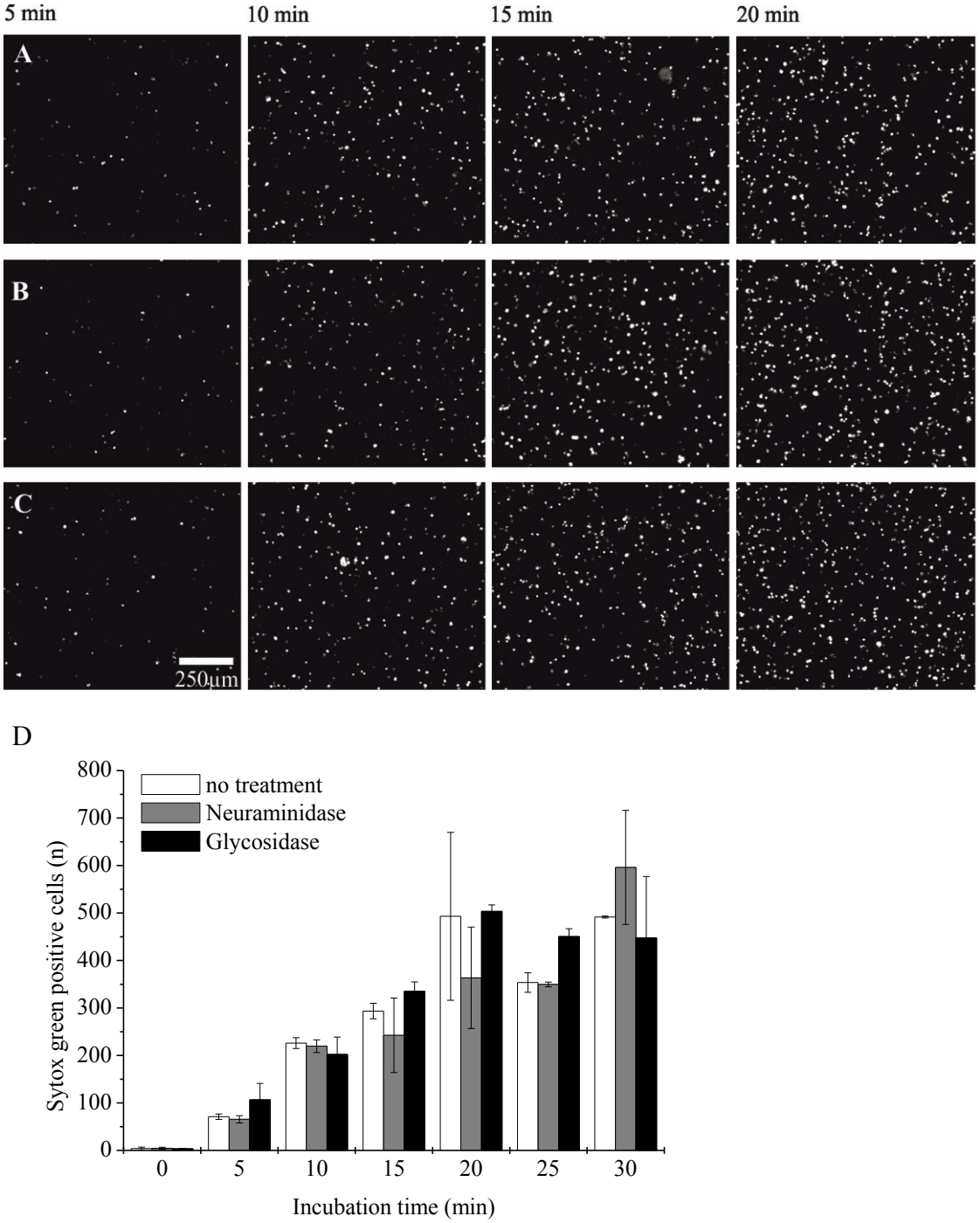

Figure 4-15 Impact of enzymatic cell pre-treatment on NK-2 activity

Activity of 3 µM NK-2 was determined over time on differently pre-treated PC-3 cells using fluorescence microscopy. Peptide-induced membrane damage was indicated by uptake of membrane impermeable DNA-intercalating dye Sytox® green (5 µg per well) by compromised cells. Two wells (4 x 10^5 cells per well) were either pre-treated with 0.1 U neuraminidase (**B**) or 0.1 U glycosidase F (**C**). Untreated cells serve as control (**A**). **A-C** show representative fluorescence pictures of one experiment. In total two independent experiments were performed. Scale bar is the same for all images. For quantitative evaluation of NK-2 activity the number of fluorescence-positive cells was determined using ImageJ software and the arithmetic mean of both experiments was calculated (**D**) to compare the effect of neuraminidase (grey bars) or glycosidase F (black bars) cell pre-treatment to the control (white bars).

Peptide-induced cell killing and time kinetics of cell death were investigated using fluorescence microscopy to compare the effectiveness of 3 µM NK-2 on adherent untreated, desialylated and deglycosylated PC-3 cells. Membrane permeabilization was visualized by PC-3 cell uptake of DNA-intercalating fluorescent dye Sytox® green. The onset of peptide effect was shown by cell dye uptake over time. Figure 4-15 shows that the first cell damages occure within 5 min, indicating a fast killing effect of NK-2, nearly completed after 20 min. The amount of fluorescence-positive cells is more or less the same at different times for all three cell groups (Figure 4-15 D). Hence, the impact of sialic acids and other carbohydrates on the activity of peptide NK-2 cannot be shown here. It should be mentioned that the same cell area had not been monitored over time, and that might have resulted in slight differences in the total cell count of the evaluated images.

Further, peptide-induced membrane permeabilization of untreated and desialylated E 42/02 and APH-R cells was determined by cell uptake of DNA-intercalating dye propidium iodide (PI) using flow cytometry (Table 4-5).

Table 4-5 Peptide induced membrane permeability of control and desialylated cells

Flow cytometry was used to compare the efficacy of the peptides on untreated and desialylated cells. Both equine cell lines were incubated either with or without 0.1 U neuraminidase in PBS, pH 7.4, for 2 h in the dark at room temperature. Then, cells (2 x 10^5) were incubated 30 min with peptides (0.1, 0.3, 1, 3, 10, 30 and 100 µM in PBS) before adding 0.5 µg PI. Control was performed by cell incubation with the highest according TFA concentration in PBS. Peptide induced cell membrane permeabilization was determined by measuring PI-positive cells with a FACSCalibur. Experiments with APH-R cells, NK-2 and melittin were done three times in duplicates; all others were done twice and in duplicates (calculating arithmetic mean values). Given are the peptide concentrations at which 50 % of the cells were PI-positive (EC_{50}). The data derived from sigmoidally fitted titration curves.

Peptide EC_{50} (µM)	E 42/02 untreated	E4 2/02 neuraminidase	APH-R untreated	APH-R neuraminidase
NK-2	5.8 ± 0.7	7.5 ± 1.1	7.3 ± 0.5	8.9 ± 0.7
C7A-D21K	3.3 ± 0.8	3.7 ± 0.5	5.6 ± 0.2	7.2 ± 0.7
LL32	12.8 ± 1.5	11.3 ± 0.9	12.7 ± 0.8	11.9 ± 1.1
Melittin	3.6 ± 0.7	3.6 ± 0.5	4.4 ± 0.3	4.1 ± 0.3

A comparison of the EC_{50} values reveals that NK-2 activity is minimally affected by desialylation of both cell lines. This is the same for the activity of C7A-D21K against APH-R cells but not against E 42/02 cells. Activity of LL32 and melittin is not affected by this enzymatic cell treatment. Thus, a minor influence of cell desialylation on NK-2 and C7A-D21K activity is shown here.

Effectiveness of 10 µM NK-2 was also tested on untreated and desialylated PC-3 cells adherently grown on biosensor chips. Peptide activity was monitored in real-time with regard to cell layer impedance and cell metabolism.
Figure 4-16 shows an immediate cell response to peptide treatment with an increase of impedance, respiration and acidification rates. Further, in contrast to untreated cells, desialylated cells show a slight decrease in cell impedance, indicating loosened cell-to-cell contact or adhesion to the chip surface. Desialylated and control cells show no significant differences in both monitored metabolic rates during NK-2 perfusion.

To sum up, the sulphated glycosaminoglycan (CS) is shown to be an effective inhibitor of peptide activity, while a sialic acid (NANA) and a sialylated protein (FE) have almost no visible effects. Further, cell desialylation has only a minor influence on the effectiveness of NK-2 and its derivate C7A-D21K against E 42/02 and APH-R cells, indicated by a slightly decreased peptide activity. Desialylated PC-3 cells respond to peptide treatment with slightly higher morphologic changes than the control cells. The metabolic cell rates are not affected by PC-3 cell desialylation. All in all, there is no significant decrease in peptide activity after the removal of cell-surface sialic acids, as should be expected if they were involved in prime peptide targeting. But the deglycosylation of PC-3 cells by glycosidase F, too, has no visible effect on peptide activity, though the proof of successful deglycosylation is pending.

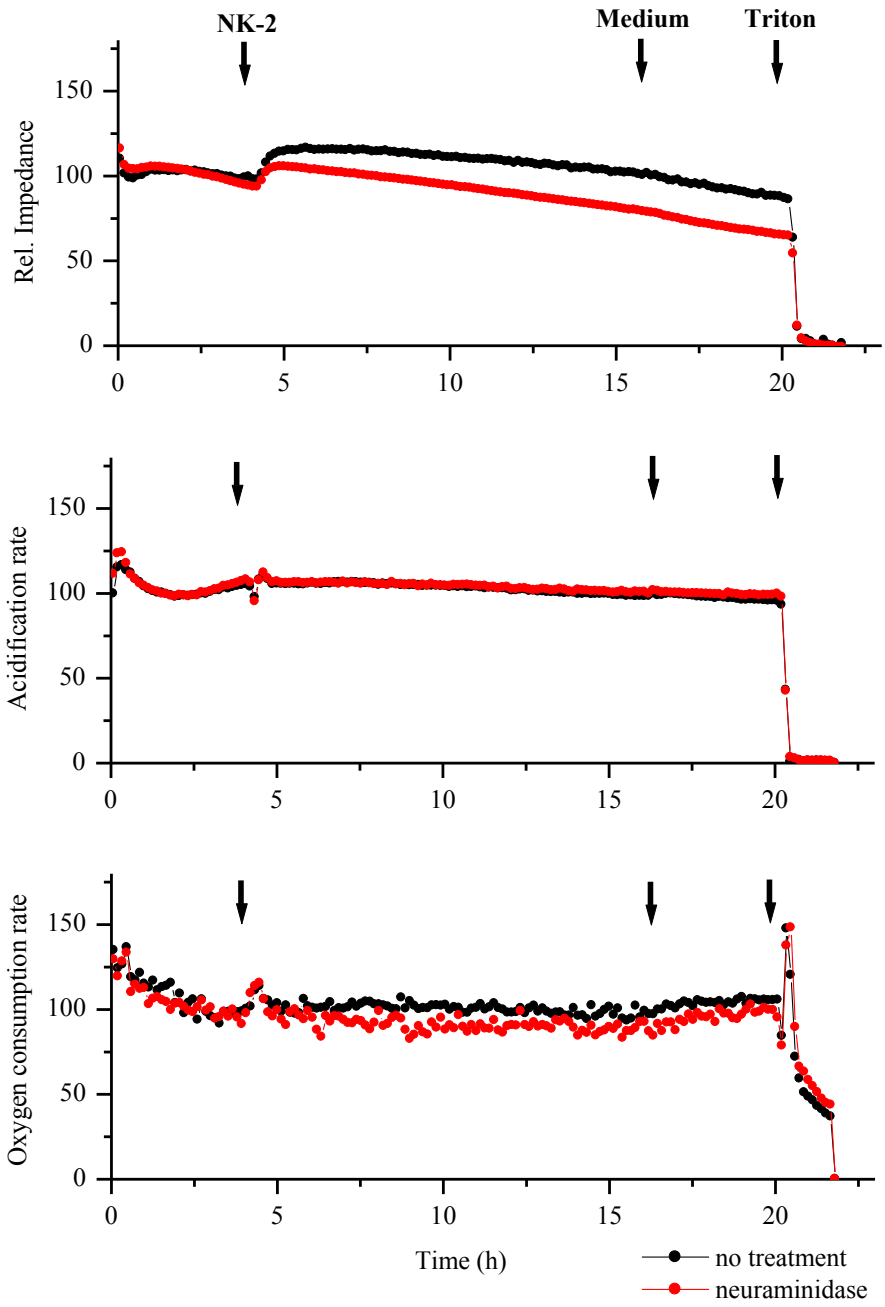

Figure 4-16 Impact of cell pre-treatment with neuraminidase on peptide activity

On biosensor-chips adherently grown PC-3 cells were pre-treated with 0.1 U neuraminidase over 2 h at 37 °C. Not pre-treated, but under the same conditions incubated cells served as control to compare peptide effectiveness on cell surfaces with (red) and without (black) sialic acids. After an initial 4 h BRM flow, cells were treated with 10 µM NK-2 for 12 h (time between left and middle arrow), followed by another 4 h BRM flow and final cell lysis by triton X-100 (right arrow). Depicted are the values for cell impedance, acidification and oxygen consumption of the surrounding medium. Four independent experiments were done which are represented by their arithmetic means.

4.3.3 Analysis of the cell surface charge of equine E 42/02 and APH-R cells

It is assumed that the cationic AMPs target cancer cells via increased anionic surface structures on these cells, thus distinguishing them from healthy cells with an almost zwitterionic surface. As, in this study, peptides showed no selectivity for the equine cancer cell line over the respective healthy cell line the Zeta potential of these cells was measured. The Zeta potential indicates the accessible surface charge of a particle, here the cell surface. It varies with the surface charge density of a particle/cell and is calculated by the electrophoretic mobility of this particle in an electric field. The higher the surface charge, the faster the movement. The obtained Zeta potentials are shown in Table 4-6. The Zeta potentials for both cell lines are similar indicating no significant difference in the surface charge between the two cell lines.

Table 4-6 Accesible surface charges of E 42/02 and APH-R cells

Zeta potential was determined using a ZetaSizer Nano. Cells were measured in 40 mM HEPES, pH 7.4 at 25 °C. Six measurements (each with 20 runs) were performed and averaged for each sample. Data presented are the mean of two independent cell preparations.

Cell line	E 42/02	APH-R
Zeta potential (mV)	-17.8 ± 0.8	-16.7 ± 1.9

4.4 Peptide oligomerization in absence and presence of liposomes

Published models suggest the formation of peptide oligomers. Here, aggregation of peptides in the absence and presence of a mimic target membrane was determined by SDS-PAGE. In the absence of liposomes, covalent linked oligomers of single peptides in solution, which are heat- and SDS-stable, were detected. Therefore, all non-covalent bindings such as hydrogen, ionic and van-der-Waals bonds as well as hydrophobic interactions were destroyed inter- and intramolecular by the addition of SDS and heating of the samples for 5 min at 100 °C before gel electrophoresis. Further, peptides were incubated both with liposomes, and with liposomes and DSP crosslinker. In the latter case, the previous incubation of the samples with DSP crosslinker fixed all

covalently and non-covalently linked molecules and, thereby, preserved all existing oligomers, which, otherwise, would have been destroyed by SDS and heating.

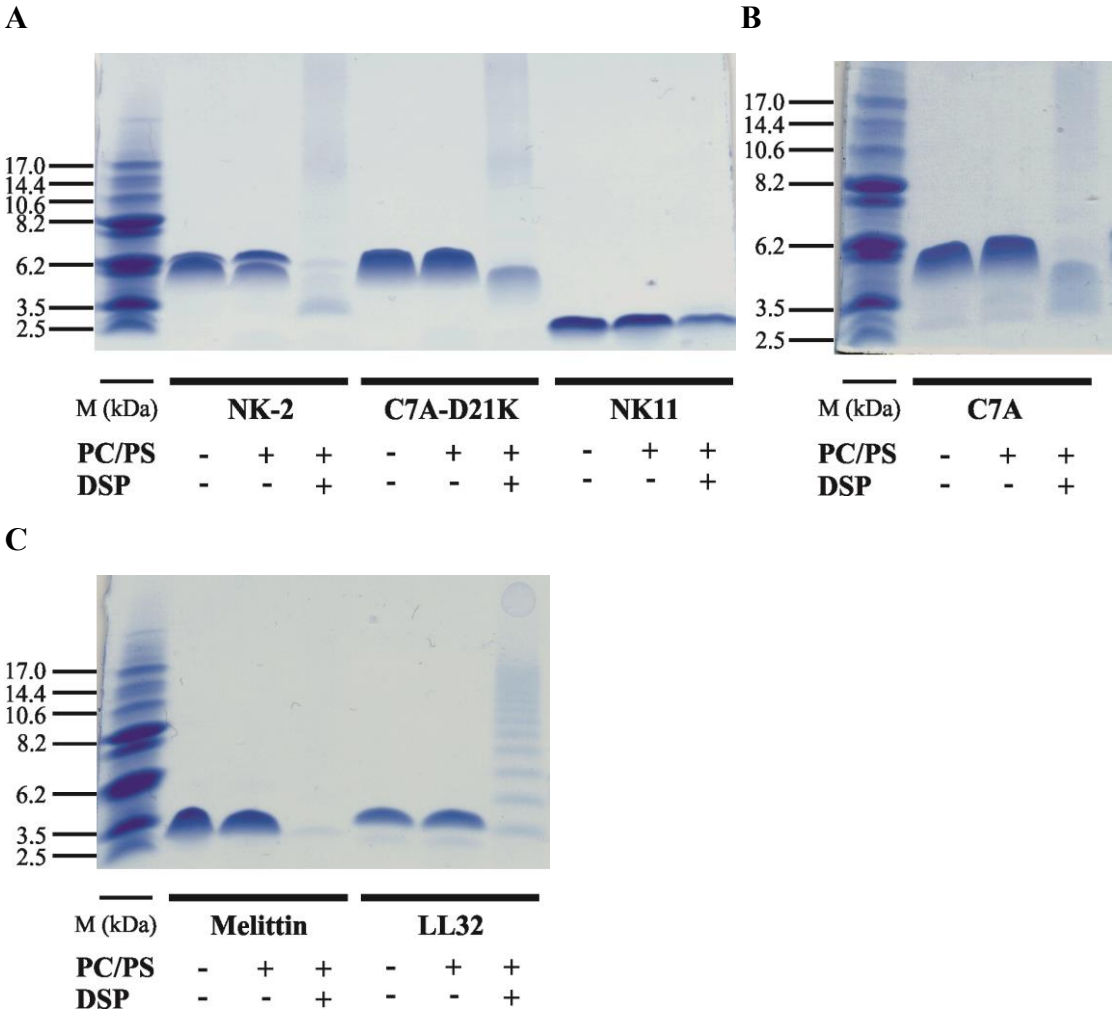

Figure 4-17 Oligomerization of peptides

SDS-PAGE was used to determine peptides oligomerization in the absence and presence of lipid layers. Peptides were incubated 30 min at room temperature either without or with PC/PS (90/10) liposomes and DSP crosslinker in PBS. The lanes were loaded with a final concentration of 1 µg peptide, 500 µM liposomes and 100 µM DSP crosslinker. Shown are separating gels of representative experiments. Experiments with peptides and liposomes/DSP were made only once for each shown peptides but thrice for NK-2 and twice for C7A-D21K. Experiments with only peptides were made five times for NK-2, twice for C7A, twice for C7A-D21K, thrice for NK11, and twice for melittin. Reference is performed by 10 µg of molecular weight marker (M). Gels were stained with Roti®-blue solution.

Figure 4-17 (A-C) depicts SDS-PAGEs of NK-2 and its derivates C7A, C7A-D21K, NK11 as well as LL32 and melittin. Peptides were incubated without and with

liposomes, and also with DSP crosslinker. The crosslinker fixed all non-covalent and covalent bindings, conserving heat- and SDS-instable oligomers.

According to the molecular weight marker, most peptides form heat- and SDS-stable dimers in the absence of liposomes; only the band of LL32 is in the range of its molecular weight, indicating a monomeric existence. For most of the peptides, there is no visible difference of heat- and SDS-stable oligomerization of peptides in and without the presence of liposomes. A difference can only be seen at NK-2 and C7A-D21K, which have an additional weak band below 2.5 kDa in the presence of liposomes. The emerging doublet of NK-2 in the absence of DSP cannot be explained by this data. It cannot be ruled out that these are monomers/ dimers or dimers/trimers with an individual electrophoretic mobility that do not exactly correlate with the mass. Such observation had been made in the laboratory before (unpublished data). The addition of DSP crosslinker to the peptide-liposome-mixture reveals the formation of several different oligomers for all the peptides with the exception of NK11. It is interesting that the only inactive peptide, NK11, shows, even with DSP, just a weak second band, indicating no further oligomerization. Melittin has one clear band in its dimeric molecular weight range but only a weak band remains after crosslinking. It is likely that the crosslinked oligomers are too large to enter the gel.

To summarize, small heat- and SDS-stable oligomers of peptides in the absence and presence of lipid layers could be shown in SDS-PAGEs. Moreover, heat- and SDS-instable oligomers of different sizes could be crosslinked with DSP in the presence of liposomes.

5 Discussion

Cancer is the leading cause of death in developed countries and the second most common cause of death worldwide [126]. Most of the used cancer therapeutics causes severe side effects by targeting not only degenerate cells but also healthy tissue. Besides, formerly successful therapeutics lose their effectiveness, as cancer cells develop increased resistance [3]. Hence, there is an urgent need for new anti-cancer drugs. As promising candidates, antimicrobial peptides (AMPs) have come into the focus of research. While they are known for their effectiveness against microorganisms, some of them have also been found to exhibit potent anti-cancer activity [24], [29], [127], [128]. Several of these AMPs show selective targeting of cancer cells [6], [71], [129], [130], thereby, causing fewer potential side effects. Further, in contrast to chemotherapeutics, they kill cells very fast by primarily causing cell membrane disruption [2], [71], [131]. This new mode of action against cancer cells has also been shown to be effective to cancer-drug resistant cells [62], [128]. It may be said in conclusion, AMPs show several properties that potentially make them new anti-cancer drugs.

In this thesis, the effectiveness of different α-helical peptides with focus on NK-2 and its derivates, was determined against two cancer cell lines (equine sarcoid cell line E 42/02 and human prostate cancer cell line PC-3) and two healthy cell lines (equine skin cell line APH-R and human keratocyte cell line HaCaT). The two cancer cell lines were chosen as representatives of frequently occurring cancer types demanding challenging treatment. Moreover, the equine sarcoid is, as skin cancer, an appropriate model for a topical application of peptides avoiding complexities that accompany a systemic treatment. Peptide optimization with respect to activity and serum stability was tested on three sequence variants of peptide NK-2. The peptides mode of action was investigated by analyzing peptides oligomerization and kinetics of cell killing. In addition, this thesis aimed at shedding light on the cell surface structures that might be important for targeting and killing of cancer cells by peptides. Hence, a closer look was taken at different anionic surface structures that were found to increase on the surface of cancer cells, thus making them putative targets for the positively charged peptides.

5.1 Tested peptides exhibit anti-cancer activity

Previous studies have already documented the anti-cancer activities of the α-helical peptides NK-2, LL-37 and melittin. NK-2, especially, features a broad spectrum activity against cancer cells including human neuroblastoma, leukaemia, and colorectal adenocarcinoma [71], as well as non-small-cell lung carcinoma [63]. The activity of peptide LL-37, from which the peptide LL32 tested in this study is derived [85], against a human squamous cancer cell line and human gastric cancer were demonstrated [2], [72], while reference peptide melittin was shown to exhibit non-selective activity against various cancer cell lines [2], [29], [130]. Successful treatment of human prostate cancer cells by peptides [132], [133] including melittin [2] has been shown already. The present study could also demonstrate the anti-cancer activities of peptides NK-2 and LL32 against the human prostate cancer cell line PC-3. Conversely, the effects of peptides on equine sarcoid cell lines have not been published till now. This is documented in this study for the first time by showing a potent activity of peptides NK-2, LL32, and melittin against equine sarcoid cells.

The favorable method of real-time measurements of cell physiological parameters was used in this study, and its differences and advantages over classical cytotoxicity assays will be discussed below. In this experimental setup, two metabolic biosensor-chips are connected to a perfusion system and serve as the bottom of small culture plates. Three different types of electrodes allow the measurement of medium acidification and medium oxygen consumption by cells, and also of cell adhesion [121]. In contrast to classical endpoint tests like the MTT assay or the PI-uptake assay, this setup allows insights into kinetics by monitoring cell reactions at any time of the treatment, thus giving a much better mimicry of the *in vivo* situation [122]. It is also possible to compare the normal metabolic activities of the tested cells. Here, PC-3 cells showed a higher cell metabolism than their healthy counterparts as is expected of cancerous cells because of their high proliferation rate [134]. This was not the case with equine sarcoid cells, which indicate no increased cell metabolism for this cancer cell line. Regarding cell-treatment experiments, it has been noticed that the use of this metabolic biosensor can also make low peptide concentrations effective, as the cells are continuously supplied with fresh compound allowing peptide accumulation on the cells. This is in

contrast to classical cytotoxic end-point tests, where cells are treated by a fixed amount of drug. In the real-time measurements, cell responses are indicated by changes in two metabolic values and cell adhesion. Increased values here, typically seen right in the beginning of peptide-treatment, can be interpreted as a stress response to peptide-induced cell damage and as attempt to overcome this deleterious attack. In this case, values will stay above or go back to control cell levels after an initial increase. Cell killing is indicated by a decline of all three values to zero. Decreased acidification, oxygen consumption, and impedance that do not drop to zero probably indicate partial cell killing. In case of temporary cell damage, cell recovery should occur after peptide treatment, but that was not seen in this study. It is noteworthy that biosensor measurements allow the assumption of the point of attack of substances in cell metabolism. This can be assumed when the two metabolic values are affected one after the other. In this case, the point of attack should be correlated to a metabolic pathway connected with the at first decreased value (e.g., glycolysis inhibition or respiratory chain inhibition) [121], [122]. The peptides of this study obviously do not have their target in one specific pathway of cell metabolism, as there is no time-shift in the reaction of cell acidification and respiration. Of the three parameters, cell adhesion turned out to be the most sensitive one in this study. An increase in impedance with non-toxic peptide doses indicates cell morphology changes to a denser cell layer, while the metabolic values stay at control cell levels. In a study by Ceriotti *et al.* cell respiration and adhesion had a similar sensitivity at 24 h of cell treatment with different chemical compounds [121], while Drechsler and Andrä also reported cell adhesion to be the most sensitive parameter in cell treatment with peptides [80]. This is further supported by the fact that they could show that inactive peptide NK11, too, increases cell impedance, which is consistent with a study of Hammer *et al.* who showed that NK11, similar to NK-2, intercalated into negatively charged phosphatidylglycerol membranes [135].

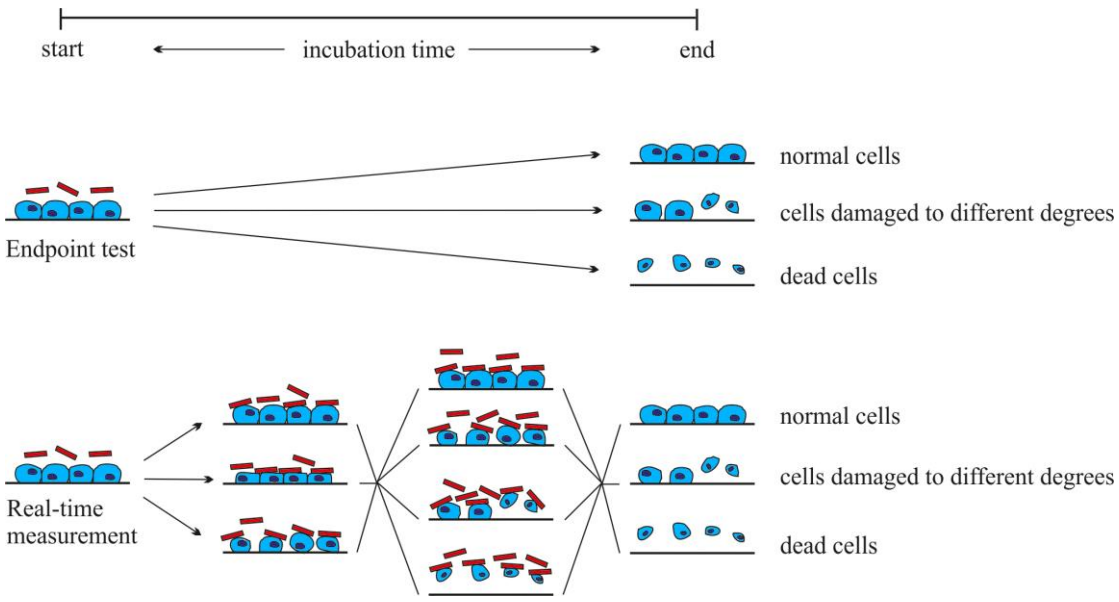

Figure 5-1 Comparison of endpoint test with real-time measurement

The figure depicts different morphological cell reactions to peptide treatment. While endpoint test and real-time measurement might bring the same result (no cell reaction to the tested agent, cell damage to different degrees, or cell death), the real-time measurement also shows cell reactions during the whole incubation time. Thus, this method provides more information about the kinetic of cell killing showing also cell restistance (indicated by closer cell-to-cell contact, flattening of the cell layer or enhanced cell adhesion) and cell recovery.

As observed in this study, usually adherent cells might not grow on the sensor chip surface. As a result, morphologic cell measurements were not possible for the equine cell lines, but metabolic cell activity could be monitored without limitation. In future experiments, a standard coating (like collagen, laminin or fibronectin) can be applied on the chip surface to facilitate an adherent cell growth. Another thing that could be changed in future experiments is the high glucose concentration in the utilized media. Commercial BRM and also DMEM contain 4.5 g/l glucose, while the human blood sugar level is around 1 g/l. To imitate the *in vivo* situation as closely as possible and to investigate whether a lower glucose concentration influences peptide effectiveness, the media composition should be adjusted to match the lower concentration in the blood. As metabolic biosensor measurements provide several advantages over classical cytotoxicity assays, this method is recommended for future experiments with decreased glucose concentrations.

5.2 Optimization of peptides

NK-2 was chosen as lead structure for the design of new peptides because of its known potency against different cancer cell lines [63], [71] and its low haemolytic activity [77]. However, further potency improvement was desired as well as size reduction to reduce the extreme high synthesis cost of peptides. Additionally, the new peptides should exhibit an increased serum stability to overcome the low efficacy of NK-2 under full medium conditions.

The most basic modification of the NK-2 sequence here is the replacement of the non-functional sole cysteine (C) residue on position seven with an alanine (A) residue (peptide C7A). This replacement is expected to improve stability by reducing the sensitivity of the peptide by oxidation. It is noticed that in the parent peptide of NK-2, NK-lysin, the cysteine residue on position seven is involved in intra-molecular disulfide bonding [76], and is, thus, not available for oxidation reactions. Previous studies have shown that an enhanced positive net charge can improve the antibacterial activity of peptides [55] and might also be relevant for their anti-cancer activity [132]. Here, an enhanced positive net charge of +2 was achieved by substituting the aspartic acid (D) residue in the C7A sequence on position twenty-one by a lysine (K) residue (peptide C7A-D21K). Finally, size reduction of C7A was achieved removing the amino acid residues 18 to 21, including an anionic aspartate and a cationic lysine residue (peptide C7A-Δ).

Actually, all three derivates showed an improved anti-cancer activity compared to their parent peptide NK-2. Substitution or deletion of anionic aspartate on position twenty-one do not lead to further activity improvement against equine sarcoid cells, while C7A-D21K (net charge +12) showed the highest potency against PC-3 cells. One possible explanation for this might be the unusual low anionic surface charge of the equine sarcoid cells (see 5.3.3), making them unattractive for peptides with higher cationic charge. It is important to note that the shortened derivate C7A-Δ, too, represents a substantially improved version of NK-2 against PC-3 cells accompanied by a significantly reduced synthesis effort. In an earlier study on the antibacterial activity of NK-2-derived peptides, the same consecutive deletion of amino acid residues 18-21 was found to be successful [55]. Here, the substitution was based on a Cys/Ser instead of the Cys/Ala exchange on position seven. The Cys/Ser exchange, however, turned out

to be not valuable for the anti-cancer cell activity (unpublished data). The potent anti-cancer activity of the NK-2 derivates is accompanied with a low haemolytic activity (Gross *et. al*, 2013), making these peptides promising candidates for new cancer drugs.

In previous studies [71], [80], and in this study as well, it was recognized that some peptides apparently exhibit reduced efficacy under full medium conditions. A higher resistance of cells because of a better nutrient supply could be considered as a possible explanation for the loss of activity of peptides in medium. This is contradicted, however, by the fact that not all peptides are affected to the same extent. Hence, it seems to be more likely that individual peptides become inactive in media to varying degrees, while the activity of others is nearly unaffected. This corresponds with several publications reporting serum inactivation of peptides due to potential susceptibility to proteases and inactivation by anionic serum components [24], [61], [68], [129]. Low-density lipoproteins are also reported to be a potent inhibitor of peptide activity, while albumin and high-density lipoproteins seem to be only slightly inhibitory [136]. In the present study, the replacement of the non-functional cysteine residue on position seven is assumed to be the key substitution to maintain the peptide´s activity also under medium conditions. Actually, C7A-D21K exhibits an enhanced medium stability compared with NK-2. As this derivate also includes an amino acid replacement on position 21, future experiments determining optimized serum stability for NK-2 derivates should include peptide C7A. Some other studies have already shown how to increase serum stability of certain peptides. Synthetic diasteromeric peptides, which are composed of both D and L amino acids, have been shown to resist the inhibitory effects of the serum [129], [137], [138]. Other ways to overcome serum instability include packing of peptides, for example, in liposomes, the designing of peptides to protease resistant pro-drug molecules, the use of peptidomimetics with altered backbones [139], [140], as well as the intergration of a peptide into human serum albumin [141]. Moreover, a recent study demonstrated the complete regression of B16 melanoma in mice after intratumoral injection of a bovine lactoferricin derived peptide [142], which, of course, is another possibility to deal with the problem of serum instability in cases of solid and accessible tumors .

5.3 Peptides' mode of action

Peptides' mode of action was investigated in this study with regard to i) peptides killing kinetics, ii) the preferred binding structures on the cell surface, and iii) peptide cancer cell selectivity.

5.3.1 Killing kinetics of antimicrobial peptides

Several studies reported a fast mode of action for antimicrobial peptides. NK-2's effective and fast cancer cell killing was shown for neuroblastoma cells [71], [80], and the AMP polybia-MPI killed sensitive and multi-drug resistant K562 cells within minutes [131]. In the present study, all experiments with regard to killing kinetics demonstrated also a rapid cell-peptide interaction. The time kinetic measurements performed by classical MTT assay showed that most of the peptides had their highest effectiveness within the first 30 min. The chip-based sensor noticed an immediate cell response to the peptides by short increases of mainly cell adhesion and oxygen consumption. These observations correspond with the results from light microscopy, where the membrane permeabilization caused by NK-2 could be monitored by cellular uptake of a fluorescent dye. The first fluorescent positive cells were noticed already within 5 min with a fluorescent maximum after 20 min, indicating a completed peptide activity. These results are in accordance with confocal fluorescence microscopy experiments. Here, NK-2 bound to the cell surfaces within seconds and, above a critical concentration, caused almost immediate membrane blebbing and membrane permeabilization. A similar cell reaction was noticed by Wang *et al.,* who reported swelling and bursting of cancer cells treated with peptide polybia-MPI [131]. In the confocal fluorescence microscopy experiments, subsequently, NK-2's entry into the cytosol could be observed. Obviously, the accumulation dynamics were dependent on the peptide concentration applied and lasted up to 10 min. Interestingly, NK-2 also bound with intracellular membranes after traversing the plasma membrane, induced the formation of intracellular bubbles, and entered the nucleus in a fast sequence. Cell killing by intracellular-targeting, including mitochondrial membrane permeabilization, inhibition of DNA and protein synthesis, has been shown for some AMPs [26], and was also suggested for NK-2 before [80]. Due to its fast killing it is assumed that NK-2

causes cell death in this study via membrane permeabilization, although it might have secondary intracellular targets as indicated by fluorescence microscopy.
Here, in all experiments the action of the tested peptides is seen to be extremely fast with rapid cell binding and membrane permeabilization. This induces massive cell stress, triggering membrane blebbing, enhanced energy metabolism, and changes in cell morphology. Depending on the concentration of the peptides, the cells might resist the attack or die.

The exact mode of membrane permeabilization by individual peptides is still under discussion. During this study, some results indicated that different peptides might differ in their modes of action. This can be seen in the various inhibitory effects of PS-containing liposomes, as well as in the fact that melittin, in comparison with NK-2 and its derivates, does not cause an increase of cell impedance. From the postulated models of membrane disruption, the “barrel-stave mechanism” was found to fit mainly non-selective lytic peptides [5]. It could accordingly be shown that melittin forms barrel-like pores [143]. An extremely high overall hydrophobicity is postulated to be the reason for melittin’s non-selective membranolytic activity [144]. Previous studies showed for melittin a charge-independent binding and model membrane permeabilization as well as high haemolytic and cytotoxic activity [55], [73]. In contrast, the latter study revealed that, for NK-2, a positive net charge and an amphipathic anchor point were essential for its antibacterial activity, which could also be true of LL32, exhibiting a cationic amphipathic α-helix as secondary structure [85]. In the “carpet mechanism”, positively charged peptides bind in a carpet-like manner to the negatively charged target membrane. Their amphipathic secondary structure allows an orientation between the lipids and the phospholipid head groups, and the membrane is permeated or disintegrated after reaching a threshold concentration. This process might include also the formation of toroidal pores [5]. LL-37 has been shown to act via this mechanism [145], [146], which is also assumed for peptide NK-2 in two studies on its antifungal and antibacterial activity [77], [147]. Their fast killing process accompanied by membrane permeabilization and their α-helical secondary structure indicates that NK-2 and its derivates act against the cancer cells used here via the “carpet mechanism” also. However, it seems likely that individual peptides have their own modes of action, depending on their nature, membrane composition, peptide concentration and environmental conditions. This would explain why, for example,

melittin has also been found to form toroidal pores [148]. Regarding pore formation, it is still a matter of discussion whether peptides form oligomers in order to disrupt the cell membrane [30]. One study could confirm this by documenting that a tetrameric peptide was embedded into a membrane-mimic while its monomeric counterpart was located only on the surface of the membrane [149]. In the present study, SDS-PAGE experiments reveal that the peptides tested here can oligomerize to different extents. Interestingly, only the inactive NK11 did not show higher oligomerization, thereby supporting the assumption that peptide-to-peptide interaction is important for cell killing.

The rapid killing process of peptides, which comes along with physical membrane destruction, represents a new mode of action in killing of cancer cells. As might be expected, several studies could show that peptides are also effective against multi-drug resistant cells [58], [63], [131]. Classical chemotherapeutics are slower compared to the action of membrane-disrupting peptides. Their targets are generally intracellular and their effect is mainly achieved by interaction with the cell metabolism. As a result, the main resistance mechanisms of cancer cells in case of classical chemotherapeutics include factors that reduce the intracellular drug concentration, lead to alterations in the drug-target interaction as well as improved cell responses like improved DNA damage repair or defects in apoptotic pathways [3]. To illustrate this, Figure 5-2 shows different chemoresistance mechanisms of cancer cells. On the contrary, it can be assumed that the rapid action of the peptides might complicate the generation of resistance in the cells due to a lack of adaptation time before being killed. Additionally, the interaction of peptides and target membranes seems not to be receptor-related but due to electrostatic interaction. Thus, inhibition of interaction would require radical changes of membrane composition.

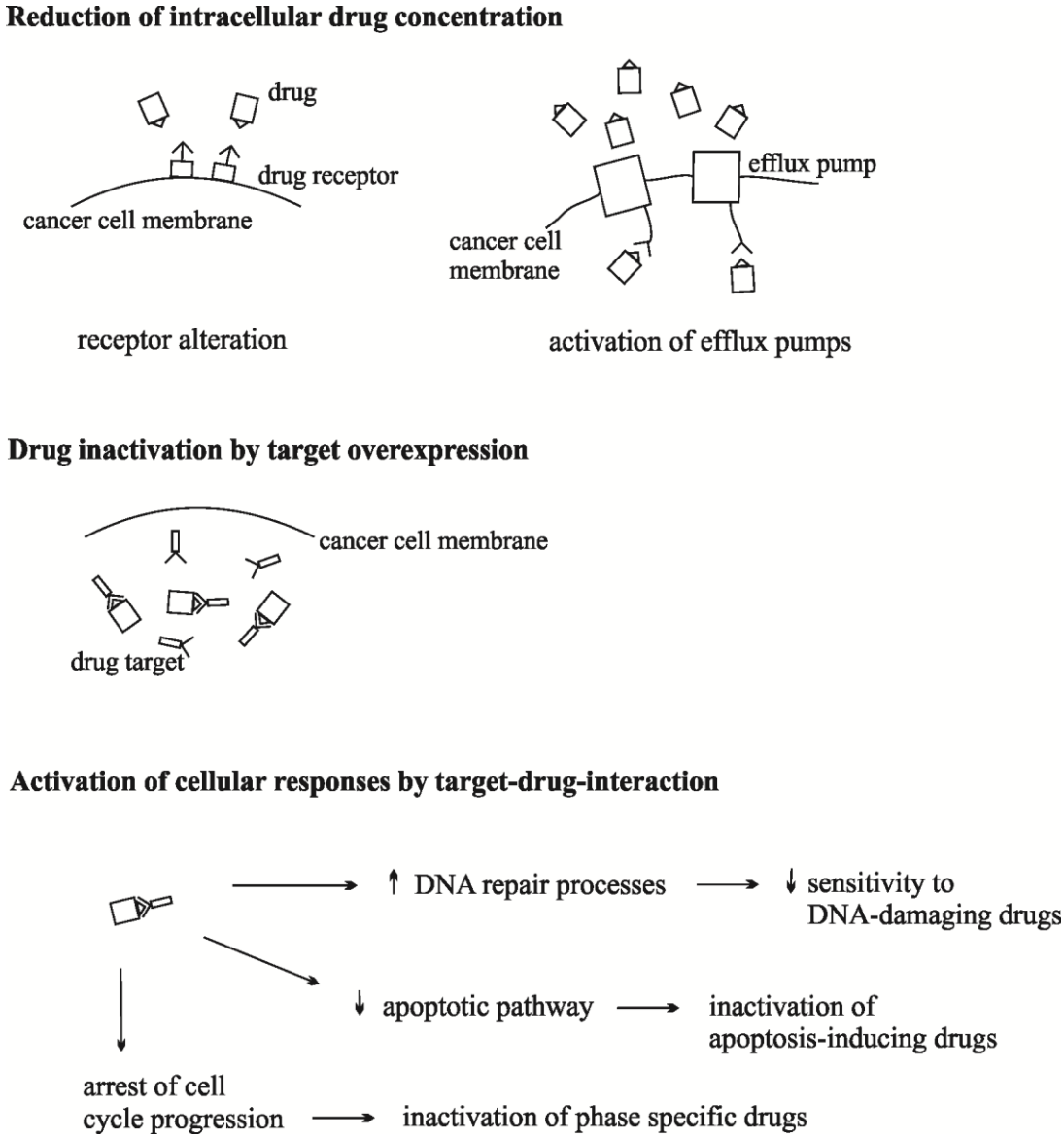

Figure 5-2 Chemoresistance mechanisms of cancer cells

The figure depicts a selection of different drug resistance mechanisms of cancer cells. The targets of classical chemotherapeutics are generally intracellular, thus giving the cells some time to develop restistance mechanisms. These mechanisms include the reduction of the intracellular drug concentration, the alteration of drug-target-interaction, and the activation of cell responses that prevent cell death.

5.3.2 Cell surface target structures of peptides

To understand the role of different cell surface structures in peptide targeting, the influence of three putative surface targets on the activity of peptides NK-2, C7A-D21K,

LL32, and melittin was examined. In contrast to the general zwitterionic surface of healthy cells, cancer cells exhibit mainly a net negative surface charge. This is due to a higher content of anionic molecules in their outer leaflet like phosphatidylserine [34]–[36], O-glycosylated mucins (glycoproteins that are rich in anionic saccharides like sialic acids and sulfates) [37], [38], sialylated gangliosides [39], and heparin sulfates [40]. Hence, phosphatidylserine, sialic acids and sulfated carbohydrates were chosen as test substances for potential peptide targets.

An enhanced content of the negatively charged membrane phospholipid phosphatidylserine (PS) in the outer membrane has been shown for several cancer cell types [34]–[36], suggesting PS to be a possible cancer marker as well [46]. For peptide magainin-2, anionic phospholipids (PS, PG) were found to be essential for its action [47], and the effectiveness of synthetic peptides derived from beetle defensins was also seen to depend on the presence of PS on the cells surface [48]. Furthermore, Lee *et al.* could show that peptide CopA3, which derived from a defensin-like peptide of the dung beetle, interacts with PS [150]. In this study, the effectiveness of NK-2 against untreated PC-3 cells and anti-PS antibody-incubated PC-3 cells was indistinguishable in flow cytometry experiments, indicating that PS is not a target of NK-2. In contrast, another experiment, with PS containing liposomes, showed an interaction of NK-2 with this phospholipid, although the concentration-dependent inhibitory effect on peptides LL32 and melittin was stronger. Interestingly, the addition of PS containing liposomes had almost no effect on the peptide C7A-D21K. These results indicate a distinct cell-membrane targeting by various peptides. To investigate the contradictory results for NK-2 interaction with the phospholipid PS, the surface PS content of PC-3 cells was determined. Therefore, immunostaining assays were performed using the anti-PS antibody as well as Annexin V, a well-known PS detection protein [35], [45]. These experiments were done with the cancerous and healthy cell lines to investigate if the increased PS content of the outer membrane, which was shown for other cancer cells [34], also applies for the cells tested here. Regrettably, the results of both PS detection methods differ for PC-3 cells, but in both tests HaCaT cells have a similar or even higher PS content. This might explain why the results for PS targeting of NK-2 are contradictory. As PS is not high on PC-3 cell surfaces, other structures might be targets of peptides in this cell line. This is especially so as previous studies documented a NK-2 selectivity due to differences in the membrane phospholipid composition of target cells

[73], and the correlation between its cancer-cell-killing activity and the exposure of negatively charged PS on the cell surface [71]. These results might indicate that individual peptides may have different target structures on different cancer cells. For the two equine cell lines, the PS surface amount is similarly low in both stainings, although the total amount differs. However, the postulated increased surface PS content could not be shown for the cancerous cell lines E 42/02 and PC-3 tested here.

Further, anionic sialic acids have been shown to increase on the cell surface of some types of cancer cells [36], [50], and, for a variety of cancer cell types, upregulation of sialyltransferases have been associated with cancer development and malignancy [151]. Thus, these anionic carboxylated carbohydrates also came into focus as potential peptide targets. Risso *et al.* showed that neuraminidase pre-treatment of diverse cancer cell lines reduced, but did not prevent, killing activity of bovine cathelicidin peptides [53]. Accordingly, Weghuber *et al.* could demonstrate an interaction of different peptides with sialylated membrane proteins and lipids [51]. Moreover, the binding of peptide LL-37 to salivary mucins could be inhibited by their desialylation [52]. In the present study, the role of sialic acids in peptide targeting of E 42/02 and PC-3 cells was investigated, on the one hand, by peptide treatment of untreated and desialylated cells and, on the other, by inhibition experiments with a sialic acid and sialylated protein. The latter was found to provide a more adequate mimicry of the membrane situation, as sialic acids on the cell surfaces are components of complex glycolipids and glycoproteins [49], [50]. The experiments revealed a negligible inhibitory effect of the single sialic acid as well as the sialylated protein on peptides' killing effectiveness, demonstrating, thereby, that the presence of multiple sialic acid residues do not enhance the affinity of the peptides. PC-3 cell desialylation also had only a minor influence on the peptide-cell interaction. In experiments with the metabolic biosensor, desialylated PC-3 cells seemed to be even more susceptible to peptide treatment. On the contrary, flow cytometry experiments showed a slightly decreased potency for NK-2 against desialylated equine sarcoid cells. This indicates that sialic acids on the surface of the equine cells are not primary but secondary targets for NK-2. All in all, there is no evidence for surface sialic acids being involved in targeting and killing of PC-3 cells by the peptides tested here and on E 42/02 cells they seem do be only secondary targets. These results, contrary to the previous reports, again indicate cell line and/or peptide specificities in cancer-cell targeting.

Glycosaminoglycans (GAGs) are large linear polysaccharids consisting of a recurring disaccharide unit, which includes an amino sugar (*N*-acetylglucose amine or *N*-acetylgalactose amine) and uronic acid (glucuronic acid or iduronic acid). The glycoseaminoglycan chains are mostly sulfated which, together with the uronic acids, gives the molecules their negative charge. GAGs, like heparan sulfate and chondroitin sulfate, are present on the surface of most cells. In cancerous tissues, they are over expressed [40], [152], [153], and expression on the cell surface seems to be positively correlated with metastasis [154], [155]. An increased amount of highly sulfated chondroitin sulfate has been especially reported for metastasis [153], [156]. To investigate the role of sulfated oligosaccharides in the targeting of the selected peptides, chondroitin sulfate was chosen as a model compound. In contrast to sialic acids and the sialylated protein fetuin, chondroitin sulfate clearly inhibited the cytotoxicity of all peptides tested here. This correlates with previous studies reporting an inhibition of the peptide LL-37 by biological fluids enriched with GAGs [157] as well as an interaction of melittin with cell-surface GAGs [158]. Fadnes *et al.* demonstrated that lager peptides were captured by heparan sulfate on the surface of cancer cells, thus preventing them from reaching the phospholipid bilayer and inducing apoptosis [159], while the cytotoxicity of smaller peptides was unaffected or increased by cell surface heparan sulfate [54]. Further, melittin's cytotoxicity to mouse fibroblasts was inhibited by sulfated sialic acid-polymers but not by their unsulfated counterparts [160]. Additionally, a glycan microarray screen showed sulfated carbohydrates, and not sialic acids, to be the preferred binding partners of NK-2 (Gross and Andrä, 2012).

All this points to sulfated and not carboxylated carbohydrates such as sialic acids playing a decisive role in peptide cell targeting. However, the deglycosylation of PC-3 cells did not influence NK-2 membrane permeabilization; although a decreased peptide activity was suspected due to the removal of all *N*-linked sugar chains, including sulfated carbohydrates. Besides, an unsuccessful deglycosylation, other possible explanations might be that the removed sugar chains covered other anionic target structures now accessible for the peptide, and/or that it is easier for the peptide to reach the lipid bilayer without the sugar molecules on the cell surface.

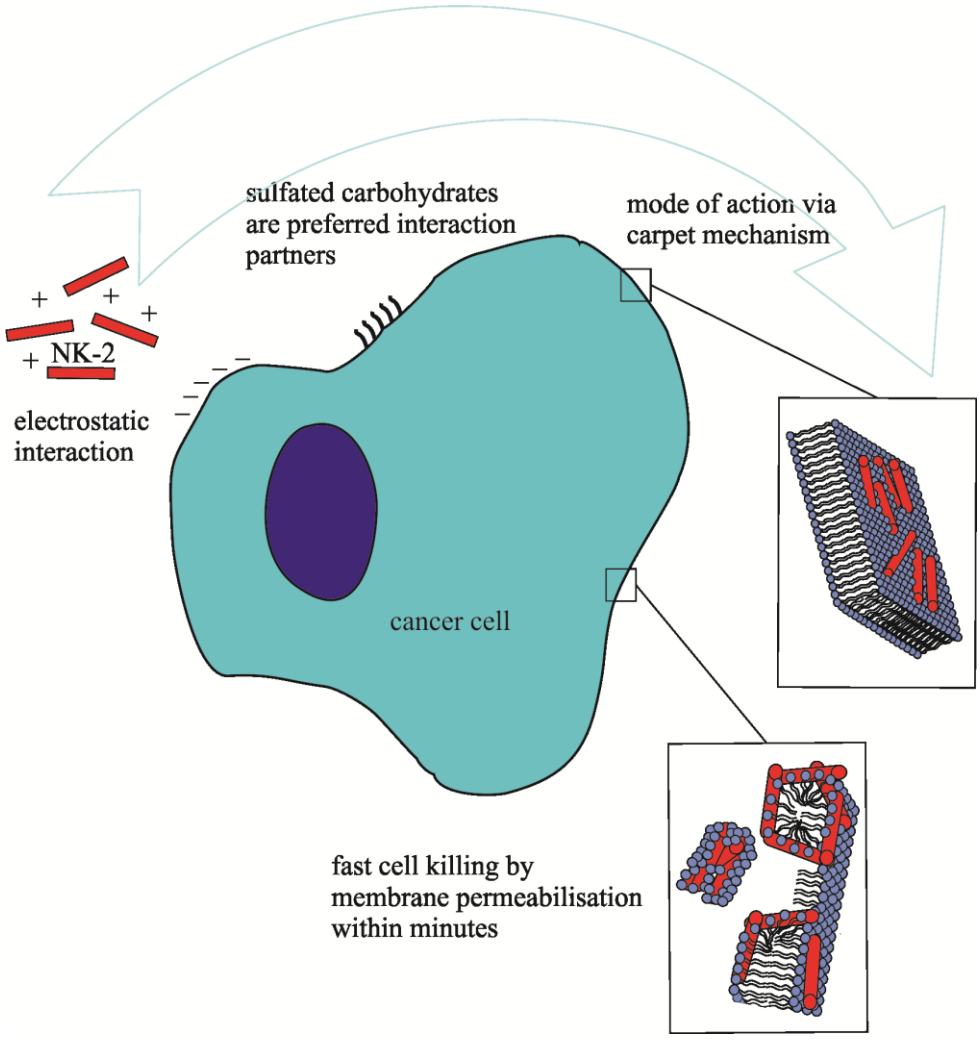

Figure 5-3 Mode of action of NK-2 and its active derivates

The figure gives an overview of cancer cell killing by NK-2 and its derivates. The binding occurs via elcectrostatic interaction but with sulfated carbohydrates as preferred interaction partners. The fast cancer cell killing is achieved by membrane permeabilization.

5.3.3 Cell type selectivity

Classical chemotherapeutics are often accompanied by more or less severe side effects [161]–[163]. Parenteral application of a drug requires a high specificity for the target tissue to minimize side effects on healthy tissue. In topical application, that is not quite as necessary because of the direct placement of the drug on the tissue to be treated. But there is, of course, the risk to the neighbouring tissue as well as that of absorption

through the skin [164]. In case of animal patients, the topical drugs might be licked off, thus, causing side effects, for example, on the mucosa of the mouth [165].

Cationic antimicrobial peptides are believed to selectively target microorganisms via an electrostatic interaction with the negatively charged membrane phospholipids phosphatidylglycerol and cardiolipin [47], [55], [73], as well as lipopolysaccharides [135]. The targeting of cancer cells also seems to be driven by electrostatic interaction [71], [166] as, unlike the zwitterionic surface of healthy cells, various cancer cells have been shown to exhibit a net negative surface charge due to a higher content of anionic molecules in their outer leaflet [34], [46], [71]. From the peptides tested here, NK-2 has been documented in a previous study to be selective to neuroblastoma cancer cells over HaCaT cells [80], the non-cancerous, spontaneously transformed human keratinocyte cell line [118] also used in this study. According to this, selectivity of the NK-2 derived peptide, C7A-D21K, could be shown in the present study for PC-3 cells over HaCaT cells by using the chip-based biosensor. Surprisingly, no selectivity of peptides NK-2 or C7A-D21K was observed in the equine cell system, and LL32 also did not show selectivity for the equine sarcoid cell line.

As NK-2 and its derivate were also expected to pick the degenerated equine cells, it was suggested that the observed lack of the peptides' selection of the equine sarcoid cell line might be due to an absence of differences in cell surface properties of E 42/02 and APH-R cells. For several cancer cell lines an increased amount of the negatively charged membrane lipid PS has been shown in the outer leaflet of their plasma membranes [34], [46], [71]. Furthermore, the preferred killing of cells with increased surface levels of PS by peptide NK-2 as well as a direct interaction of this peptide with PS was documented before [71], [167]. Suggesting PS as potential peptide target the PS content on both equine cell lines was investigated. It turned out that the detectable PS surface levels of the two equine cell lines are undistinguishable. Further investigations included the accessible surface charge of both equine cell lines by determining their Zeta potential. But also the Zeta potentials of E 42/02 and APH-R cell suspensions show no significant difference between the two cell lines, indicating that also no other charged surface factors are predominant in one of the cell lines. Assuming that the targeting of cancer cells happens via electrostatic interaction, the lack of difference in surface charge of both equine cells lines explains why the tested peptides have no specificity for the equine sarcoid cell line.

5.4 Conclusion

Cationic, amphipathic peptides are potential anti-cancer drugs with a novel mode of action. Here, various *in vitro* tests showed a fast-killing efficacy by cell membrane permeabilization of peptides NK-2, LL32 and melittin against the equine sarcoid cell line E 42/02 and the human prostate cancer cell line PC-3. Peptide improvement with regard to potency, stability and size reduction by directed amino acid substitution was determined for three derivates of NK-2, highlighting them as potential candidates for new anti-cancer drugs. But although derivate C7A-D21K shows effective and selective killing of PC-3 cells, a therapeutic use against human prostate cancer is at the moment unlikely due to obstacles associated with the parenteral application of peptides. The demonstrated activity of the peptides against equine sarcoid cells, on the other hand, makes topical application an interesting option in a therapeutic approach, especially as a combined therapy with surgical removal. Here, the peptides might eradicate residual tumor cells to prevent a relapse and, at the same time, act as an antibiotic, thereby minimizing the risk of wound infection. In the meanwhile, *in vivo* repetitively intratumoral injections of peptides C7A and C7A-D21K have been demonstrated to induce a notable reduction of tumor growth in a human *ex vivo* colon carcinoma model in mice [168].

Moreover, investigations into peptide targeting revealed that carboxylated carbohydrates like sialic acids are not the primary targets for the peptides tested here. In fact, several experiments showed an interaction of the peptides with sulfated carbohydrates, thus, stressing sulfated glycans as potential prime target structures for these AMPs on the tested cancer cells. In addition, membrane phospholipid phosphatidylserine could be assumed to be target of peptides LL32, melittin, and, to a lesser extent, of NK-2. It might be reasonably assumed that this targeting preference is not limited to the peptides and cancer cells tested here.

6 Abstract

Evaluation of antimicrobial peptides as anti-cancer agents against equine sarcoid and human prostate adenocarcinoma cells

Cancer is a frequently occurring disease in humans causing over seven million deaths per year worldwide and showing increasing morbidity. Therapy is challenging, as the disease is not curable in its advanced stages, and, in addition, medication causes severe side effects or becomes ineffective due to an increase of drug-resistant cancer types. Antimicrobial peptides (AMPs) became the focus of research, as the search of new and effective anti-cancer agents intensified. These peptides are part of the innate immune system of mammals, some showing anti-cancer activity besides targeting pathogens. To investigate the potential of AMPs as anti-cancer drugs, the present study aimed at determining the activity of a selection of natural AMPs and fragments thereof against an equine sarcoid and a human prostate cancer cell line, and to elucidate the mode of action of the selected peptides. Cytotoxicity assays and sensor-chip-based real-time measurements made evident a potent activity of the tested AMPs against both cancer cell lines. Derivates of peptide NK-2 were documented to exhibit improved anti-cancer potency, thus becoming promising candidates for future drug development. Peptides' mode of action was investigated with respect to killing kinetics, peptide-to-peptide-interaction, target structures on cell surfaces, and cancer cell selectivity. The cationic AMPs are believed to target cells via an anionic membrane surface, which several cancer cells have. The AMPs mainly inflict cell death via direct membrane destruction. It is suggested that AMPs might aggregate, especially during membrane interaction, and gel electrophoresis performed in this study supports this assumption. Cytotoxicity assays, fluorescent microscopy, and sensor-chip-based real-time measurements showed a fast cell-killing process by the tested peptides. Inhibition tests and enzymatic treatment of the cell surface evidenced that AMPs can distinguish different anionic cell surface structures. They bind sulfated carbohydrates rather than sialic acids or sialylated proteins. The anionic membrane lipid PS interacts in varying degrees with individual AMPs, pointing to different target preferences. While peptides exhibit selectivity for the prostate cancer cell line over a healthy cell line, no selectivity was seen for the equine sarcoid cell line over its healthy counterpart. This difference could be explained by a lack of anionic surface in the latter cancer cells.

7 Zusammenfassung

Evaluierung von antimikrobiellen Peptiden als Krebswirkstoffe gegen equine Sarkoid und humane Prostata Adenokarzinom Zellen

Mit über sieben Millionen Toten pro Jahr und weiter steigender Morbidität zählt Krebs zu den häufigen Erkrankungen beim Menschen. Die Therapie mit klassischen Medikamenten geht mit deutlichen Nebenwirkungen einher, wobei fortgeschrittene Krankheitsstadien meist nicht heilbar sind. Zusätzlich erschwerend ist die steigende Zahl medikamenten-resistenter Krebszellen. Auf der Suche nach neuen effektiven Krebstherapeutika rückten auch sogenannte Antimikrobielle Peptide (AMPs) in den Focus der Wissenschaft. Einige dieser Peptide besitzen neben einer Wirksamkeit gegen verschiedene Pathogene auch eine Wirkung gegen Krebszellen. In dieser Studie wurde die Aktivität ausgewählter natürlicher Peptide und Peptidfragmente gegen eine equine Sarkoid- und eine humane Prostatakrebs-Zellline untersucht. Zytotoxizitätstests und Messungen mit einem metabolischen Biosensorchip belegten eine hohe Aktivität der Peptide gegen beide Krebszelllinien. Neu designte Abkömmlinge des Peptids NK-2 zeigten dabei eine verbesserte Effektivität gegenüber ihrer Muttersubstanz, wodurch sie für zukünftige Medikamentenentwicklung interessant sind. Desweiteren wurde hier der Wirkmechanismus der AMPs untersucht bezüglich Wirkgeschwindigkeit, bevorzugten Bindungsstrukturen, Peptid-Peptid-Interaktion und Selektivität für Krebszellen. Es wird angenommen, dass die kationischen AMPs Zielzellen anhand derer negativ geladener Membranoberfläche, wie sie auch für einige Krebszellen gezeigt wurde, erkennen und diese durch Membranpermeabilisierung abtöten. Eine vermutete Aggregatbildung der Peptide bei diesem Vorgang wurde hier durch Ergebnisse einer Aggregationsstudie mittels Gelelektrophorese gestützt. Zytotoxizitätstests, Echtzeitmessungen mittels eines Sensorchips und Fluoreszenztests konnten einen sehr schnellen Wirkungseintritt der getesteten Peptide zeigen. Inhibitionsversuche und enzymatische Zelloberflächen-behandlungen zeigten, dass sulfatierte Kohlenhydrate bevorzugt gegenüber carboxy-lierten Kohlenhydraten gebunden wurden. Das anionische Membranlipid Phosphatidyl-serine interagierte in unterschiedlichem Umfang mit den einzelnen Peptiden, was auf unterschiedliche Zielstrukturen für verschiedene Peptide hinweist. Während eine Selektivität für die Prostatakrebszellen gezeigt werden konnte, bestand aufgrund fehlender anionischer Oberfläche keine Selektivität für die equine Sarkoidzelllinie.

8 References

[1] H. Jenssen, P. Hamill, and R. E. W. Hancock, “Peptide antimicrobial agents,” *Clin. Microbiol. Rev.*, vol. 19, no. 3, pp. 491–511, Jul. 2006.

[2] D. W. Hoskin and A. Ramamoorthy, “Studies on anticancer activities of antimicrobial peptides,” *Biochim. Biophys. Acta*, vol. 1778, no. 2, pp. 357–375, Feb. 2008.

[3] L. Gatti and F. Zunino, “Overview of tumor cell chemoresistance mechanisms,” *Methods Mol. Med.*, vol. 111, pp. 127–148, 2005.

[4] A. Giuliani, G. Pirri, A. Bozzi, A. Di Giulio, M. Aschi, and A. C. Rinaldi, “Antimicrobial peptides: natural templates for synthetic membrane-active compounds,” *Cell. Mol. Life Sci.*, vol. 65, no. 16, pp. 2450–2460, Aug. 2008.

[5] Y. Shai, “Mode of action of membrane active antimicrobial peptides,” *Biopolymers*, vol. 66, no. 4, pp. 236–248, 2002.

[6] F. Schweizer, “Cationic amphiphilic peptides with cancer-selective toxicity,” *Eur. J. Pharmacol.*, vol. 625, no. 1–3, pp. 190–194, Dec. 2009.

[7] M. R. Yeaman and N. Y. Yount, “Mechanisms of antimicrobial peptide action and resistance,” *Pharmacol. Rev.*, vol. 55, no. 1, pp. 27–55, Mar. 2003.

[8] R. E. Hancock and G. Diamond, “The role of cationic antimicrobial peptides in innate host defences,” *Trends Microbiol.*, vol. 8, no. 9, pp. 402–410, Sep. 2000.

[9] N. Mookherjee and R. E. W. Hancock, “Cationic host defence peptides: innate immune regulatory peptides as a novel approach for treating infections,” *Cell. Mol. Life Sci.*, vol. 64, no. 7–8, pp. 922–933, Apr. 2007.

[10] D. Gaspar, A. S. Veiga, and M. A. R. B. Castanho, “From antimicrobial to anticancer peptides. A review,” *Front Microbiol*, vol. 4, p. 294, 2013.

[11] M. Zasloff, “Antimicrobial peptides of multicellular organisms,” *Nature*, vol. 415, no. 6870, pp. 389–395, Jan. 2002.

[12] D. Takahashi, S. K. Shukla, O. Prakash, and G. Zhang, “Structural determinants of host defense peptides for antimicrobial activity and target cell selectivity,” *Biochimie*, vol. 92, no. 9, pp. 1236–1241, Sep. 2010.

[13] H. G. Boman, “Antibacterial peptides: basic facts and emerging concepts,” *J. Intern. Med.*, vol. 254, no. 3, pp. 197–215, Sep. 2003.

[14] M. Zaiou, “Multifunctional antimicrobial peptides: therapeutic targets in several human diseases,” *J. Mol. Med.*, vol. 85, no. 4, pp. 317–329, Apr. 2007.

[15] M. Zasloff, “Antimicrobial peptides in health and disease,” *N. Engl. J. Med.*, vol. 347, no. 15, pp. 1199–1200, Oct. 2002.

[16] R. E. Hancock and R. Lehrer, “Cationic peptides: a new source of antibiotics,” *Trends Biotechnol.*, vol. 16, no. 2, pp. 82–88, Feb. 1998.

[17] “Antiinfective Peptides Laboratory - Prof. Alessandro Tossi.” [Online]. Available: http://www.bbcm.units.it/~tossi/pag1.htm. [Accessed: 28-Mar-2013].

[18] Y. Rosenfeld and Y. Shai, “Lipopolysaccharide (Endotoxin)-host defense antibacterial peptides interactions: role in bacterial resistance and prevention of sepsis,” *Biochim. Biophys. Acta*, vol. 1758, no. 9, pp. 1513–1522, Sep. 2006.

[19] M. Zasloff, “Magainins, a class of antimicrobial peptides from Xenopus skin: isolation, characterization of two active forms, and partial cDNA sequence of a precursor,” *Proc. Natl. Acad. Sci. U.S.A.*, vol. 84, no. 15, pp. 5449–5453, Aug. 1987.

[20] H. G. Boman, “Antibacterial peptides: Key components needed in immunity,” *Cell*, vol. 65, no. 2, pp. 205–207, Apr. 1991.

[21] M. N. Melo, R. Ferre, and M. A. R. B. Castanho, “Antimicrobial peptides: linking partition, activity and high membrane-bound concentrations,” *Nat. Rev. Microbiol.*, vol. 7, no. 3, pp. 245–250, Mar. 2009.
[22] B. Bechinger and K. Lohner, “Detergent-like actions of linear amphipathic cationic antimicrobial peptides,” *Biochim. Biophys. Acta*, vol. 1758, no. 9, pp. 1529–1539, Sep. 2006.
[23] K. Lohner and S. E. Blondelle, “Molecular mechanisms of membrane perturbation by antimicrobial peptides and the use of biophysical studies in the design of novel peptide antibiotics,” *Comb. Chem. High Throughput Screen.*, vol. 8, no. 3, pp. 241–256, May 2005.
[24] N. Papo and Y. Shai, “Host defense peptides as new weapons in cancer treatment,” *Cell. Mol. Life Sci.*, vol. 62, no. 7–8, pp. 784–790, Apr. 2005.
[25] A. Risso, E. Braidot, M. C. Sordano, A. Vianello, F. Macrì, B. Skerlavaj, M. Zanetti, R. Gennaro, and P. Bernardi, “BMAP-28, an antibiotic peptide of innate immunity, induces cell death through opening of the mitochondrial permeability transition pore,” *Mol. Cell. Biol.*, vol. 22, no. 6, pp. 1926–1935, Mar. 2002.
[26] P. Nicolas, “Multifunctional host defense peptides: intracellular-targeting antimicrobial peptides,” *FEBS J.*, vol. 276, no. 22, pp. 6483–6496, Nov. 2009.
[27] F. Jean-François, S. Castano, B. Desbat, B. Odaert, M. Roux, M.-H. Metz-Boutigue, and E. J. Dufourc, “Aggregation of cateslytin beta-sheets on negatively charged lipids promotes rigid membrane domains. A new mode of action for antimicrobial peptides?,” *Biochemistry*, vol. 47, no. 24, pp. 6394–6402, Jun. 2008.
[28] H. W. Huang, “Action of antimicrobial peptides: two-state model,” *Biochemistry*, vol. 39, no. 29, pp. 8347–8352, Jul. 2000.
[29] C. Leuschner and W. Hansel, “Membrane disrupting lytic peptides for cancer treatments,” *Curr. Pharm. Des.*, vol. 10, no. 19, pp. 2299–2310, 2004.
[30] N. Sitaram and R. Nagaraj, “Interaction of antimicrobial peptides with biological and model membranes: structural and charge requirements for activity,” *Biochim. Biophys. Acta*, vol. 1462, no. 1–2, pp. 29–54, Dec. 1999.
[31] Y. Shai, “Mechanism of the binding, insertion and destabilization of phospholipid bilayer membranes by alpha-helical antimicrobial and cell non-selective membrane-lytic peptides,” *Biochim. Biophys. Acta*, vol. 1462, no. 1–2, pp. 55–70, Dec. 1999.
[32] J. E. Vance and G. Tasseva, “Formation and function of phosphatidylserine and phosphatidylethanolamine in mammalian cells,” *Biochim. Biophys. Acta*, vol. 1831, no. 3, pp. 543–554, Mar. 2013.
[33] J. A. Op den Kamp, “Lipid asymmetry in membranes,” *Annu. Rev. Biochem.*, vol. 48, pp. 47–71, 1979.
[34] T. Utsugi, A. J. Schroit, J. Connor, C. D. Bucana, and I. J. Fidler, “Elevated expression of phosphatidylserine in the outer membrane leaflet of human tumor cells and recognition by activated human blood monocytes,” *Cancer Res.*, vol. 51, no. 11, pp. 3062–3066, Jun. 1991.
[35] S. Ran, A. Downes, and P. E. Thorpe, “Increased exposure of anionic phospholipids on the surface of tumor blood vessels,” *Cancer Res.*, vol. 62, no. 21, pp. 6132–6140, Nov. 2002.
[36] I. Dobrzyńska, B. Szachowicz-Petelska, S. Sulkowski, and Z. Figaszewski, “Changes in electric charge and phospholipids composition in human colorectal cancer cells,” *Mol. Cell. Biochem.*, vol. 276, no. 1–2, pp. 113–119, Aug. 2005.

[37] W. H. Yoon, H. D. Park, K. Lim, and B. D. Hwang, “Effect of O-glycosylated mucin on invasion and metastasis of HM7 human colon cancer cells,” *Biochem. Biophys. Res. Commun.*, vol. 222, no. 3, pp. 694–699, May 1996.
[38] M. D. Burdick, A. Harris, C. J. Reid, T. Iwamura, and M. A. Hollingsworth, “Oligosaccharides expressed on MUC1 produced by pancreatic and colon tumor cell lines,” *J. Biol. Chem.*, vol. 272, no. 39, pp. 24198–24202, Sep. 1997.
[39] H. S. Lee, C. B. Park, J. M. Kim, S. A. Jang, I. Y. Park, M. S. Kim, J. H. Cho, and S. C. Kim, “Mechanism of anticancer activity of buforin IIb, a histone H2A-derived peptide,” *Cancer Lett.*, vol. 271, no. 1, pp. 47–55, Nov. 2008.
[40] J. Kleeff, T. Ishiwata, A. Kumbasar, H. Friess, M. W. Büchler, A. D. Lander, and M. Korc, “The cell-surface heparan sulfate proteoglycan glypican-1 regulates growth factor action in pancreatic carcinoma cells and is overexpressed in human pancreatic cancer,” *J. Clin. Invest.*, vol. 102, no. 9, pp. 1662–1673, Nov. 1998.
[41] R. A. Cruciani, J. L. Barker, M. Zasloff, H. C. Chen, and O. Colamonici, “Antibiotic magainins exert cytolytic activity against transformed cell lines through channel formation,” *Proc. Natl. Acad. Sci. U.S.A.*, vol. 88, no. 9, pp. 3792–3796, May 1991.
[42] M. Sok, M. Sentjurc, and M. Schara, “Membrane fluidity characteristics of human lung cancer,” *Cancer Lett.*, vol. 139, no. 2, pp. 215–220, May 1999.
[43] H. Steiner, D. Andreu, and R. B. Merrifield, “Binding and action of cecropin and cecropin analogues: antibacterial peptides from insects,” *Biochim. Biophys. Acta*, vol. 939, no. 2, pp. 260–266, Apr. 1988.
[44] L. Silvestro, K. Gupta, J. N. Weiser, and P. H. Axelsen, “The concentration-dependent membrane activity of cecropin A,” *Biochemistry*, vol. 36, no. 38, pp. 11452–11460, Sep. 1997.
[45] S. Manno, Y. Takakuwa, and N. Mohandas, “Identification of a functional role for lipid asymmetry in biological membranes: Phosphatidylserine-skeletal protein interactions modulate membrane stability,” *Proc. Natl. Acad. Sci. U.S.A.*, vol. 99, no. 4, pp. 1943–1948, Feb. 2002.
[46] S. Riedl, B. Rinner, M. Asslaber, H. Schaider, S. Walzer, A. Novak, K. Lohner, and D. Zweytick, “In search of a novel target - phosphatidylserine exposed by non-apoptotic tumor cells and metastases of malignancies with poor treatment efficacy,” *Biochim. Biophys. Acta*, vol. 1808, no. 11, pp. 2638–2645, Nov. 2011.
[47] K. Matsuzaki, K. Sugishita, N. Fujii, and K. Miyajima, “Molecular basis for membrane selectivity of an antimicrobial peptide, magainin 2,” *Biochemistry*, vol. 34, no. 10, pp. 3423–3429, Mar. 1995.
[48] T. Iwasaki, J. Ishibashi, H. Tanaka, M. Sato, A. Asaoka, D. Taylor, and M. Yamakawa, “Selective cancer cell cytotoxicity of enantiomeric 9-mer peptides derived from beetle defensins depends on negatively charged phosphatidylserine on the cell surface,” *Peptides*, vol. 30, no. 4, pp. 660–668, Apr. 2009.
[49] J. M. Jakielaszek, J. A. Madej, and K. A. Sobiech, “[Glycoproteins and sialoproteins in the serum and internal organs of mice with transplantable leukemia],” *Pol. Arch. Weter.*, vol. 26, no. 1–2, pp. 95–105, 1986.
[50] K. M. Erbil, S. E. Sen, H. Zincke, and J. D. Jones, “Significance of serum protein and lipid-bound sialic acid as a marker for genitourinary malignancies,” *Cancer*, vol. 57, no. 7, pp. 1389–1394, Apr. 1986.
[51] J. Weghuber, M. C. Aichinger, M. Brameshuber, S. Wieser, V. Ruprecht, B. Plochberger, J. Madl, A. Horner, S. Reipert, K. Lohner, T. Henics, and G. J. Schütz, “Cationic amphipathic peptides accumulate sialylated proteins and lipids

in the plasma membrane of eukaryotic host cells," *Biochim. Biophys. Acta*, vol. 1808, no. 10, pp. 2581–2590, Oct. 2011.

[52] R. Bucki, D. B. Namiot, Z. Namiot, P. B. Savage, and P. A. Janmey, "Salivary mucins inhibit antibacterial activity of the cathelicidin-derived LL-37 peptide but not the cationic steroid CSA-13," *J. Antimicrob. Chemother.*, vol. 62, no. 2, pp. 329–335, Aug. 2008.

[53] A. Risso, M. Zanetti, and R. Gennaro, "Cytotoxicity and apoptosis mediated by two peptides of innate immunity," *Cell. Immunol.*, vol. 189, no. 2, pp. 107–115, Nov. 1998.

[54] B. Fadnes, L. Uhlin-Hansen, I. Lindin, and Ø. Rekdal, "Small lytic peptides escape the inhibitory effect of heparan sulfate on the surface of cancer cells," *BMC Cancer*, vol. 11, p. 116, 2011.

[55] J. Andrä, D. Monreal, G. Martinez de Tejada, C. Olak, G. Brezesinski, S. S. Gomez, T. Goldmann, R. Bartels, K. Brandenburg, and I. Moriyon, "Rationale for the design of shortened derivatives of the NK-lysin-derived antimicrobial peptide NK-2 with improved activity against Gram-negative pathogens," *J. Biol. Chem.*, vol. 282, no. 20, pp. 14719–14728, May 2007.

[56] M. Leippe, J. Andrä, and H. J. Müller-Eberhard, "Cytolytic and antibacterial activity of synthetic peptides derived from amoebapore, the pore-forming peptide of *Entamoeba histolytica*," *Proc. Natl. Acad. Sci. U.S.A.*, vol. 91, no. 7, pp. 2602–2606, Mar. 1994.

[57] N. Yang, M. B. Strøm, S. M. Mekonnen, J. S. Svendsen, and O. Rekdal, "The effects of shortening lactoferrin derived peptides against tumour cells, bacteria and normal human cells," *J. Pept. Sci.*, vol. 10, no. 1, pp. 37–46, Jan. 2004.

[58] S. Kim, S. S. Kim, Y. J. Bang, S. J. Kim, and B. J. Lee, "In vitro activities of native and designed peptide antibiotics against drug sensitive and resistant tumor cell lines," *Peptides*, vol. 24, no. 7, pp. 945–953, Jul. 2003.

[59] J. A. Werkmeister, A. Kirkpatrick, J. A. McKenzie, and D. E. Rivett, "The effect of sequence variations and structure on the cytolytic activity of melittin peptides," *Biochim. Biophys. Acta*, vol. 1157, no. 1, pp. 50–54, May 1993.

[60] S. E. Blondelle and R. A. Houghten, "Hemolytic and antimicrobial activities of the twenty-four individual omission analogues of melittin," *Biochemistry*, vol. 30, no. 19, pp. 4671–4678, May 1991.

[61] J. S. Mader and D. W. Hoskin, "Cationic antimicrobial peptides as novel cytotoxic agents for cancer treatment," *Expert Opin Investig Drugs*, vol. 15, no. 8, pp. 933–946, Aug. 2006.

[62] A. J. Moore, D. A. Devine, and M. C. Bibby, "Preliminary experimental anticancer activity of cecropins," *Pept. Res.*, vol. 7, no. 5, pp. 265–269, Oct. 1994.

[63] J. Banković, J. Andrä, N. Todorović, A. Podolski-Renić, Z. Milošević, D. Miljković, J. Krause, S. Ruždijić, N. Tanić, and M. Pešić, "The elimination of P-glycoprotein over-expressing cancer cells by antimicrobial cationic peptide NK-2: the unique way of multi-drug resistance modulation," *Exp. Cell Res.*, vol. 319, no. 7, pp. 1013–1027, Apr. 2013.

[64] J. S. Mader, J. Salsman, D. M. Conrad, and D. W. Hoskin, "Bovine lactoferricin selectively induces apoptosis in human leukemia and carcinoma cell lines," *Mol. Cancer Ther.*, vol. 4, no. 4, pp. 612–624, Apr. 2005.

[65] R. Okuyama, A. Aruga, T. Hatori, K. Takeda, and M. Yamamoto, "Immunological responses to a multi-peptide vaccine targeting cancer-testis antigens and VEGFRs in advanced pancreatic cancer patients," *Oncoimmunology*, vol. 2, no. 11, p. e27010, Nov. 2013.

[66] K. C. L. Mulder, L. A. Lima, V. J. Miranda, S. C. Dias, and O. L. Franco, "Current scenario of peptide-based drugs: the key roles of cationic antitumor and antiviral peptides," *Front Microbiol*, vol. 4, Oct. 2013.
[67] J. Hu, C. Chen, S. Zhang, X. Zhao, H. Xu, X. Zhao, and J. R. Lu, "Designed antimicrobial and antitumor peptides with high selectivity," *Biomacromolecules*, vol. 12, no. 11, pp. 3839–3843, Nov. 2011.
[68] R. E. W. Hancock and H.-G. Sahl, "Antimicrobial and host-defense peptides as new anti-infective therapeutic strategies," *Nat. Biotechnol.*, vol. 24, no. 12, pp. 1551–1557, Dec. 2006.
[69] M. A. Baker, W. L. Maloy, M. Zasloff, and L. S. Jacob, "Anticancer efficacy of Magainin2 and analogue peptides," *Cancer Res.*, vol. 53, no. 13, pp. 3052–3057, Jul. 1993.
[70] L. Hui, K. Leung, and H. M. Chen, "The combined effects of antibacterial peptide cecropin A and anti-cancer agents on leukemia cells," *Anticancer Res.*, vol. 22, no. 5, pp. 2811–2816, Oct. 2002.
[71] H. Schröder-Borm, R. Bakalova, and J. Andrä, "The NK-lysin derived peptide NK-2 preferentially kills cancer cells with increased surface levels of negatively charged phosphatidylserine," *FEBS Lett.*, vol. 579, no. 27, pp. 6128–6134, Nov. 2005.
[72] W. K. K. Wu, G. Wang, S. B. Coffelt, A. M. Betancourt, C. W. Lee, D. Fan, K. Wu, J. Yu, J. J. Y. Sung, and C. H. Cho, "Emerging roles of the host defense peptide LL-37 in human cancer and its potential therapeutic applications," *Int. J. Cancer*, vol. 127, no. 8, pp. 1741–1747, Oct. 2010.
[73] H. Schröder-Borm, R. Willumeit, K. Brandenburg, and J. Andrä, "Molecular basis for membrane selectivity of NK-2, a potent peptide antibiotic derived from NK-lysin," *Biochim. Biophys. Acta*, vol. 1612, no. 2, pp. 164–171, Jun. 2003.
[74] M. Andersson, H. Gunne, B. Agerberth, A. Boman, T. Bergman, B. Olsson, A. Dagerlind, H. Wigzell, H. G. Boman, and G. H. Gudmundsson, "NK-lysin, structure and function of a novel effector molecule of porcine T and NK cells," *Vet. Immunol. Immunopathol.*, vol. 54, no. 1–4, pp. 123–126, Nov. 1996.
[75] M. Andersson, H. Gunne, B. Agerberth, A. Boman, T. Bergman, R. Sillard, H. Jörnvall, V. Mutt, B. Olsson, and H. Wigzell, "NK-lysin, a novel effector peptide of cytotoxic T and NK cells. Structure and cDNA cloning of the porcine form, induction by interleukin 2, antibacterial and antitumour activity," *EMBO J.*, vol. 14, no. 8, pp. 1615–1625, Apr. 1995.
[76] E. Liepinsh, M. Andersson, J. M. Ruysschaert, and G. Otting, "Saposin fold revealed by the NMR structure of NK-lysin," *Nat. Struct. Biol.*, vol. 4, no. 10, pp. 793–795, Oct. 1997.
[77] J. Andrä and M. Leippe, "Candidacidal activity of shortened synthetic analogs of amoebapores and NK-lysin," *Med. Microbiol. Immunol.*, vol. 188, no. 3, pp. 117–124, Dec. 1999.
[78] T. Jacobs, H. Bruhn, I. Gaworski, B. Fleischer, and M. Leippe, "NK-lysin and its shortened analog NK-2 exhibit potent activities against Trypanosoma cruzi," *Antimicrob. Agents Chemother.*, vol. 47, no. 2, pp. 607–613, Feb. 2003.
[79] J. Andrä, M. H. J. Koch, R. Bartels, and K. Brandenburg, "Biophysical characterization of endotoxin inactivation by NK-2, an antimicrobial peptide derived from mammalian NK-lysin," *Antimicrob. Agents Chemother.*, vol. 48, no. 5, pp. 1593–1599, May 2004.

[80] S. Drechsler and J. Andrä, “Online monitoring of metabolism and morphology of peptide-treated neuroblastoma cancer cells and keratinocytes,” *J. Bioenerg. Biomembr.*, vol. 43, no. 3, pp. 275–285, Jun. 2011.
[81] J. Andrä, T. Goldmann, C. M. Ernst, A. Peschel, and T. Gutsmann, “Multiple peptide resistance factor (MprF)-mediated Resistance of *Staphylococcus aureus* against antimicrobial peptides coincides with a modulated peptide interaction with artificial membranes comprising lysyl-phosphatidylglycerol,” *J. Biol. Chem.*, vol. 286, no. 21, pp. 18692–18700, May 2011.
[82] J. W. Larrick, M. Hirata, R. F. Balint, J. Lee, J. Zhong, and S. C. Wright, “Human CAP18: a novel antimicrobial lipopolysaccharide-binding protein,” *Infect. Immun.*, vol. 63, no. 4, pp. 1291–1297, Apr. 1995.
[83] T. Sigurdardottir, P. Andersson, M. Davoudi, M. Malmsten, A. Schmidtchen, and M. Bodelsson, “In silico identification and biological evaluation of antimicrobial peptides based on human cathelicidin LL-37,” *Antimicrob. Agents Chemother.*, vol. 50, no. 9, pp. 2983–2989, Sep. 2006.
[84] U. H. N. Dürr, U. S. Sudheendra, and A. Ramamoorthy, “LL-37, the only human member of the cathelicidin family of antimicrobial peptides,” *Biochim. Biophys. Acta*, vol. 1758, no. 9, pp. 1408–1425, Sep. 2006.
[85] T. Gutsmann, S. O. Hagge, J. W. Larrick, U. Seydel, and A. Wiese, “Interaction of CAP18-derived peptides with membranes made from endotoxins or phospholipids.,” *Biophys J*, vol. 80, no. 6, pp. 2935–2945, Jun. 2001.
[86] C. E. Dempsey, “The actions of melittin on membranes,” *Biochim. Biophys. Acta*, vol. 1031, no. 2, pp. 143–161, May 1990.
[87] Fürst, Anton, Martens, Ann, and Bogaert, Lies, “Das Equine Sarkoid.” CVE Pferd, VET Impulse, Mar. 2009.
[88] Derek C. Knottenbelt, “A Suggested Clinical Classification for the Equine Sarcoid,” *Clin Tech Equine Practice*, no. 4, pp. 278–295, 2005.
[89] L. Goodrich, H. Gerber, E. Marti, and D. F. Antczak, “Equine sarcoids,” *Vet. Clin. North Am. Equine Pract.*, vol. 14, no. 3, pp. 607–623, vii, Dec. 1998.
[90] H. Broström, “Equine sarcoids. A clinical and epidemiological study in relation to equine leucocyte antigens (ELA),” *Acta Vet. Scand.*, vol. 36, no. 2, pp. 223–236, 1995.
[91] N. Bloch, M. Breen, and P. B. Spradbrow, “Genomic sequences of bovine papillomaviruses in formalin-fixed sarcoids from Australian horses revealed by polymerase chain reaction,” *Vet. Microbiol.*, vol. 41, no. 1–2, pp. 163–172, Jul. 1994.
[92] S. W. Reid, K. T. Smith, and W. F. Jarrett, “Detection, cloning and characterisation of papillomaviral DNA present in sarcoid tumours of Equus asinus,” *Vet. Rec.*, vol. 135, no. 18, pp. 430–432, Oct. 1994.
[93] L. Bogaert, A. Martens, W. M. Kast, E. Van Marck, and H. De Cock, “Bovine papillomavirus DNA can be detected in keratinocytes of equine sarcoid tumors,” *Vet. Microbiol.*, vol. 146, no. 3–4, pp. 269–275, Dec. 2010.
[94] A. Martens, A. De Moor, and R. Ducatelle, “PCR detection of bovine papilloma virus DNA in superficial swabs and scrapings from equine sarcoids,” *Vet. J.*, vol. 161, no. 3, pp. 280–286, May 2001.
[95] L. Nasir and S. W. Reid, “Bovine papillomaviral gene expression in equine sarcoid tumours,” *Virus Res.*, vol. 61, no. 2, pp. 171–175, Jun. 1999.
[96] G. Chambers, V. A. Ellsmore, P. M. O’Brien, S. W. J. Reid, S. Love, M. S. Campo, and L. Nasir, “Association of bovine papillomavirus with the equine sarcoid,” *J. Gen. Virol.*, vol. 84, no. Pt 5, pp. 1055–1062, May 2003.

[97] Z. Yuan, E. A. Gault, M. S. Campo, and L. Nasir, "Different contribution of bovine papillomavirus type 1 oncoproteins to the transformation of equine fibroblasts," *J. Gen. Virol.*, vol. 92, no. Pt 4, pp. 773–783, Apr. 2011.

[98] S. Brandt, R. Haralambus, A. Schoster, R. Kirnbauer, and C. Stanek, "Peripheral blood mononuclear cells represent a reservoir of bovine papillomavirus DNA in sarcoid-affected equines," *J. Gen. Virol.*, vol. 89, no. Pt 6, pp. 1390–1395, Jun. 2008.

[99] L. Bogaert, A. Martens, C. De Baere, and F. Gasthuys, "Detection of bovine papillomavirus DNA on the normal skin and in the habitual surroundings of horses with and without equine sarcoids," *Res. Vet. Sci.*, vol. 79, no. 3, pp. 253–258, Dec. 2005.

[100] B. A. Valentine, "Survey of equine cutaneous neoplasia in the Pacific Northwest," *J. Vet. Diagn. Invest.*, vol. 18, no. 1, pp. 123–126, Jan. 2006.

[101] B. K. Wobeser, J. L. Davies, J. E. Hill, M. L. Jackson, B. A. Kidney, M. N. Mayer, H. G. G. Townsend, and A. L. Allen, "Epidemiology of equine sarcoids in horses in western Canada," *Can. Vet. J.*, vol. 51, no. 10, pp. 1103–1108, Oct. 2010.

[102] Cecil Jackson, "The incidence and pathology of tumours of domesticated animals in south africa - A study of the Onderstepoort Collection of Neoplasms with Special Reference to their Histopathology," 1936.

[103] E. Cotchin, "A general survey of tumours in the horse," *Equine Vet. J.*, vol. 9, no. 1, pp. 16–21, Jan. 1977.

[104] R. R. Pascoe and P. M. Summers, "Clinical survey of tumours and tumour-like lesions in horses in south east Queensland," *Equine Vet. J.*, vol. 13, no. 4, pp. 235–239, Oct. 1981.

[105] J. P. Teifke, "[Morphologic and molecular biologic studies of the etiology of equine sarcoid]," *Tierarztl Prax*, vol. 22, no. 4, pp. 368–376, Aug. 1994.

[106] S. Mattil-Fritz, D. Scharner, K. Piuko, N. Thönes, L. Gissmann, H. Müller, and M. Müller, "Immunotherapy of equine sarcoid: dose-escalation trial for the use of chimeric papillomavirus-like particles," *J. Gen. Virol.*, vol. 89, no. Pt 1, pp. 138–147, Jan. 2008.

[107] E. Marti, S. Lazary, D. F. Antczak, and H. Gerber, "Report of the first international workshop on equine sarcoid," *Equine Vet. J.*, vol. 25, no. 5, pp. 397–407, Sep. 1993.

[108] D. C. Knottenbelt and D. F. Kelly, "The diagnosis and treatment of periorbital sarcoid in the horse: 445 cases from 1974 to 1999," *Vet Ophthalmol*, vol. 3, no. 2–3, pp. 169–191, 2000.

[109] F. F. McConaghy, R. E. Davis, G. P. Reppas, J. Rawlinson R, S. A. McClintock, D. R. Hutchins, and D. R. Hodgson, "Management of equine sarcoids: 1975-93," *N Z Vet J*, vol. 42, no. 5, pp. 180–184, Oct. 1994.

[110] B. Carstanjen, P. Jordan, and O. M. Lepage, "Carbon dioxide laser as a surgical instrument for sarcoid therapy--a retrospective study on 60 cases," *Can. Vet. J.*, vol. 38, no. 12, pp. 773–776, Dec. 1997.

[111] "Prostate Cancer." [Online]. Available: http://www.cancer.org/cancer/prostatecancer/index. [Accessed: 30-Jul-2013].

[112] A. Jemal, R. Siegel, J. Xu, and E. Ward, "Cancer statistics, 2010," *CA Cancer J Clin*, vol. 60, no. 5, pp. 277–300, Oct. 2010.

[113] "S3-Leitlinie Prostatakarzinom - s3-leitlinie-prostatakarzinom_2012_kurz.pdf." .

[114] H. G. Sim and C. W. S. Cheng, "Changing demography of prostate cancer in Asia," *Eur. J. Cancer*, vol. 41, no. 6, pp. 834–845, Apr. 2005.

[115] S. K. Park, L. C. Sakoda, D. Kang, A. P. Chokkalingam, E. Lee, H.-R. Shin, Y.-O. Ahn, M.-H. Shin, C.-W. Lee, D.-H. Lee, A. Blair, S. S. Devesa, and A. W. Hsing, "Rising prostate cancer rates in South Korea," *Prostate*, vol. 66, no. 12, pp. 1285–1291, Sep. 2006.

[116] "Cancer of the Prostate - SEER Stat Fact Sheets." [Online]. Available: http://seer.cancer.gov/statfacts/html/prost.html. [Accessed: 18-Mar-2011].

[117] "Prostate Cancer Treatment (PDQ®) - National Cancer Institute." [Online]. Available: http://www.cancer.gov/cancertopics/pdq/treatment/prostate/HealthProfessional/page4. [Accessed: 18-Mar-2011].

[118] P. Boukamp, R. T. Petrussevska, D. Breitkreutz, J. Hornung, A. Markham, and N. E. Fusenig, "Normal keratinization in a spontaneously immortalized aneuploid human keratinocyte cell line," *J. Cell Biol.*, vol. 106, no. 3, pp. 761–771, Mar. 1988.

[119] U. K. Laemmli, "Cleavage of structural proteins during the assembly of the head of bacteriophage T4," *Nature*, vol. 227, no. 5259, pp. 680–685, Aug. 1970.

[120] H. Schägger and G. von Jagow, "Tricine-sodium dodecyl sulfate-polyacrylamide gel electrophoresis for the separation of proteins in the range from 1 to 100 kDa," *Anal. Biochem.*, vol. 166, no. 2, pp. 368–379, Nov. 1987.

[121] L. Ceriotti, A. Kob, S. Drechsler, J. Ponti, E. Thedinga, P. Colpo, R. Ehret, and F. Rossi, "Online monitoring of BALB/3T3 metabolism and adhesion with multiparametric chip-based system," *Anal. Biochem.*, vol. 371, no. 1, pp. 92–104, Dec. 2007.

[122] E. Thedinga, A. Kob, H. Holst, A. Keuer, S. Drechsler, R. Niendorf, W. Baumann, I. Freund, M. Lehmann, and R. Ehret, "Online monitoring of cell metabolism for studying pharmacodynamic effects," *Toxicol. Appl. Pharmacol.*, vol. 220, no. 1, pp. 33–44, Apr. 2007.

[123] "Zeta potential, short tutorial." [Online]. Available: http://www.dispersion.com/zeta-potential-short-tutorial. [Accessed: 01-Oct-2014].

[124] "Electroacoustics Tutorial 1.PDF - TN-ZP-zetapotential.pdf." [Online]. Available: http://www.titanex.com.tw/doc/tecsupport/TN-ZP-zetapotential.pdf. [Accessed: 01-Oct-2014]

[125] "Zetasizer_Nano_user_manual_Man0317-1.1.pdf." [Online]. Available: http://www.biophysics.bioc.cam.ac.uk/files/Zetasizer_Nano_user_manual_Man0317-1.1.pdf. [Accessed: 03-Oct-2014]

[126] "Cancer Facts and Statistics | American Cancer Society." [Online]. Available: http://www.cancer.org/research/cancerfactsstatistics/index. [Accessed: 18-Jun-2013].

[127] L. T. Eliassen, G. Berge, B. Sveinbjørnsson, J. S. Svendsen, L. H. Vorland, and Ø. Rekdal, "Evidence for a direct antitumor mechanism of action of bovine lactoferricin," *Anticancer Res.*, vol. 22, no. 5, pp. 2703–2710, Oct. 2002.

[128] Y. Ohsaki, A. F. Gazdar, H. C. Chen, and B. E. Johnson, "Antitumor activity of magainin analogues against human lung cancer cell lines," *Cancer Res.*, vol. 52, no. 13, pp. 3534–3538, Jul. 1992.

[129] N. Papo, M. Shahar, L. Eisenbach, and Y. Shai, "A novel lytic peptide composed of DL-amino acids selectively kills cancer cells in culture and in mice," *J. Biol. Chem.*, vol. 278, no. 23, pp. 21018–21023, Jun. 2003.

[130] Y. Q. Chen, C. Min, M. Sang, Y. Y. Han, X. Ma, X. Q. Xue, and S. Q. Zhang, "A cationic amphiphilic peptide ABP-CM4 exhibits selective cytotoxicity against leukemia cells," *Peptides*, vol. 31, no. 8, pp. 1504–1510, Aug. 2010.

[131] K. Wang, J. Yan, B. Zhang, J. Song, P. Jia, and R. Wang, "Novel mode of action of polybia-MPI, a novel antimicrobial peptide, in multi-drug resistant leukemic cells," *Cancer Lett.*, vol. 278, no. 1, pp. 65–72, Jun. 2009.

[132] P. Warren, L. Li, W. Song, E. Holle, Y. Wei, T. Wagner, and X. Yu, "In vitro targeted killing of prostate tumor cells by a synthetic amoebapore helix 3 peptide modified with two gamma-linked glutamate residues at the COOH terminus," *Cancer Res.*, vol. 61, no. 18, pp. 6783–6787, Sep. 2001.

[133] N. Papo, D. Seger, A. Makovitzki, V. Kalchenko, Z. Eshhar, H. Degani, and Y. Shai, "Inhibition of tumor growth and elimination of multiple metastases in human prostate and breast xenografts by systemic inoculation of a host defense-like lytic peptide," *Cancer Res.*, vol. 66, no. 10, pp. 5371–5378, May 2006.

[134] M. Yun, "Imaging of Gastric Cancer Metabolism Using 18 F-FDG PET/CT," *J Gastric Cancer*, vol. 14, no. 1, pp. 1–6, Mar. 2014.

[135] M. U. Hammer, A. Brauser, C. Olak, G. Brezesinski, T. Goldmann, T. Gutsmann, and J. Andrä, "Lipopolysaccharide interaction is decisive for the activity of the antimicrobial peptide NK-2 against Escherichia coli and Proteus mirabilis," *Biochem. J.*, vol. 427, no. 3, pp. 477–488, May 2010.

[136] K. A. Peck-Miller, R. P. Darveau, and H. P. Fell, "Identification of serum components that inhibit the tumoricidal activity of amphiphilic alpha helical peptides," *Cancer Chemother. Pharmacol.*, vol. 32, no. 2, pp. 109–115, 1993.

[137] N. Papo and Y. Shai, "New lytic peptides based on the D,L-amphipathic helix motif preferentially kill tumor cells compared to normal cells," *Biochemistry*, vol. 42, no. 31, pp. 9346–9354, Aug. 2003.

[138] M. V. Buri, T. M. Domingues, E. J. Paredes-Gamero, R. L. Casaes-Rodrigues, E. G. Rodrigues, and A. Miranda, "Resistance to degradation and cellular distribution are important features for the antitumor activity of gomesin," *PLoS ONE*, vol. 8, no. 11, p. e80924, 2013.

[139] J. B. McPhee, M. G. Scott, and R. E. W. Hancock, "Design of host defence peptides for antimicrobial and immunity enhancing activities," *Comb. Chem. High Throughput Screen.*, vol. 8, no. 3, pp. 257–272, May 2005.

[140] W. Huang, J. Seo, S. B. Willingham, A. M. Czyzewski, M. L. Gonzalgo, I. L. Weissman, and A. E. Barron, "Learning from host-defense peptides: cationic, amphipathic peptoids with potent anticancer activity," *PLoS ONE*, vol. 9, no. 2, p. e90397, 2014.

[141] M. R. Joshi, N. Yao, K. A. Myers, and Z. Li, "Human serum albumin and p53-activating peptide fusion protein is able to promote apoptosis and deliver fatty acid-modified molecules," *PLoS ONE*, vol. 8, no. 11, p. e80926, 2013.

[142] K. A. Camilio, G. Berge, C. S. Ravuri, O. Rekdal, and B. Sveinbjørnsson, "Complete regression and systemic protective immune responses obtained in B16 melanomas after treatment with LTX-315," *Cancer Immunol. Immunother.*, vol. 63, no. 6, pp. 601–613, Jun. 2014.

[143] S. F. Sui, H. Wu, Y. Guo, and K. S. Chen, "Conformational changes of melittin upon insertion into phospholipid monolayer and vesicle," *J. Biochem.*, vol. 116, no. 3, pp. 482–487, Sep. 1994.

[144] M. Dathe and T. Wieprecht, "Structural features of helical antimicrobial peptides: their potential to modulate activity on model membranes and biological cells," *Biochim. Biophys. Acta*, vol. 1462, no. 1–2, pp. 71–87, Dec. 1999.

[145] Z. Oren, J. C. Lerman, G. H. Gudmundsson, B. Agerberth, and Y. Shai, "Structure and organization of the human antimicrobial peptide LL-37 in

phospholipid membranes: relevance to the molecular basis for its non-cell-selective activity," *Biochem. J.*, vol. 341 (Pt 3), pp. 501–513, Aug. 1999.

[146] K. A. Henzler Wildman, D.-K. Lee, and A. Ramamoorthy, "Mechanism of lipid bilayer disruption by the human antimicrobial peptide, LL-37," *Biochemistry*, vol. 42, no. 21, pp. 6545–6558, Jun. 2003.

[147] R. Willumeit, M. Kumpugdee, S. S. Funari, K. Lohner, B. P. Navas, K. Brandenburg, S. Linser, and J. Andrä, "Structural rearrangement of model membranes by the peptide antibiotic NK-2," *Biochim. Biophys. Acta*, vol. 1669, no. 2, pp. 125–134, May 2005.

[148] L. Yang, T. A. Harroun, T. M. Weiss, L. Ding, and H. W. Huang, "Barrel-stave model or toroidal model? A case study on melittin pores," *Biophys. J.*, vol. 81, no. 3, pp. 1475–1485, Sep. 2001.

[149] R. Saravanan and S. Bhattacharjya, "Oligomeric structure of a cathelicidin antimicrobial peptide in dodecylphosphocholine micelle determined by NMR spectroscopy," *Biochim. Biophys. Acta*, vol. 1808, no. 1, pp. 369–381, Jan. 2011.

[150] J. H. Lee, I.-W. Kim, S.-H. Kim, E.-Y. Yun, S.-H. Nam, M.-Y. Ahn, D.-C. Kang, and J. S. Hwang, "Anticancer activity of CopA3 dimer peptide in human gastric cancer cells," *BMB Rep*, Jul. 2014.

[151] L. Yang, J. O. Nyalwidhe, S. Guo, R. R. Drake, and O. J. Semmes, "Targeted Identification of Metastasis-associated Cell-surface Sialoglycoproteins in Prostate Cancer," *Mol Cell Proteomics*, vol. 10, no. 6, Jun. 2011.

[152] J. Tímár, K. Lapis, J. Dudás, A. Sebestyén, L. Kopper, and I. Kovalszky, "Proteoglycans and tumor progression: Janus-faced molecules with contradictory functions in cancer," *Semin. Cancer Biol.*, vol. 12, no. 3, pp. 173–186, Jun. 2002.

[153] A. Weyers, B. Yang, D. S. Yoon, J.-H. Park, F. Zhang, K. B. Lee, and R. J. Linhardt, "A structural analysis of glycosaminoglycans from lethal and nonlethal breast cancer tissues: toward a novel class of theragnostics for personalized medicine in oncology?," *OMICS*, vol. 16, no. 3, pp. 79–89, Mar. 2012.

[154] R. D. Sanderson, "Heparan sulfate proteoglycans in invasion and metastasis," *Semin. Cell Dev. Biol.*, vol. 12, no. 2, pp. 89–98, Apr. 2001.

[155] H. Nakanishi, K. Oguri, K. Yoshida, N. Itano, K. Takenaga, T. Kazama, A. Yoshida, and M. Okayama, "Structural differences between heparan sulphates of proteoglycan involved in the formation of basement membranes in vivo by Lewis-lung-carcinoma-derived cloned cells with different metastatic potentials," *Biochem. J.*, vol. 288 (Pt 1), pp. 215–224, Nov. 1992.

[156] F. Li, G. B. Ten Dam, S. Murugan, S. Yamada, T. Hashiguchi, S. Mizumoto, K. Oguri, M. Okayama, T. H. van Kuppevelt, and K. Sugahara, "Involvement of highly sulfated chondroitin sulfate in the metastasis of the Lewis lung carcinoma cells," *J. Biol. Chem.*, vol. 283, no. 49, pp. 34294–34304, Dec. 2008.

[157] W. Barańska-Rybak, A. Sonesson, R. Nowicki, and A. Schmidtchen, "Glycosaminoglycans inhibit the antibacterial activity of LL-37 in biological fluids," *J. Antimicrob. Chemother.*, vol. 57, no. 2, pp. 260–265, Feb. 2006.

[158] G. Klocek and J. Seelig, "Melittin interaction with sulfated cell surface sugars," *Biochemistry*, vol. 47, no. 9, pp. 2841–2849, Mar. 2008.

[159] B. Fadnes, ?ystein Rekdal, and L. Uhlin-Hansen, "The anticancer activity of lytic peptides is inhibited by heparan sulfate on the surface of the tumor cells," *BMC Cancer*, vol. 9, p. 183, Jun. 2009.

[160] Y. Oda, M. Kinoshita, K. Hamada, K. Nakayama, Y. Ohta, S. Yamaguchi, Y. Tsukada, Y. Kawai, and K. Kakehi, "Sulfated sialic acid-polymers inhibit the

cytotoxic action of bee and snake venom," *Glycoconj. J.*, vol. 16, no. 8, pp. 457–463, Aug. 1999.

[161] S. Stortecky and T. M. Suter, "Insights into cardiovascular side-effects of modern anticancer therapeutics," *Curr Opin Oncol*, vol. 22, no. 4, pp. 312–317, Jul. 2010.

[162] J. Cassidy and J.-L. Misset, "Oxaliplatin-related side effects: characteristics and management," *Semin. Oncol.*, vol. 29, no. 5 Suppl 15, pp. 11–20, Oct. 2002.

[163] D. Simpson and G. L. Plosker, "Paclitaxel: as adjuvant or neoadjuvant therapy in early breast cancer," *Drugs*, vol. 64, no. 16, pp. 1839–1847, 2004.

[164] B. C. Böckle, D. Jara, W. Nindl, W. Aberer, and N. T. Sepp, "Adrenal Insufficiency as a Result of Long-Term Misuse of Topical Corticosteroids," *Dermatology (Basel)*, Apr. 2014.

[165] L. Venco, M. Mortarino, C. Carro, M. Genchi, F. Pampurini, and C. Genchi, "Field efficacy and safety of a combination of moxidectin and imidacloprid for the prevention of feline heartworm (Dirofilaria immitis) infection," *Vet. Parasitol.*, vol. 154, no. 1–2, pp. 67–70, Jun. 2008.

[166] A. Makovitzki, A. Fink, and Y. Shai, "Suppression of human solid tumor growth in mice by intratumor and systemic inoculation of histidine-rich and pH-dependent host defense-like lytic peptides," *Cancer Res.*, vol. 69, no. 8, pp. 3458–3463, Apr. 2009.

[167] C. Gelhaus, T. Jacobs, J. Andrä, and M. Leippe, "The antimicrobial peptide NK-2, the core region of mammalian NK-lysin, kills intraerythrocytic Plasmodium falciparum," *Antimicrob. Agents Chemother.*, vol. 52, no. 5, pp. 1713–1720, May 2008.

[168] C. Maletzki, U. Klier, S. Marinkovic, E. Klar, J. Andrä, and M. Linnebacher, "Host defense peptides for treatment of colorectal carcinoma - a comparative in vitro and in vivo analysis," *Oncotarget*, vol. 5, no. 12, pp. 4467–4479, Jun. 2014.

9 Publications

Parts of this thesis have been published as indicated below:

Peer-reviewed papers

Gross S, Wilms D, Krause J, Brezesinski G, Andrä J. Design of NK-2-derived peptides with improved activity against equine sarcoid cells. J. Pept. Sci., Oct. 2013.

Gross S, Andrä J. Anticancer peptide NK-2 targets cell surface sulphated glycans rather than sialic acids. Biol. Chem. 2012; 393: 817–827.

Proceedings

Gross S, Andrä J. Glycan targets of the anti-cancer peptide NK-2. In:
Kokotos G, Constantinou-Kokotou V, Matsoukas J, editors. Peptides 2012; Proceedings of the 32nd European Peptide Symposium: European Peptide Society, 2012:38-39.

10 Acknowledgement

I would like to express my great gratitude to my supervisor Prof. Dr. Jörg Andrä for giving me the opportunity to carry out this thesis, for his guidance and support during all phases of the work, for fruitful discussions, teaching of laboratory technics, and helpful advices.

I deeply thank Prof. Dr. Susanne Hartmann for agreeing to examine this thesis as first refereer.

I would like to thank Prof. Dr. Thomas Gutsmann for the possibility to perform this study in his lab group.

I am grateful to Rainer Bartels and Volker Grote for their supply with antimicrobial peptides.

I thank the FLI Federal Research Institute for Animal Health on the island Riems for providing the equine cell lines.

I would like to thank Sabrina Groth for taking care of the cells, introducing me into flow cytometry, and her excellent technical assistance.

I thank Jannike Krause for her help with the confocal fluorescence microscopy.

I thank Christine Hamann for teaching me the preparation of liposomes.

I would like to thank Franziska Kopp and Annika Saathoff for their proof-reading and their constructive remarks.

I am especially greatfull to Nina Hahlbrock for being an enjoyable lab companion.

I would like to express my appreciation to all members of the biophysics laboratory group at the Research Center Borstel for the friendly atmosphere, many inspiring conversations, and various help with smaller and bigger problems.

I would like to thank Prof. Dr. Hermine Brunner and Nicole Deplace for correcting my English in some parts of this work and further helpful remarks, although they have quite time-consuming jobs.

Last but not least I am outmost grateful to Christof for his continous sarcastic comments which always push me to complete this thesis, find a new job, and thus regain financial independence.

Finally, I offer my regards to all those who have not been mentioned personally but supported me in any respect in the successful completion of this thesis.

11 Selbstständigkeitserklärung

Hiermit bestätige ich, dass ich die vorliegende Arbeit selbstständig angefertigt und ausschließlich die angegebenen Quellen und Hilfen in Anspruch genommen habe. Diese Arbeit wurde weder in gleicher noch ähnlicher Form an einer anderen Stelle im Rahmen eines Prüfungsverfahrens vorgelegt.

Norderstedt, den 15. Oktober 2014

Stephanie Groß